

Investigating Spatial Signatures of Spin-Glass Criticality in the Human Brain

Thesis submitted in partial fulfillment
of the requirements for the degree of

Master of Science
in
Computational Natural Sciences
by Research
by

Anirudh Palutla
2018113007

`anirudh.palutla@research.iiit.ac.in`



International Institute of Information Technology
Hyderabad - 500 032, INDIA
December 2023

Copyright © Anirudh Palutla, 2023
All Rights Reserved

International Institute of Information Technology
Hyderabad, India

CERTIFICATE

It is certified that the work contained in this thesis, titled “**Investigating Spatial Signatures of Spin-Glass Criticality in the Human Brain**” by **Anirudh Palutla**, has been carried out under my supervision and is not submitted elsewhere for a degree.

Date

Adviser: Prof. Marimuthu Krishnan

To my Family

Acknowledgments

When I arrived in IIIT Hyderabad back in 2018, I could not have imagined the person I would become, the people I would meet, the work I would do, or the path I would take in life. This college will forever be home to me.

First and foremost, I want to thank my father. He is the reason I even got a chance to attend IIIT, and he is the reason I am who I am today. This thesis belongs to him as much as it belongs to me. I want to thank my mother and my brother for the constant support they have given me. I want to thank my family for being the best family one could ask for.

Most importantly, I want to thank Prof. Marimuthu Krishnan for being the best possible advisor and for being the most kind and understanding mentor. When I first started working with him in my third year of college, I had absolutely no idea what research meant. He taught me how to research from the very ground-up. He taught me how to approach a new field, and he gave me the confidence to explore stuff without being afraid. I am incredibly grateful to him for teaching me valuable life skills, which I will be sure to carry with me for the rest of my days.

I would like to thank my other mentor Dr. S.S. Ashwin, for teaching me a new perspective on research, and for helping me publish my first ever paper. Although I worked with him for less than a year, I will always remember his tireless attitude and the time spent in the lab with him.

I want to thank my best friend, Aditya, for being there for me in the years past and the years to come.

I owe half of everything to my closest friend throughout college, Shivansh, to whom I am eternally grateful. He has been the best friend and research mate I could have ever found, and has been with me every single step of the way starting from the very first day of college. Without him, I would never have made it through my research work or through college. I cannot imagine how my life would have been without him.

Finally, I want to thank my college group of friends, “Daddycated”. I never could have imagined meeting this many people so similar to me, yet so different. There could not have been a better group of 27 individuals to spend my college years with. Thank you for helping me grow and for growing with me. You all inspire me, and you will always be my family.

Abstract

The human brain is a highly complex network of interconnected neurons exhibiting emergent phenomena. The theory of the brain functioning at a critical state - near a second-order phase transition where its capabilities for memory, learning, and information processing - has gained widespread popularity in recent years. This criticality has often been likened to the critical state observed in the Ising model, which is influenced by a temperature parameter. Neural dysfunction due to neurodegenerative conditions such as Alzheimer's Disease influences the proximity to this critical state. We study the disrupted proximity to criticality of the dysfunctional Alzheimer's brain using a spin-lattice pairwise maximum entropy model where connectivity is inferred from resting-state fMRI data. The closeness to criticality is quantified through the critical temperature, which is derived by analysing the susceptibility of the system. We find an insignificant difference between the two classes, which we attribute to the dependence of susceptibility on spatial dynamics, with the hypothesis that the existence of a spin-glass-like criticality could hinder the sensitivity of this metric. To characterise the nature of brain criticality, we explore the spatial characteristics and temporal correlations of criticality for both normal and Alzheimer's brains. We find a weak distinction in the spatial dynamics between the two classes - the sizes and number of spatial domains formed, as well as the self-averaging behaviour of the system, were not found to vary significantly. However, we notice a stretched exponential form in the temporal relaxation times, which is characteristic of spin-glasses. We find a significant difference between the relaxation behaviour of Alzheimer's and Cognitively Normal subjects. In spin-glass systems, a third phase exists near the phase transition boundary - the spin-glass phase. This phase is characterised by frustration and competing interactions. It allows for the emergence of complex properties such as long-term memory, which are features not found in simple Ising-like criticality. Despite the difference in closeness to criticality, the lack of a significant distinction in the spatial correlation lengths can be attributed to local frustrations, which might not allow the system to reach equilibrium domain distributions. Based on the differences observed between the spatial and temporal correlations, we conclude that the criticality found in the brain is more akin to a spin-glass criticality, which is more sensitive to temporal rather than spatial measures.

Contents

1	Introduction	1
1.1	Overview	1
1.2	fMRI and Alzheimer’s Disease	2
1.3	The Critical State Brain	4
1.4	Statistical Modelling	4
1.5	Criticality in Statistical Models	5
1.6	Motivation	6
1.7	Thesis Outline	6
2	Theory and Related Work	8
2.1	fMRI Studies	8
2.2	Statistical Mechanics and Applications in Neuroscience	10
2.2.1	The Ising Model	10
2.2.2	The Sherrington-Kirkpatrick Model	12
2.3	Criticality	13
2.3.1	Ising Model	13
2.3.2	The Critical State	16
2.3.3	Spin-Glasses	17
2.3.4	Frustration	17
2.3.5	Self-Averageness	19
2.3.6	Ergodicity Breaking	19
2.3.7	The Spin-Glass Phase	20
2.4	The Critical-State Brain	22
2.5	Aspects of Criticality	25
2.5.1	Self-Averaging	25
2.5.2	Domain Formation	26
2.5.3	Signal Relaxation Behaviour	27
2.6	Alzheimer’s Disease	29

2.7	Relevant Literature	30
2.8	Overview	31
3	Investigating Disrupted Criticality in Alzheimer’s through the Pairwise Maximum-Entropy Model	33
3.1	Introduction	33
3.2	Methods	35
3.2.1	Dataset	35
3.2.2	Preprocessing and Parcellation	36
3.2.3	Functional Connectivity	37
3.2.4	Pairwise Maximum-Entropy Model	37
3.2.5	Binarisation	39
3.2.6	Pseudo-likelihood Maximisation	39
3.2.7	Hyperparameter Optimisation	41
3.2.8	Archetype Construction	43
3.2.9	Magnetisation and Susceptibility	44
3.3	Results	45
3.3.1	Reconstruction	45
3.3.2	Magnetization and Susceptibility	47
3.4	Discussion	52
4	Spatial Aspects of Criticality in fMRI	54
4.1	Introduction	54
4.2	Methods	57
4.2.1	Datasets	57
4.2.2	Preprocessing	57
4.2.3	Self-Averaging	58
4.2.3.1	Relative Variance (R_X)	58
4.2.3.2	Generating Systems to Study Self-Averaging	59
4.2.4	Domain Formation	61
4.2.5	Relaxation Times: τ Calculation	63
4.3	Results	64
4.3.1	Self-Averaging	64
4.3.2	Domain Formation	70
4.3.3	Relaxation Times	74
4.4	Discussion	77

5 Conclusion and Future Work	79
-------------------------------------	-----------

Bibliography	84
---------------------	-----------

List of Figures

2.1 Free Energy in an Ising Ferromagnet [22]	15
2.2 Frustration [22]	18
2.3 Free Energy of a Spin-Glass System [22]	21
2.4 Domain Formation near Criticality	27
2.5 Stretched Exponential and Simple Exponential	28
3.1 Reconstruction Accuracy	46
3.2 Variation in Average Magnetization with Temperature	47
3.3 Absolute Average Magnetization vs Temperature along with critical Temperature marked using the dotted-dashed lines	48
3.4 Susceptibility vs T along with critical Temperature (marked using the dotted-dashed lines)	50
4.1 Visualisation of Subsystems Generated from the Primary System for R_X calculation.	58
4.2 Generating subsystems from fMRI	60
4.3 R_X vs N after averaging in log-space for $t = 80$	65
4.4 $\log(R_X)$ vs $\log(N)$ averaged over subjects for $t = 80$	67
4.5 Distributions of α_{sub}	69
4.6 Domain Size Distributions	71
4.7 Number of Domains Distributions	71
4.8 Volume of Spins within Domains of Varying Sizes	72
4.9 Mean Lifetime of Largest Domain	73
4.10 Representative exponential and stretched exponential fits on ACF $\rho(t)$	74
4.11 Distributions of the stretched exponential parameters over all voxels for all subjects	75
4.12 Distributions of the stretched exponential parameters across voxels averaged over subjects	76

List of Tables

3.1	Dataset Information	36
3.2	Parameters for Gradient Ascent on J	43
3.3	Simulation Parameters for M and χ Calculation	45
3.4	Magnetisation and Susceptibility Results	51
4.1	Parameters to Generate Systems for R_X Analysis	61
4.2	Results of R_X Fits	68

Chapter 1

Introduction

1.1 Overview

The brain is an intricate network that consists of numerous interconnected components working together to exhibit highly complex dynamics. The theory that the brain operates at a “critical state” has gained considerable popularity in recent years. The critical state is where a system is poised at a phase transition of the second order. In this state, information processing is at an optimal level, allowing for rapid responses to stimuli, the system has the capacity to adapt to external conditions efficiently, and small fluctuations can have disproportionately large effects.

The critical state or critical point is a concept that emerges from statistical physics. The critical state in the brain has typically been compared to the system being at the critical temperature of an Ising model, which is the phase transition boundary between its paramagnetic and ferromagnetic states. Neural dysfunction often alters the proximity to this critical state, resulting in sub-optimal brain functioning. Alzheimer’s Disease is one such neurodegenerative disorder in which the brain exhibits abnormal dynamics. Such disorders can be studied using statistical modelling of the brain. Since the concept of criticality akin to the Ising model is invoked, a model comprised of a system of spins (known as a spin-lattice model) can be employed to emulate the brain and investigate criticality. Empirical data can be used as the basis for statistical modelling owing to advances in imaging technology, which have enabled us to capture neuronal activity in real-time. Functional magnetic resonance imaging (fMRI) is one such valuable tool that allows us to capture activity in the brain. It has seen widespread use in recent years and is often used to study the brain’s response to stimulus and to study neural diseases and disorders.

In this thesis, we first investigate the proximity to criticality of Alzheimer’s Disease-afflicted (AD) and Cognitively Normal (CN) subjects through resting-state fMRI data to study the relation between disrupted criticality and connectivity. We use a pairwise maximum-entropy model (pMEM) to infer neuronal connectivity, which is a spin-lattice system where the connection strength between spins is derived through likelihood-maximisation techniques. Then, we study the susceptibility of the system at

various temperatures to determine its critical point, which can inform us about its relative proximity to criticality for the AD and CN groups. While significant contrasts were expected between the two classes, we noticed only a weak distinction, leading us to hypothesise that the type of criticality itself may be more complex than just being at a paramagnetic-ferromagnetic transition, in which case susceptibility would be too superficial of an order parameter to study this data. This motivates us to investigate further the type of phase transition in the brain's critical state by studying the spatial and temporal aspects of criticality, where we hope to identify signatures of the type of criticality.

At criticality, numerous spatial metrics - such as the correlation length, susceptibility, and spin-spin correlations - tend to show power-law behaviour. We investigate these aspects of criticality to determine the proximity to the critical state of the brain in general and the distinction between AD and CN subjects. We hypothesise that the criticality found in the brain might be more complex than a simple Ising-like paramagnetic-ferromagnetic phase transition. A more elaborate version of the Ising model with long-range interactions - the Sherrington-Kirkpatrick model - is used to simulate spin-glass systems which can be taken to be analogous to the brain. In such systems, a third phase exists - the spin-glass phase, which is dominated by frustration and disorder. Spin-glass systems are more sensitive to temporal measures rather than spatial measures, compared to a simple Ising system where both spatial and temporal measures are significantly expected to diverge as we approach criticality. To this end, we further investigate the temporal aspects of criticality in the case of AD and CN subjects. With the knowledge that AD and CN differ in their proximity to the critical state, ascertaining the distinction between the two classes in these measures will allow us to determine the type of phase transition. This thesis investigates the distinctions in the spatial aspects followed by the temporal aspects of criticality between AD and CN subjects in order to determine the type of criticality found in the human brain.

1.2 fMRI and Alzheimer's Disease

The scientific study of the brain and its related components is termed as neuroscience. One of the key goals of neuroscience is to understand the underlying factors that enable neural functioning. This is done by studying the brain's structure and function and furthering this understanding through modelling it. With the rapid advancement of neural imaging technology in the past few years, neuroscience has made great strides in unravelling the intricate functioning of the human brain by studying it.

Functional Magnetic Resonance Imaging or functional MRI (or fMRI for short) is one such imaging technique used to measure neural activity by detecting the changes in oxygenation and blood flow that occur as a consequence of activity. This technique takes advantage of the coupling between blood flow and neuronal activity.

The primary principle of fMRI is Blood Oxygen Level-Dependent (BOLD) imaging. This technique relies on the fact that haemoglobin is diamagnetic when oxygenated but paramagnetic when deoxygenated. When a certain area of the brain is in use, more blood flows into it in order to facilitate the increased demand for oxygen. By measuring the magnetisation of haemoglobin and the amount of oxygenation in this blood, the amount of neuronal activation in the area can be computed. The change in the signal resulting from neuronal activity is known as the “haemodynamic response”. The haemodynamic response typically lags behind actual activity by a couple of seconds due to the time taken by the blood flow to respond to the oxygen needs of the brain.

Since its development in 1990, fMRI has been used extensively for studying tasks of cognition. Being able to study neuronal activity has enabled us to understand the workings of the brain further and come up with more accurate and improved models of cognition. fMRI is especially useful as it allows us to image the entire brain instead of having to select regions or place electrodes at exact locations (such as in electroencephalography). This whole brain imaging allows us to study the evolution of various networks of the brain and reactions to stimuli. This line of methodology has resulted in significant advancements in our understanding of behaviour, language processing, and motor control. This thesis uses fMRI as a tool to investigate neuronal activity in healthy and dysfunctional brains to gain greater insight into the critical state functioning of the human brain.

Studying the intricacies of brain function and dysfunction is of great importance for the advancement of our understanding of biology and medicine. Neurological disorders not only have a profound impact on the lives of millions of people but also pose significant challenges to society. Among these, Alzheimer’s Disease stands out not only due to its prevalence but also due to the devastating effects it has on families and society at large. Alzheimer’s Disease (or AD for short) affects millions of people worldwide, with numbers projected to rise as the average age of the world population increases. AD places great stress on society, impacting healthcare systems, caregivers and economies at large. Therefore, there is an urgent need to deepen our understanding of the disease in order to develop more effective interventions, enable earlier detection and develop preventive strategies.

By studying neural dynamics, we can make great progress in unravelling the mechanisms underlying Alzheimer’s. In Alzheimer’s, there is progressive neurodegeneration, which causes significantly altered neuronal connectivity and brain function, resulting in symptoms such as impaired memory, cognitive decline, and a plethora of behavioural and psychological symptoms. Examining the fundamental workings of the brain in the case of neurodegenerative diseases such as Alzheimer’s can lead to profound insights into how disruptions occur and how they lead to cognitive impairment. Understanding the effect of the dysfunctional aspects of the Alzheimer’s brain on closeness to criticality can further pave the way for earlier intervention, identifying potential biomarkers and more effective treatments to alleviate the profound impact of this disease.

1.3 The Critical State Brain

The human brain demonstrates a wide range of phenomena that require a quantitative understanding of its underlying principles. Concepts from statistical mechanics offer a valuable structure for comprehending the behaviour of complex systems like the brain. By employing the framework of statistical mechanics, we can uncover valuable insights into the brain's dynamics, emergent properties and information-processing capabilities. The brain is a complex system with an enormous number of interacting parts. These parts exhibit non-linearity and emergent collective behaviour, which cannot simply be attributed to a sum of their functions. This kind of behaviour has been shown to be akin to models of criticality near a phase transition often found in statistical physics, such as the Ising model.

As a system approaches criticality, its behaviour undergoes a rapid and discontinuous change. At this state, interesting properties of the system, such as scale-invariance, increased susceptibility and oscillatory patterns arise. Across varying length and time scales, similar behaviour and trends are observed. The system is extremely sensitive to stimuli in this state due to the existence of long-range correlations across varying scales. At the critical state, the observed patterns of fluctuations exhibit a certain degree of organisation. These properties enable the system to be highly adaptable, adept at information processing, and exhibit emergent behaviour. Critical systems tend to exhibit universal scaling laws that are independent of the system themselves, allowing them to be highly generalisable to various domains.

A brain that operates in a critical state has long-range correlations and minuscule fluctuations that can bring about changes on a global level in neuronal activity patterns. These qualities make it a system that is extremely efficient in learning and information-processing and enables it to perform complex cognitive functions. Owing to these properties, investigating the brain as a critical state system is highly beneficial as it provides a comprehensive framework to study its functioning.

1.4 Statistical Modelling

A powerful class of statistical physics models that are often used in the study of neuronal dynamics is based on pairwise interactions. These models allow the analysis of collective behaviours and emergent patterns by capturing the intricacies of interactions between individual components of the brain. Statistical models such as the Ising model allow us to understand critical behaviour within the brain by transferring over well-studied concepts from statistical mechanics. The collective behaviour of neuronal populations can be analysed using this model, leading to a better understanding of the origin of global patterns from local interactions. The pairwise maximum-entropy model is a variant of the Ising model wherein connectivity is inferred from empirical data and can be employed to generate representations of neural connectivity by encapsulating the latent statistical dependencies among regions. By employing models

such as the Ising model and the pairwise maximum-entropy model, we can gain insight into information processing, synchronisation, and network dynamics and assess how alterations in the complex patterns of connectivity in disorders such as Alzheimer's can affect the critical state functioning of the brain.

Through the use of the Pairwise Maximum-Entropy Model (pMEM), we establish a base to study criticality within the brain. fMRI data can be modelled as a spin-lattice system, with each Region of Interest (RoI) being modelled as a spin. Inferring spin-lattice connectivity from empirical data through such a model then allows us to simulate systems at different temperatures. In Ising-like systems, criticality is characterised by the temperature parameter, which defines the phase boundary. At this phase boundary, the susceptibility of the system is maximised. Hence, the critical temperature (T_c) of a spin-lattice system with defined connectivity can be established by simulating the system at various temperatures. This allows us to determine the T_c of the Alzheimer's and Cognitively Normal classes separately, enabling us to then determine the relative proximity to criticality of the dysfunctional brain by comparing it to the control case.

1.5 Criticality in Statistical Models

Criticality in the Ising model is defined by a phase transition boundary between the ferromagnetic and paramagnetic phases. In the ferromagnetic phase, all the spins are aligned due to conforming spins, resulting in an aligned net magnetisation. In the paramagnetic phase, randomness within the system due to high temperature dominates, and there is no order in the alignment of spins, resulting in near-zero net magnetisation. Typically, when the brain is studied using statistical modelling, there is a control parameter in the form of temperature, and the critical behaviour is established through this phase boundary between ferromagnetic and paramagnetic phases, as seen in the Ising model. We refer to this criticality with the transition between these two phases as "Ising criticality".

There is another type of phase that could arise in more complex variants of the Ising model such as the Sherrington-Kirkpatrick (SK) model -this model allows for interactions between any two spins in the lattice, and not just between nearest neighbours like in the simple Ising model. This third type of phase is often found in a class of magnetic materials known as spin-glasses, thereby giving the phase the name "spin-glass phase". Spin-glass systems have quenched disorder where the connectivity between spins is not uniform like in the simple Ising case but is random. This allows the system to enter states which are marked by frustration and competing interactions. The phase comprising these states is known as the spin-glass phase. In this phase, spins struggle to align together despite being at low temperatures. When this phase exists, there are numerous critical transitions in the phase diagram between all combinations of the three phases - ferromagnetic, spin-glass, and paramagnetic. If the phase transition observed involves the spin-glass phase, we refer to this type of criticality as "spin-glass criticality".

1.6 Motivation

Understanding the correlation between disrupted proximity to criticality due to neurodegeneration and neural connectivity can give us valuable insight into the functioning of the brain. We first applied conventional statistical modelling to study the critical behaviour of Alzheimer's Disease-afflicted subjects. Upon finding results that did not display the expected significant distinctions due to the disrupted critical state functioning of the AD, we further investigated the nature of criticality - exploring the possibility that susceptibility, which is typically used to study the Ising phase-transition, may not be robust enough to capture the critical dynamics of the brain. The presence of a spin-glass phase may require a more intricate measure. There is a need to further study the spatial growth dynamics in order to find the underlying cause for the deficient distinctions found.

We hypothesise that there is a possibility of the brain being more akin to a system with spin-glass-like criticality than it is to Ising-like criticality which could affect the sensitivity of innately spatial metrics such as susceptibility. To this end, we set out to investigate the spatial aspects of the system that are known to exhibit certain behaviours at criticality in order to confirm closeness to the phase boundary of the brain in general. Here, we study the spatial correlations by studying the domains formed and self-averaging behaviour within the system. Even if there are no distinctions found between the two cases, this study will allow us to ascertain whether the brain truly is working close to a critical state. Upon determining the proximity to the phase transition, we further study the temporal aspects to determine whether the disruptions due to AD indeed do not affect critical functioning, or if in reality there is a distinction that evades detection by spatial measures but is sensitive to temporal measures. Understanding the distinctions found in the spatial correlations and the self-averaging behaviour, and additionally, the temporal measures between the AD and CN classes can give us a better idea of the type of criticality in the human brain as we will be able to ascertain the type of phase transition given the unique signatures we identify.

1.7 Thesis Outline

The thesis starts off by introducing and elaborating on the necessary theory and other relevant literature in Chapter 2. This chapter covers the required knowledge to understand the rest of the thesis. We first explore the background of fMRI and the current state of the field, exploring applications of fMRI. We proceed to discuss the necessary theory behind the criticality hypothesis and select studies leveraging the theory in neuroscience. The statistical mechanics concepts and models used in the thesis - the Ising model and SK model - along with their types of critical behaviours and phases are introduced and modelled formally. Following this, there is a detailed discussion on the spatial aspects of criticality that are investigated in this thesis - domain formation and self-averaging - as well as a brief discussion of

temporal correlations. Then, we discuss neural dysfunction in Alzheimer's Disease and how its study can help us understand the brain better. This section aims to be a comprehensive guide for approaching neuroscience through the lens of statistical mechanics and serve as a possible starting point for physicists to explore neuroscience.

In Chapter 3, we delve into the use of the Pairwise Maximum-Entropy Model to study Alzheimer's. It introduces the formal modelling of it, as well as inference of connectivity and determination of critical temperature. The results from this study are then discussed. This chapter illustrates the typical method in which statistical mechanics models are employed to study criticality in the brain.

Chapter 4 forms the core of this thesis. This chapter serves to investigate our hypothesis that the criticality in the human brain is more akin to a spin-glass system than a simple Ising system. In this chapter, we introduce relevant concepts and the formulation of the data in order to study its spatial and temporal behaviour with respect to criticality. The study of phase-ordering, spatial correlations, and self-averaging is discussed. Then, the temporal aspects are also explored to substantiate the hypothesis. Finally, the chapter concludes with a compilation of the results and their interpretation to make inferences regarding the type of criticality that the brain exhibits.

We finish the thesis with a final chapter discussing conclusions that can be drawn from these investigations and discuss future work that can build upon this thesis.

Chapter 2

Theory and Related Work

The fields of neuroscience and statistical mechanics both offer a wide variety of concepts and methods that can be used to further our understanding of the human brain. This chapter examines the theory necessary to understand the background of our study and discusses the application of these concepts in the context of our thesis in detail.

2.1 fMRI Studies

Neurological studies use numerous techniques to collect empirical data and investigate the brain. One of the primary methods that has emerged in recent years is fMRI. Functional Magnetic Resonance Imaging, or fMRI for short, has revolutionised our understanding of the brain and the way we study it. Advancements in fMRI techniques have contributed significantly to enhancing our ability to study brain function [82, 38, 56]. High-resolution fMRI has provided unprecedented spatial resolution and allowed us to now be able to identify fine-scale functional networks and subcortical structures in the magnitude of millimetres [18]. Multimodal imaging, such as combining fMRI studies with anatomical techniques such as diffusion tensor imaging (DTI) or other functional techniques such as electroencephalography (EEG), has enabled highly comprehensive studies of the human brain [34, 37].

Task-based fMRI studies have greatly contributed to our understanding of the brain areas responsible for different cognitive tasks. By examining neural activity during tasks such as reading, listening and speaking, we have been able to identify key regions of the brain responsible for speech processing [52, 45]. For example, the left inferior frontal gyrus, including Broca's area, has been widely associated with being responsible for language production while the superior temporal gyrus, which includes the Wernicke's area, has been associated with language comprehension [26]. Not only have fMRI studies confirmed the areas traditionally associated with language, but they have brought to light more regions of the brain that might be responsible for syntactic processing, semantic retrieval, and discourse comprehension [80]. By studying the brain during activities such as memory encoding, consolidation, and retrieval

phases, researchers have also been able to identify the areas responsible for memory and learning - the hippocampus and surrounding medial temporal lobe have been linked with episodic memory formation while working memory has been attributed to the pre-frontal cortex and parietal regions [79]. fMRI studies have also contributed to our understanding of attentional networks and their interplay with higher cognitive processes by helping identify the role of pre-frontal and parietal cortex in selective attention, cognitive control, and decision-making [95, 45]. Functional magnetic resonance imaging studies have revolutionised the field of cognitive neuroscience by providing valuable insights into the neural substrates underlying various cognitive tasks and hold great potential for clinical applications.

fMRI plays a crucial role in studying the advancement of diseases or disorders that alter neural function, such as Alzheimer's [21], Parkinson's [91] or Autism [72]. Extensive studies have been performed using fMRI to study the advancement and effects of these diseases on brain function, helping identify network disruptions and altered connectivity [73, 39, 84]. Advancements in machine learning (ML) have also augmented the power of fMRI by providing a framework for early detection, classification, and monitoring of neurodegenerative diseases or disorders on a scale beyond the human capacity for direct study. ML techniques are capable of detecting subtle differences which are not comprehensible to the human eye and show great promise when working with large sets of data [70]. They have been used in the identification of disorders such as Autism Spectrum Disorder (ASD), Alzheimer's Disease (AD), and Schizophrenia [10, 54]. ML techniques use fMRI data from a wide range of tasks such as listening, reading, or cognitive control tasks and have been useful with resting-state fMRI data as well [49]. Since these techniques do not require manual feature extraction, they can be used without the requirement of domain expertise and can mitigate human error.

fMRI studies have contributed to the understanding of neurological conditions such as epilepsy and stroke by mapping functional reorganisation and identifying regions critical for recovery through ML techniques [75]. In neurodegenerative diseases such as Parkinson's, fMRI has helped to identify characteristic patterns of cortical or subcortical atrophy and highlight the regions primarily affected by the disease processes, showing altered activity in regions responsible for emotion processing, reward circuitry, and control [91]. Advancements in fMRI-based understanding of disease-related dysfunctions have shown significant promise to guide target therapies and interventions. For example, fMRI has enabled targeted rehabilitation strategies by making possible the identification of regions showing potential for neural recovery following a stroke or traumatic brain injury [48, 98]. Resting-state fMRI (rs-fMRI) is a form of fMRI that is typically used to study the functioning of the brain in the absence of any stimulus, i.e., at rest. rs-fMRI has revolutionised our understanding of resting brain activity by identifying spontaneous fluctuations and activity patterns that occur in the BOLD signal [51, 13]. They have helped identify Resting-State Networks (RSNs), such as the Default Mode Network (DMN), responsible for mind-wandering and self-referential thoughts, providing insight into the functional organisation of the

brain at rest. By examining the amplitude, frequency, and spatial patterns of spontaneous fluctuations, researchers have gained valuable insights into spontaneous activity and studied the role of resting-state neuronal dynamics in cognitive functions, brain plasticity, and information processing. The analysis of these dynamics has also led to the emergence of the concept of brain criticality, where the brain operates with a balance between stability and flexibility, allowing for efficient information processing and adaptability and enabling complex cognition [17, 90, 20].

2.2 Statistical Mechanics and Applications in Neuroscience

The field of statistical mechanics offers an arsenal of concepts and frameworks to study neural function. Statistical mechanics applies statistical methods and probability theory to systems of microscopic elements at a large scale to study their collective behaviour at a macroscopic level. It is used to study the behaviour that arises from the interaction of sizeable systems of minute entities. Its applications are found in every field, ranging from biology and chemistry to finance and social sciences [97, 6, 14, 33]. It provides the framework to describe and predict the collective behaviour of large ensembles, bridging the gap between the microscopic and macroscopic scales. The brain is one such ensemble system comprising an enormous number of interacting neurons. Statistical mechanics thus offers an expansive toolkit to study the brain by treating it as a complex statistical system. By analysing the behaviour of the brain through the lens of statistical mechanics, we can gain insight into the emergent behaviour and underlying dynamics of neuronal networks.

2.2.1 The Ising Model

The Ising model is a mathematical model describing the behaviour of interacting particles. It was proposed in 1925 as a model of ferromagnetism in statistical mechanics by Ernst Ising. Since then, the model has evolved and found applications in a wide range of domains [12, 19, 65]. The model consists of a lattice, usually two- or three-dimensional, with each lattice site containing a spin. A spin can take values of up (+1) or down (-1). The spins in the Ising model only interact with their nearest neighbours in the lattice, i.e., spins that are exactly adjacent to them in the lattice. The total energy of the model is determined by interactions between the spins. Spins that are oriented in the same direction contribute to lesser energy than those that are oriented in opposite directions. A common mathematical formulation of the energy of the simple Ising model is given by the Hamiltonian:

$$H(\sigma) = - \sum_{\langle i,j \rangle} J_{ij} \sigma_i \sigma_j - \sum_i h_i \sigma_i \quad (2.1)$$

Here, J denotes the connectivity strengths, with J_{ij} indicating the connectivity strengths between sites i and j . The summation over $\langle i, j \rangle$ denotes the summation over the nearest neighbours.

$\sigma = \{\sigma_i\} \forall i \in \{1, \dots, N\}$ denotes the lattice in the Ising model, with N being the total number of spins σ_i representing the site i (without loss of generality in 2D or 3D). h_i denotes the external field acting at site i .

The configuration probability of a certain state σ can be given by:

$$P_\beta(\sigma) = \frac{e^{-\beta H(\sigma)}}{Z_\beta} \quad (2.2)$$

where the $\beta = (k_B T)^{-1}$ is the inverse temperature with temperature T and Boltzmann constant k_B , and the normalisation constant

$$Z_\beta = \sum_{\sigma} e^{-\beta H(\sigma)} \quad (2.3)$$

is the partition function of the system.

The Ising model can be studied using various methods such as Monte Carlo simulations, mean-field theory (especially in the case of greater than three dimensions), and exact solutions [50, 7]. There are numerous properties defined in the Ising model, such as magnetisation, susceptibility and specific heat, which can be studied at different temperatures.

Often, the Ising model is further simplified by setting the external field $h = 0$, and by setting the coupling values equal to a positive constant, $J_{ij} = J$. This gives us what is known as the “ferromagnetic Ising model” with zero external field [65]. This leads to the Hamiltonian:

$$H(\sigma) = -J \sum_{\langle i,j \rangle} \sigma_i \sigma_j \quad (2.4)$$

This is the simplest form of the model and is exactly solvable in 1-D and 2-D [7]. Any form of the model that is more complicated than this version (non-constant J , for example) requires the use of approximate methods, one of the most common ones being Mean-Field Theory. This variant of the Ising model serves as a baseline to qualitatively understand the behaviour of magnetic systems while also finding a variety of other applications.

A key aspect of the Ising model is its ability to model phase transitions and critical phenomena. As the temperature increases, the system undergoes a transition from order to disorder, passing through a critical point at the “critical temperature” (T_c). This critical state is classified by its critical exponents which govern the divergence of certain thermodynamic variables at this state. By studying the Ising model, researchers gain valuable insights into the nature of phase transitions, critical phenomena, and universality. The Ising model serves as a base for simplifying and understanding complex systems and phenomena such as ferromagnetism, superconductivity, and even social behaviour, which are observed in nature. It was first introduced as a simplified model of the behaviour of ferromagnetic materials, as Ernst Ising was trying to understand how the magnetic properties of a material change with temperature and

how a magnetic phase transition could come about. Since then, the Ising model has found widespread use in various fields: in condensed matter physics to describe spin-glasses, magnetic materials and phase transitions in general; in social sciences to describe opinion dynamics, voter behaviour, and social networks; and even in computer science to solve optimisation problems and simulate neural networks [86, 106, 93, 53].

2.2.2 The Sherrington-Kirkpatrick Model

Ising models, in general, can be defined by their interactions and the external perturbation applied to the model. The matrix J , which defines these interactions, is largely responsible for the dynamics and the analytical behaviour of the system. The model can be fully defined by the distribution $P(J_{ij})$ in the absence of h .

The conventional Ising model (as described by Eq. 2.1) only considers interactions between nearest neighbours. This means that each spin only interacts with four other spins in a 2-D model or six other spins in a 3-D model. In this model, $J_{ij} = J$ if i and j are neighbours and $J_{ij} = 0$ otherwise. Although this simplification allows for wider analytical study and can be studied without relying on numerical or approximate solutions, it abstracts away an aspect found in many systems: long-range interactions.

The Sherrington-Kirkpatrick model (or SK model for short), introduced by David Sherrington and Scott Kirkpatrick in 1975, is a variant of the Ising model which allows for the modelling of more complex behaviour [81]. The SK model allows for interactions between any two spins in the lattice with their interaction strength defined by the coupling matrix J . This increased complexity makes the SK model harder to study but also allows for the modelling of complex systems. The Hamiltonian of this model can be written as:

$$H(\sigma) = - \sum_{i < j} J_{ij} \sigma_i \sigma_j - \sum_i h_i \sigma_i \quad (2.5)$$

which is very similar to Eq. 2.1 but allows for long-range interactions.

In this model, the interaction strengths J_{ij} are selected from a Normal distribution $P(J_{ij}) \sim \exp(-N J_{ij}^2 / J^2)$ where J is the characteristic strength of the interaction. The SK model is analytically solvable only using the mean-field approximation as the nature of its space of states is quite complex, given that the connectivity J is random between all spin pairs. There is a voluminous literature on the subject as it has found numerous applications. The SK model is used in many cases where there is a need for modelling long-range spin interactions.

The advantage of the SK model over the conventional Ising model is its ability to integrate long-range interactions and randomness into the model. The modelling of the interactions in the SK model allows us to draw a more direct analogy with the brain, with neurons or brain regions being akin to spin sites. This

model also enables the existence of a third phase - the spin-glass phase - due to the complex dynamics of the model. As we will discuss later, the existence of the spin-glass phase is very important due to the nature of its dynamics differing significantly from the other phases. The SK model was selected for our study since it strikes the correct balance between accuracy and simplification.

This model has found significant applications in the field of neuroscience as well since it allows for the study of collective dynamics and information processing within neural systems. It is often used to model neuronal activity, with each neuron being considered a spin. This allows for the study of synchronisation, information encoding, and phase transitions.

An application of the SK model termed the Pairwise-Maximum Entropy Model (or pMEM), has also been used to infer connectivity between neurons from experimental data. Given a certain time-series of spins, this model can estimate the connectivity between the lattice sites using methods such as maximum likelihood estimation (MLE) and provides a framework for inferring connectivity [89]. This has found various uses, such as modelling neuronal activity as a spin-lattice inferring its connectivity. It has also found use in predicting the response to external stimuli. By treating stimulus as an additional input parameter to the model, typically in the field term, encoding and sensory information processing by neural populations can be studied. This approach has been used to predict the responses of neurons in sensory systems, such as the visual cortex, auditory system, and olfactory system [102, 76].

2.3 Criticality

Criticality is a feature exhibited by statistical models. The critical state is a state poised at a second-order phase transition where interesting phenomena, such as scale-invariance, long-range correlations, and increased susceptibility - are observed. The concept of criticality is extremely generalisable as numerous models tend to display similar behaviour at the critical state. In this section, we explore the emergence of criticality in statistical models and understand its qualitative nature.

2.3.1 Ising Model

Let us consider the Ising model in more than two dimensions. In this case, mean-field theory is applied since an exact analytical solution is not possible [22]. The Bragg-Williams mean-field approximation is a method to simplify the effect of all other spins on a particular spin site, i.e., to simplify the effect of all $j \neq i$ on the spin i . The assumption is that the distribution function in the equilibrium state is a factorisation of the products of the independent distribution functions for each site:

$$P_\beta(\sigma) = \frac{1}{Z} \exp(-\beta H(\sigma)) \simeq \prod_i P_i(\sigma_i) \quad (2.6)$$

leading to the normalised site distribution functions being taken as:

$$P_i(\sigma_i) = \frac{1 + m_i}{2} \delta(\sigma_i - 1) + \frac{1 - m_i}{2} \delta(\sigma_i + 1) \quad (2.7)$$

The average magnetisation per site of the system can then be derived from the probability function to be:

$$m_i = \langle \sigma_i \rangle \quad (2.8)$$

Using the mean-field approximation, the entropy can be computed as:

$$\begin{aligned} S &= - \langle \log(P[\sigma]) \rangle \simeq - \langle \log\left(\prod_i P_i[\sigma_i]\right) \rangle \\ &= - \sum_i \left[\frac{1 + m_i}{2} \log\left(\frac{1 + m_i}{2}\right) + \frac{1 - m_i}{2} \log\left(\frac{1 - m_i}{2}\right) \right] \end{aligned} \quad (2.9)$$

Then, we can derive the free energy $F = E - TS$ where $T = 1/\beta$ as:

$$\begin{aligned} F &= \left(- \sum_{\langle i,j \rangle} J_{ij} m_i m_j - h \sum_i m_i \right) \\ &+ T \sum_i \left[\frac{1 + m_i}{2} \log\left(\frac{1 + m_i}{2}\right) + \frac{1 - m_i}{2} \log\left(\frac{1 - m_i}{2}\right) \right] \end{aligned} \quad (2.10)$$

The system wants to minimise its free energy, and the condition for that would be $\frac{\delta F}{\delta m_i} = 0$:

$$\begin{aligned} (-2 \sum_j J_{ij} - h) + T \left(\log\left[\frac{1 + m_i}{2}\right] - \log\left[\frac{1 - m_i}{2}\right] \right) &= 0 \\ (-2 \sum_j J_{ij} - h) + (T \tanh^{-1}(m_i)) &= 0 \end{aligned} \quad (2.11)$$

$$m_i = \tanh \left[\beta \left(2 \sum_j J_{ij} m_j + h \right) \right] \quad (2.12)$$

Let us take the case of the simple ferromagnetic Ising system in the 3-D case with no external field. It would then have six nearest-neighbour interactions for each spin. Since the system is homogeneous, it is reasonable to expect that the magnetisation per site $m_i = m$ is some constant parameter. m is, hence, a parameter that defines the state of the system. Then, for some site i , this approximation leads to:

$$\sum_j J_{ij} m_j = 6Jm \quad (2.13)$$

Then, the magnetisation evaluates to:

$$m = \tanh [12\beta Jm] \quad (2.14)$$

Since we want the minimum of the free energy, we can further evaluate the condition $\frac{\delta^2 F}{\delta m^2} > 0$ from the Eq. 2.11 to the constraint:

$$\frac{1}{1 - m^2} > 12\beta J \quad (2.15)$$

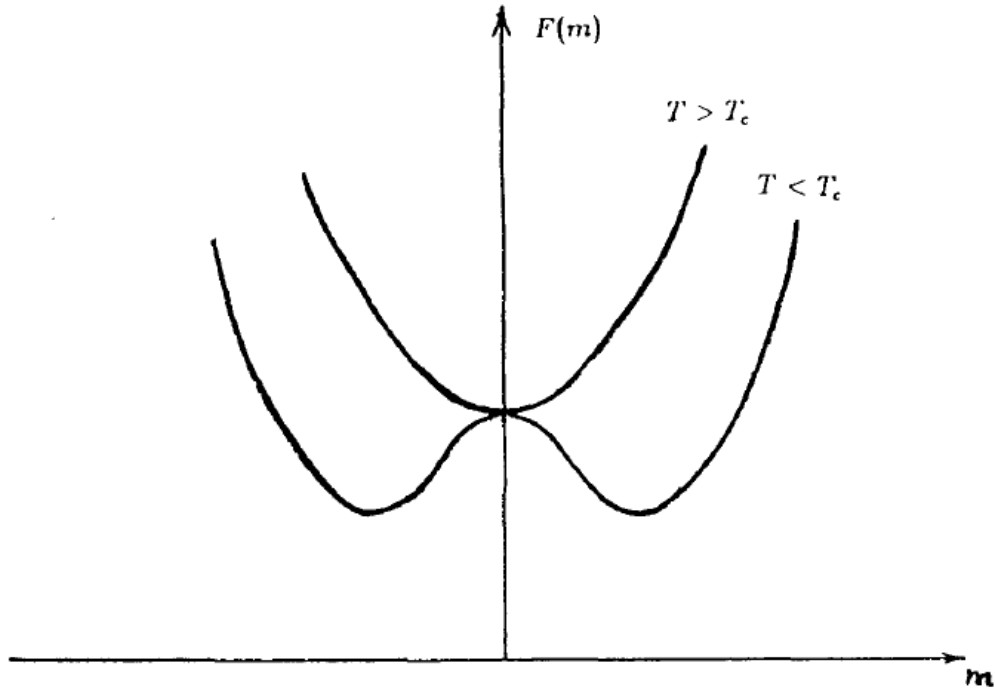


Figure 2.1: Free Energy in an Ising Ferromagnet [22]

From Eq. 2.15, it can then be shown that in the case where the external field $h = 0$, we achieve the minimum of the free energy at $m = 0$ when $T > T_c$. But, when $T < T_c$, $m = 0$ becomes the maximum of the free energy, and the minimum is instead obtained at the non-zero magnetisation values $m = \pm m(T)$. Near T_c , the magnetisation $m(T)$ is small and can be expanded in powers of $m(T)$. In this case, the magnetisation can then be shown to be:

$$\begin{aligned} m(T) &= \text{const} * \tau^{1/2} \\ &= \text{const} * \left(1 - \frac{T}{T_c}\right)^{1/2} \ll 1 \end{aligned} \quad (2.16)$$

The behaviour of the system spontaneously changes as the system moves from one side of T_c to the other and changes the fundamental nature of the free-energy curve. This is known as a phase transition of the second order. The qualitative shape of the curve when the system is on either side of T_c is visualised in Fig. 2.1. The two ground states that appear in the case of $T < T_c$ now differ by their sign of the

average spin magnetisation. The symmetry with respect to the global change of signs of the spins is broken, and there are two ground states at $T < T_c$ instead of just one at $T > T_c$. This phenomenon is known as “spontaneous symmetry breaking”.

The free energy of the system itself is proportional to the volume of system N , and hence, the barrier separating these two states is also proportional to it. Hence, the value of $m(T)$ itself is proportional to the volume of the system. In statistical mechanics, we often study the case of large or infinite systems, i.e., $N \rightarrow \infty$. In this case, the barrier separating the two states at $T < T_c$ will also be infinite.

2.3.2 The Critical State

At the temperature $T = T_c$, the system displays unique behaviour. It is poised at a phase transition between two phases that completely differ in their behaviour. This temperature T_c is known as the “critical temperature”, and the state at which the system is at this temperature is known as the “critical state”. The critical state is, therefore, an important state to study.

As we get closer to the critical state, the behaviour of the system changes rapidly. One such change in behaviour occurs in the correlation functions near the critical state. Correlation functions characterise the correlations between different spins of the system in both spatial and temporal aspects. Near criticality, these functions tend to display power-law or scale-invariant behaviour, meaning that they seem to show similar behaviour at all the scales studied. This is also closely related to self-similarity and the emergence of fractals. This signifies the presence of interactions across large ranges both over time (as the system evolves) and space (across the entire lattice). These power-laws can be characterised using critical exponents and can reveal meaningful information about the emergence of long-range order.

The behaviour of order parameters when in a critical state is also interesting. Quantities that describe how the system breaks its symmetry are known as order parameters. In the Ising model, the key order parameter is magnetisation (discussed above). Close to the critical state, order parameters go through a phase transition and also tend to demonstrate power-law behaviour. Studying such order parameters offers valuable insights into the characteristics of the phase transition and the emergence of spontaneous magnetisation.

Additionally, at this stage, the vulnerability or responsiveness of the system to an external field - known as susceptibility (represented by χ) - is maximised. In the vicinity of T_c , susceptibility displays a peak or divergence following a power-law behaviour and can be characterised by a critical exponent. This enables the system to be extremely responsive to external stimuli at this state and allows for rapid transmission throughout the system from perturbations.

Another interesting thing that happens at the critical state is the emergence of collective behaviour. In this state, the behaviour that occurs cannot simply be equated to the sum of its parts, and this is strongly linked to the long-range order that occurs close to criticality. Seemingly insignificant connections could

play a great role when it comes to the critical state and vice versa. This is a very important property that allows this model of criticality to be generalised to various domains and apply these concepts in order to study emergent behaviour. This gives rise to the concept of universality - the phenomenon where these concepts have been applied in widely varied domains, and the existence of criticality and even sharing of critical exponents has been observed. Thus, the idea of the critical state and criticality has found widespread application in a multitude of different problems.

2.3.3 Spin-Glasses

Criticality can vary widely between different models with differing connectivity types and strengths. In the previous sections, we have explored criticality in the ferromagnetic Ising model, which is one of the simplest models. The methodology applied to study this model can be repeated and extended to many such variants of the Ising model that are used to model a wide variety of phenomena. An interesting case to study is that of spin-glasses, which display rather unique behaviour.

Spin-glasses are a form of magnetic substances in which the interaction between each pair can either be ferromagnetic ($J_{ij} > 0$) or anti-ferromagnetic ($J_{ij} < 0$). The exact value of the interaction strength is random. Spin-glasses are characterised by competing interactions and “disorder”. The name itself comes from an analogy drawn between magnets and solids. The atoms in conventional glasses (amorphous solids) are typically randomly positioned in comparison with crystalline solids, which have a very ordered structure. Similarly, in contrast to simple Ising ferromagnets, spin-glasses lack regular magnetic order and have random or disordered interaction strengths between spins. Taking this into account, it is easy to see how the Sherrington-Kirkpatrick model (introduced in Section 2.2.2) is a popular model for spin-glass systems as it accounts for connections of varying strengths and long-range interactions.

2.3.4 Frustration

The main way in which the dynamics within spin-glasses differ is through frustration, which occurs due to the randomness in the interaction strengths. The random interaction strengths are said to be “quenched” for a given system. This means that they maintain fixed values and do not change over time. This causes the system to experience competing interactions.

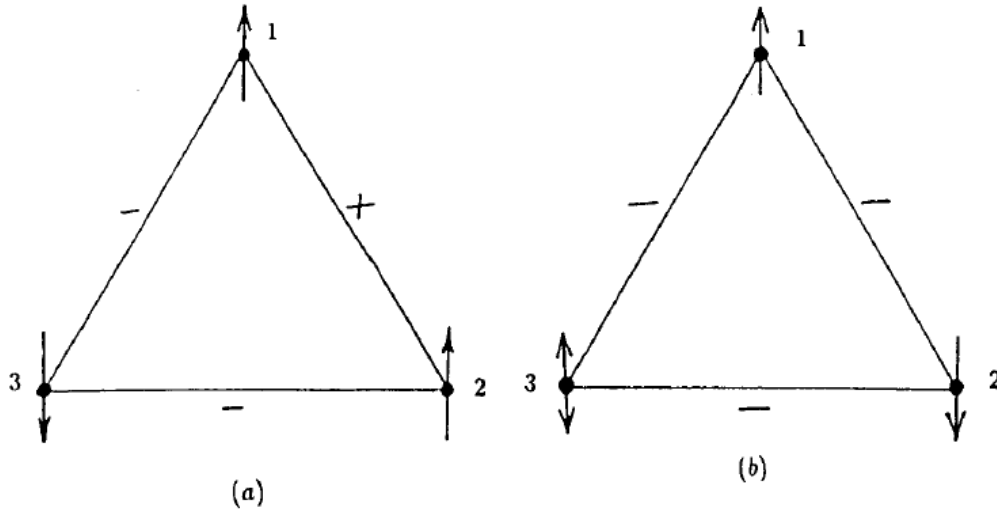


Figure 2.2: Frustration [22]

Consider the example of 3 interacting spins ($i = \{1, 2, 3\}$). Here, we have 3 interactions: J_{12} , J_{23} , J_{13} . For simplicity's sake, let us consider them to be of the same characteristic strength J , with the variation coming only in signs. Now, there can be a few different cases for the ground state here:

1. If all J_{ij} are positive, then they all align together and take on the same spin value $\sigma_i = k$.
2. If two J_{ij} are negative, but one is positive - suppose $J_{12} > 0$ and $J_{23} < 0$, $J_{13} < 0$ - then 1 and 2 can take the value $\sigma_1 = \sigma_2 = k$, whereas 3 takes the value $\sigma_3 = -k$.
3. If two J_{ij} are positive, but one is negative - suppose $J_{12} < 0$ and $J_{23} > 0$, $J_{13} > 0$ - and $\sigma_1 = k$, we can set $\sigma_2 = -k \because J_{12} < 0$. But now, we run into a conflict: according to $J_{13} > 0$, we should get $\sigma_3 = k$ and according to $J_{23} > 0$, we should get $\sigma_3 = -k$.
4. If all J_{ij} are negative, a similar situation occurs. We set $\sigma_1 = k$ and $\sigma_2 = -k \because J_{12} < 0$, but according to $J_{13} < 0$, we should get $\sigma_3 = -k$ and according to $J_{23} < 0$, we should get $\sigma_3 = k$.

This situation is illustrated in Fig. 2.2. In both cases 1 and 2, the system is perfectly fine since all the interactions agree with each other, leading to a clear ground state. However, in cases 3 and 4, we have interactions that disagree with each other, and we run into a conflict that cannot be resolved. This leads to multiple ground states - each in which there are some interactions that do not agree with each other. This phenomenon is called "frustration".

Without frustration, the system would behave the same as a regular ferromagnet. These frustrations that arise due to competing interactions are the reason why disordered systems (random J) differ fundamentally from ordered systems. Frustrations can be expected to exist in any system which has

interactions which have inherent randomness in the sign of the interaction. This phenomenon would hence result in the existence of *multiple ground states* or, at the very least, have numerous states close to the ground state.

2.3.5 Self-Averageness

Consider the thermodynamic limit $N \rightarrow \infty$ of a macroscopic system. Since we know that the free energy of the system itself is proportional to the volume N of the system, it is reasonable to deduce that the main contribution to the free energy in this limit comes not from the boundary but from the volume of the system. In this case, the macroscopic system could be subdivided into multiple macroscopic systems, and these could, in turn, further be subdivided into multiple macroscopic systems and so on recursively in the ∞ volume limit. The free energy of the entire system could then be taken as the sum of the individual subdivided systems and the energy from their interaction at the boundaries of subsystems. The contributions from the mutual interactions of these systems are simply the boundary effects which vanish in this thermodynamic limit, hence leaving the total free energy to just be a sum of macroscopic terms - each of which themselves are a random quenched quantity as they are dependent on the random interaction strengths of J_{ij} . We can apply the law of large numbers here - which states that the sum of a large number of random values can be represented as their average value multiplied by their number - to reason that the free energy of a macroscopic system must be self-averaging over the realisations of the random interactions. In disordered systems, the self-averaging described above is not followed perfectly.

2.3.6 Ergodicity Breaking

Another interesting property of spin-glasses is ergodicity-breaking. The ergodic hypothesis states that over long periods of time, the time spent by a system in some microstates is proportional to the volume of this corresponding region of the phase space, essentially meaning that all microstates are equally probable. In complex systems, the ergodic hypothesis breaks down in certain phases. This happens when the system is unable to fully explore the allowed state space, thereby violating the condition of the time spent being proportional to the volume of the region in the phase space. A system can get stuck in such phases when its kinetics are simply too slow (in experimental time scales) to be able to explore all the possible states.

Consider a system of water molecules in a jar in a supercooled state below freezing which is in quasi-equilibrium with a thermal bath at a temperature T . A thermal bath is essentially a store of molecules that can transfer or receive energy while maintaining a set temperature and is used as a control for equilibrium processes. As the temperature of the bath is slowly reduced, the system of water molecules also cools down along with the bath in equilibrium. Since the velocity of the molecules is dependent on temperature, the molecules slow down with a reduction in temperature. These water molecules are in equilibrium

with the bath via energy transfer. After enough cooling, however, the dynamics of the molecules become extremely slow. At this point, as we keep reducing the temperature of the bath, the system of water molecules is not able to keep up with the temperature due to its slow dynamics. Its molecules compete with their own neighbours for movement and become trapped to the point of becoming extremely slow in movement. Hence, the system is not able to lose temperature fast enough to stay in equilibrium with the bath. The molecules are no longer able to freely explore throughout the system as they were able to at higher temperatures due to these slow kinetics. This inability to explore all possible states is known as “ergodicity breaking”.

Similarly, a spin-glass system will also fall out of equilibrium with a thermal bath below a certain temperature due to the competing interactions and frustration between its spins. The spins are competing with each other and thereby make it extremely difficult for the system to explore all the possible configurations at that temperature. The spin-glass system is hence stuck in a “valley” of free energy, which it struggles to get out of below a certain temperature. This is called ergodicity-breaking in the spin-glass case. As the temperature is reduced further and further, more and more such valleys are formed, causing further ergodicity-breaking.

2.3.7 The Spin-Glass Phase

Spin-glass systems are a class of spin models that model complex and disordered behaviour. Their defining feature is the presence of quenched disorder in the interactions between spins. This leads to states of frustration between the spins, resulting in a state of competing and conflicting interactions. Additionally, spin-glasses also display slow dynamics and aging phenomena, allowing for the modelling of longer-lasting traits like memory. These properties of spin-glasses makes them functionally distinct from conventional Ising systems (such as ferromagnetic or antiferromagnetic systems), and allows us to use the properties of spin-glasses to model increasingly complex behaviour. An interesting feature in spin-glass systems arising due to the aforementioned properties is the existence of a new phase known as the spin-glass phase. We discuss the emergence of this phase in the following section.

The Sherrington-Kirkpatrick is typically used to model spin-glass systems. The Hamiltonian of a simple version of this model can be written as:

$$H = -\frac{1}{2} \sum_{i \neq j}^N J_{ij} \sigma_i \sigma_j \quad (2.17)$$

The probability distribution of the SK model is taken as a Gaussian distribution, and a simple such distribution can be written as:

$$P(J_{ij}) = \frac{1}{\sqrt{2\pi J^2}} \exp\left(-\frac{J_{ij}^2}{2J^2}\right) \quad (2.18)$$

where J is the characteristic strength of interaction.

Spin-glasses also have a form of spontaneous symmetry-breaking taking place. This symmetry-breaking not only happens at T' , but it is a continuous sequence of symmetry-breaking occurring below T' as we move through the state space. Above T' , the system is in the paramagnetic state where there is no phase transition and no ergodicity-breaking, as all states are explored with equal probability. As we go to low temperatures, however, the system undergoes a phase transition at T' . Here, there could be a large number of states which all differ in their free energy, and the space of states can be split into many “valleys”, and a representative state diagram is visualised in 2.3. Some of these valleys could have free energy much lower than the others, and there could technically exist a lot of such states. This causes the system to “freeze” in these states at low temperatures and not fully explore the allowed state space.

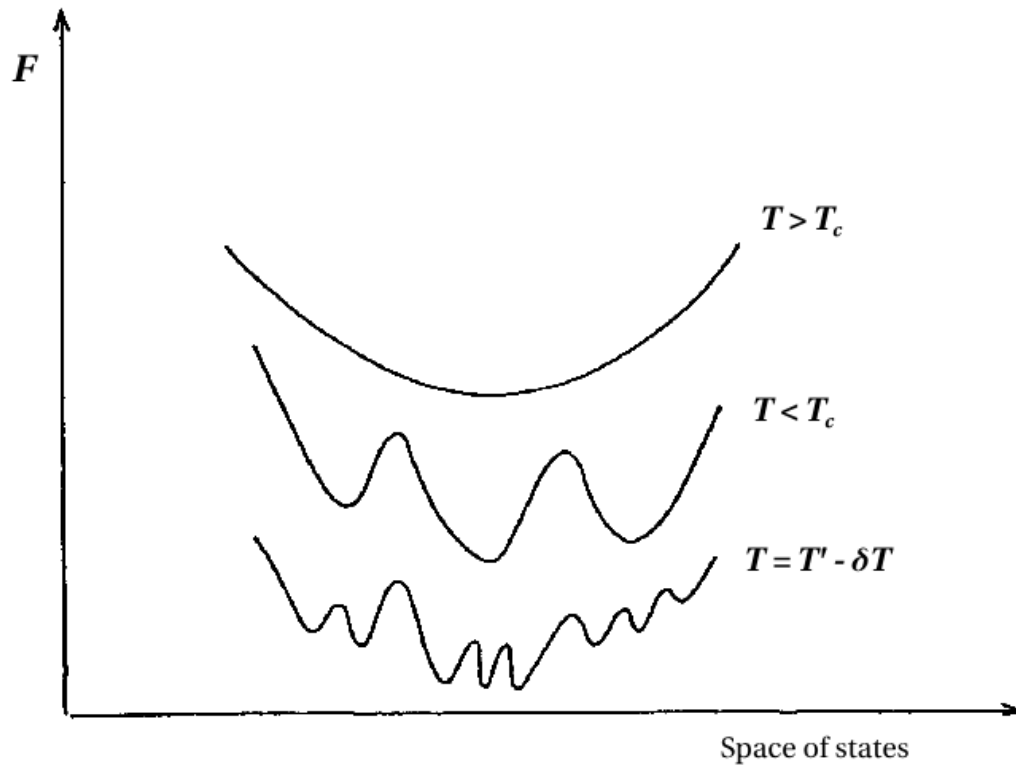


Figure 2.3: Free Energy of a Spin-Glass System [22]

In the large limit, as $N \rightarrow \infty$, the number of such states also goes to ∞ . Just below T' , the ergodicity is broken, and subsequently, the free energy separating these valleys goes to ∞ in the thermodynamic limit $N \rightarrow \infty$. Between each of these states, another phase transition occurs where a new kind of ergodicity-breaking occurs. Hence, there is an infinite number of symmetry breaking occurring as we move through these states. At a given temperature $T = T' - \delta T$, each of these valleys are unique in their (non-zero) average site-wise spin magnetisations $\langle \sigma_i \rangle_\alpha$ where α denotes the particular valley. Each

site now has unique $\langle \sigma_i \rangle_\alpha$ since all states (i.e., all combinations of $\sigma = \{\sigma_i\}$) are not visited with the same probability even when given infinite time. Each of these valleys can be split up into numerous smaller valleys separated by an infinite barrier. Furthermore, they also contain many valleys, which are separated by finite free-energy barriers of varying heights. The free-energy spectrum is, therefore, continuous, going all the way to infinity. Hence, the free energy of a spin-glass system is non-analytic at any temperature below T' .

The space of states at temperatures below T' is known as the spin-glass phase. In contrast to the paramagnetic phase, which is dominated by complete randomness and the ferromagnetic phase, which is dominated by order, the spin-glass phase is characterised by its inherent disorder and frustrated interactions, which causes the system to get stuck in metastable zones within the phase space. Consequently, there is a wide variety of configurations that the system can now take. This allows for the concept of long-term memory as there might be certain valleys where a part of the system is paralysed, allowing for slow relaxation dynamics in comparison to the other two phases. The spin-glass phase can also display robustness to perturbations and, therefore, be able to self-correct to stable states more easily while also not being completely static and enabling self-correction. Since this phase typically has numerous ground states, there is a high level of redundancy, allowing for multiple operational modes depending on the situation. These properties hence make spin-glasses unique in their behaviour, and the spin-glass phase has hence found numerous practical applications [61, 87, 88].

2.4 The Critical-State Brain

In the realm of statistical physics, the concept of criticality is a fundamental concept that describes systems that are in a phase transition. At the critical point, a qualitative change in the properties of the system occurs from a minor change in these control parameters. At this point between phases, the system exhibits phenomena that are unique compared to any of the phases in particular.

Scale-invariance is one of these phenomena - the properties of the system remain the same at different scales [15]. This means that in certain observables, when the system is scaled up or down, the qualitative nature of the trend observed remains the same. This kind of scale-invariance leads to the emergence of power-law behaviours. A power-law distribution is followed - rather than a linear or exponential - which can be described by the equation:

$$y = a \cdot x^k + \epsilon \tag{2.19}$$

where y represents the physical quantity (such as magnetisation or susceptibility) and x is an independent variable (such as temperature or distance). Here, k is known as the critical exponent. These power-laws can be described by the critical exponent k as the nature of the curve depends only on this exponent.

When x is scaled to some value cx , the nature of the y curve remains the same as now we have:

$$\begin{aligned}
 y &= a \cdot (cx)^k + \epsilon \\
 &= ac^k \cdot x^k + \epsilon \\
 &= b \cdot x^k + \epsilon
 \end{aligned}
 \tag{2.20}$$

for some other constant b . This can be contrasted with a non-scale-invariant function - such as $y = e^x$, which changes to $y = e^{cx}$ upon scaling - where the shape of the curve is fundamentally altered. In power-laws, we can zoom out to any level, and the observed trend would remain the same and is, therefore, a signature of scale-invariance. Some properties that display scale-invariance near criticality are the susceptibility, specific heat and correlation lengths [15].

The presence of fluctuations is another hallmark of criticality. These are spontaneous and unpredictable variations in the properties of the system. Fluctuations become important in the critical state and have a significant impact on the behaviour of the system as a whole. These are responsible for the scale invariance and the critical phenomena that are observed at the critical point.

The concept of criticality of the brain has gained significant attention in neuroscience research due to the valuable insights it offers into the dynamics of the brain [17]. The criticality hypothesis states that the brain operates at a critical state similar to systems in statistical physics since the brain shares a multitude of features with these systems and exhibits similar behaviour. Similar to critical-state systems, scale-invariance is observed in the brain in temporal dynamics of neuronal activity where similar patterns emerge at varying time scales [68]. At criticality, systems are extremely sensitive to small perturbations and are poised at the edge of a phase transition. The brain, at rest, demonstrates high sensitivity and responsiveness to external stimuli and sensory input. This allows for efficient information processing and high adaptability, which are also seen in critical-state systems across different scales. The brain exhibits non-linear dynamics and emergent behaviour, where the complex activity that occurs at scale cannot be attributed to a simple sum of the activity of its components [8].

Understanding the critical-state operation of the brain and its implications for neurological disorders provides a promising avenue for developing our understanding of brain function and dysfunction. Several studies have investigated the relationship between criticality and altered neural states or dynamics. One such study from 2012 by C. Meisel et al. shows that the brain deviates from the normally observed power-law distributions, which is a hallmark of criticality, during epileptic seizures using invasive electroencephalogram (EEG) recordings, and goes on to suggest that the cause of these seizures is due to the failure of criticality through computational modelling [59]. Another study by S. Liu et al. suggests the possibility of Early Warning Signal identification for epileptic seizures using the Distance to Tipping Point (DTP), a metric proposed to be the distance from criticality using dynamic network biomarker theory and random matrix theory. They observe a shape transition in the DTP before and after the onset of epileptic seizures and suggest that the brain loses its quasi-critical state during these seizures [55].

Self-organised criticality is another interesting aspect of criticality that has gained widespread attention in neuroscience in recent years. This refers to a type of criticality where systems naturally evolve to and maintain a critical state without external tuning and was proposed to be exhibited by the brain in the paper “Self-organized Criticality” by P. Bak, C. Tang, and K. Wiesenfeld in 1988 [5]. In their seminal work, Bak et al. identify and propose a governing principle for spatially extended dynamical systems - systems with both temporal and spatial degrees of freedom - that display two widely occurring but seemingly isolated phenomena. The first is the temporal effect of “flicker noise” or $1/f$ noise, where the power spectrum $S(f)$ of the system scales as $1/f$ at low frequencies. The second is spatial self-similarity, which is the evolution of spatial structure with scale-invariance and self-similar fractal-like properties. These are cooperative critical phenomena that are well-known in statistical mechanics to occur at the critical point or the transition point.

They identify these phenomena naturally occurring in a wide range of systems in seemingly unrelated and distant fields in - it is identified in the formation of sandpiles, the light from quasars, the intensity of sunspots, the flow of rivers such as the Nile, the current through resistors, and stock exchange prices [31, 74]. They argue and demonstrate that these critical phenomena do not occur by accident in systems and that these systems evolve naturally into these “self-organised” critical states without any external tuning. The critical state is an attractor of the dynamics, and this self-organised criticality is the underlying principle behind the phenomena observed in the aforementioned natural systems. While self-organised criticality is a method of organisation towards the critical point, the behaviour at the critical point itself is interesting to study in the context of the brain. This thesis focuses particularly on the behaviour near the critical state rather than the methods through which a system organises towards that state.

Investigations of criticality with regard to the progression of neurodegenerative diseases, such as Alzheimer’s Disease and Parkinson’s Disease, have also yielded promising results. An early study by T. Montez et al. measured magnetoencephalography (MEG) recordings from Alzheimer’s-afflicted (AD) and control subjects. They found that AD patients had a reduced incidence of alpha-band oscillation bursts with long life-times (≥ 1 s) over temporoparietal regions, weaker autocorrelations on long time scales, and greatly increased life- and waiting times of theta oscillations over medial pre-frontal regions [63]. They suggest that amplitude modulation of neuronal oscillations is important for cognition and that these altered oscillations, linked with information retrieval and retention, could serve as a potential biomarker of early-stage Alzheimer’s. A resting-state EEG study of a large number of subjects by Vyšata et al. compared the power-law exponents of spectral densities of AD patients with control subjects [100]. They noted a statistically significant difference in the frontal and pre-frontal lobes and recorded a large separation value in the receiver operating characteristic (ROC) in the temporal areas, noting a deviation from criticality. In an fMRI study into the comparison of AD, Mild Cognitive Impairment (MCI) and Cognitively Normal (CN) subjects by Jiang et al., they developed an index of functional criticality derived

from non-linear dynamics which could successfully distinguish the three groups, whereas the standard deviation of the time-series could only distinguish between AD and CN subjects [44]. The criticality hypothesis has opened up new avenues to analyse, detect, and study abnormal dynamics of altered neural states and shows great promise in clinical studies [107].

2.5 Aspects of Criticality

There are numerous phenomena observed at the critical state, and these phenomena can be utilised to characterise the nature of criticality observed. The behaviour at the critical state could vary widely - it could be similar to the one observed in Ising models or similar to the functioning of spin-glass systems. We explore certain aspects of criticality which can be used to investigate in detail and ascertain the type of criticality exhibited in the human brain.

2.5.1 Self-Averaging

Self-averaging is a concept that describes the behaviour of an observable or physical quantity as the system size varies. This behaviour is seen in many of the observables in systems with quenched randomness. In such systems, the disorder can lead to spatial or temporal variations in the observables of the constituents or the environment. As a result, the properties in these systems can exhibit significant sample-to-sample fluctuations due to the randomness in the disorder realisation [4]. Self-averaging emerges when the system size increases, and the fluctuations in observables diminish relative to their average values in certain systems with quenched disorder. This means that for large enough system sizes, the fluctuations become less significant, and the behaviour of the observable becomes more predictable and representative of the average behaviour of the system. This property of systems allows the use of ensemble averaging, allowing the simplification of statistical analysis of large systems with quenched disorder. When this property holds, it becomes possible to describe the behaviour of the entire system using a single disorder realisation instead of needing to consider multiple disorder realisations, thereby simplifying analysis.

The Central Limit Theorem (CLT) states that fluctuations within a system are proportional to $N^{\frac{1}{2}}$, where N is the size of the system. This means that as we increase the size of a region that is being averaged, the measurements obtained from it are more reliable. One of the core assumptions of the CLT is that the variables in the system are independent and identically distributed. However, as individual signals in the system evolve differently due to increasing correlation across long ranges, this underlying assumption of the CLT is violated. These correlations lead to certain signals being dependent on other signals, which can give unreliable averages that are not truly representative of the underlying phenomena. Such systems are said to be experiencing imperfect or weak self-averaging. Self-averaging,

however, can exist on a spectrum. Systems can have self-averaging that ranges all the way from no self-averaging (implying a completely interconnected system with correlations) to perfect self-averaging (where the variables in the system are independent and identically distributed). To account for the correlated signals and to have adequate self-averaging in the system, it is necessary to have an adequate system size to average over. As we increase the realisation size that is averaged over, the influence of individual dependencies and individual components diminishes, and the overall average becomes more representative of the true nature of the system [105]. With larger and larger realisation sizes, we average over all correlations and possible states within the, covering more of the allowed state space.

The quantification of self-averaging can help us understand the behaviour of the system. At criticality, the system is expected to show a breakdown in self-averaging behaviour as described in 2.3.5 [4]. This breakdown occurs due to the presence of long-range order close to the critical state and the violation of CLT. However, this breakdown can be compensated for as the volume over which the averaging is done keeps increasing, allowing for an increased ensemble to average over. Although systems such as the SK model are inherently disordered, they can still exhibit self-averaging behaviour [77], and self-averaging within these systems can serve as a good marker of criticality. Numerous studies have been done using fMRI data at many different scales, but the nature of self-averaging in these systems is generally not explored thoroughly, and the size, which is parcellated, is an important metric to consider for accurate and reliable averaging of signals. This is an additional goal of the study of self-averaging. We mainly studied self-averaging in order to examine indicators of criticality. Self-averaging is an inherently spatial property - it quantifies the behaviour of the system as we go through different regions and examine different scales. As the spatial distribution of the constituents and the state of the system changes, it can tell us a fair amount about the evolution of spatial behaviour as we get closer to criticality. Hence, self-averaging is a good indicator of the spatial aspect of criticality. We explore the effect of system size self-averaging in the human brain at the critical state through rs-fMRI in detail, employing a plethora of methods to treat the critical-state brain as a disordered system to which this concept of self-averaging is applicable.

2.5.2 Domain Formation

In an Ising system, the low-temperature regime is dominated by alignment between the spins and is known as the ferromagnetic phase. The high-temperature regime is dominated by randomness, leading to misalignment and is known as the paramagnetic phase. As we approach criticality, however, something interesting happens. The spins are neither completely aligned nor misaligned. Localised regions of spins start to align with each other while still competing with the randomness of spins from outside this local region. This leads to the formation of regions of spins which are all aligned with each other, bordered by other regions of spins which are all aligned with each other, but the two regions in question are of

opposite spin. These regions are then called “domains”. Domains are regions of uniform spin bordered by other domains of opposite spin. These arise due to the complex balance between randomness and spin-spin interactions [15].

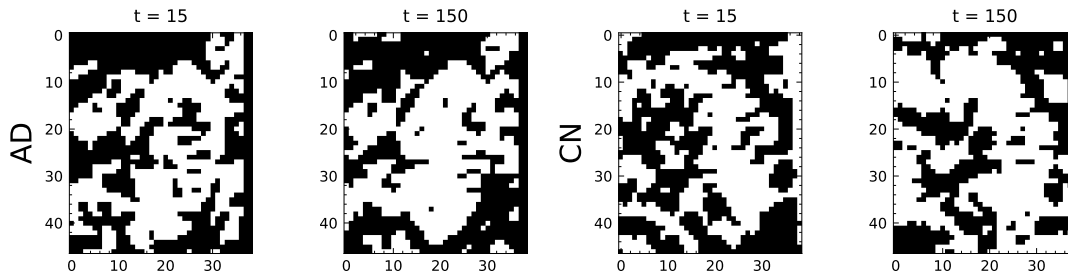


Figure 2.4: Domain Formation near Criticality

A representative example can be seen in Fig. 2.4. Near criticality, as the system undergoes a phase transition, domains become highly disordered and fluctuating. They constantly rearrange themselves over space as the system evolves. The domain sizes tend to diverge as the system approaches criticality, leading to large, percolating clusters. Domains at this point often combine with other domains due to a few random flips at the domain boundary connecting two isolated domains and also die out as smaller isolated regions are taken over by the larger domains. This leads to long-range order through the wide-spanning domains, making the system all the more sensitive to external perturbations. Studies have also shown that the domain boundaries (or domain walls) tend to constantly fluctuate but converge towards certain time-dependent positions, which are dependent on the system configuration but independent of the initial conditions. This indicates that the system reaches a sort of dynamic equilibrium near criticality, allowing it to be stable and yet responsive to stimulus.

The brain in the resting state has also been shown to form networks of correlated spins. The existence of such networks, which are distributed spatially and temporally, is a signature of domain formation [23, 29]. The formation of domains is a key indicator of the proximity to criticality for an Ising-like system. It is an important spatial property when it comes to criticality and plays a vital role in information flow within systems. Quantifying domain formation and further studying the evolution and behaviour of these domains at equilibrium (in resting state) can shed light on the nature of the criticality of the system.

2.5.3 Signal Relaxation Behaviour

The relaxation behaviour of the signals (or the spins in a spin-lattice system) is a good indicator of the phase of the system. Temporal relaxation refers to the time evolution of a signal towards an equilibrium state or a stable state after being perturbed. It characterises the persistence of effects on the system through the time taken to return to equilibrium. The temporal relaxation behaviour of a signal can

typically be quantified through correlation functions. Namely, the temporal autocorrelation quantifies the relaxation.

The form of relaxation is often studied for a clearer idea of the nature of the system in question. They act as valuable indicators of various effects: topological defects, ageing, criticality, fluctuations within the system, and complex dynamics. As the signal becomes uncorrelated with itself with increasing time gap t , this relaxation is generally expected to follow an exponential decay (of the form $y(t) = const * e^{-t/\tau}$) pattern in the paramagnetic phase of an Ising model. The relaxation time τ can be calculated by fitting the equation to the curve. As we approach criticality, the relaxation times tend to diverge as the system takes longer and longer to recover from perturbations due to long-range correlations.

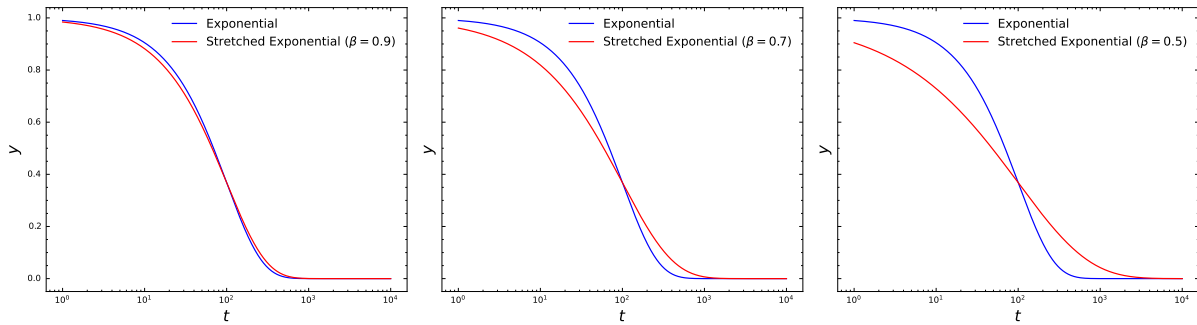


Figure 2.5: Stretched Exponential and Simple Exponential

Spin-glass systems have been widely shown to display a form of decay that is best described by a function known as the stretched exponential or the Kohlrausch-Williams-Watts stretched exponential form [103]. A stretched exponential is similar in shape to a regular exponential but shows a marked deviation from it (by a factor β) through the stretching of the curve. This can be written as $y(t) = const * exp[(\frac{-t}{\tau})^\beta]$. Fig. 2.5 shows a stretched exponential with varying β values where the deviation from regular exponential behaviour can be seen. The stretched exponential form involves a two-step relaxation pattern, which is a classic signature of the presence of metastable states [9]. This is observed in spin-glass systems as we approach the glass transition.

As we draw nearer to the critical state, we expect to see larger and larger relaxation times (τ) regardless of the presence of a stretched exponential. [101, 27] Temporal correlation lengths are typically not disrupted by the type of transition and exhibit distinctive behaviour regardless of the type of phase transition. If there is indeed a difference in proximity to criticality, we expect to see it reflected well in the temporal relaxation behaviour. Therefore, signal relaxation analysis can serve as a good final step to clarify and add weight to the findings from other experiments.

2.6 Alzheimer's Disease

Alzheimer's Disease is a neurodegenerative disorder characterised by cognitive decline and memory impairment. The disruption of neuronal connectivity - both functional and structural - plays a key role in the progression of this disease. Numerous studies have investigated connectivity alterations using various modalities. Resting-state connectivity studies using fMRI investigate the functional connectivity of the subject in a state where there is no stimulus, and the subject is typically in a resting position [40]. Disrupted connectivity within the default mode network (DMN), which is a set of brain regions associated with memory and introspection, has often been observed in these studies [35]. Abnormal connectivity within other networks, such as the salience network and executive control network, have also been identified [3]. Additionally, task-based studies have shown disrupted connectivity patterns in various cognitive domains affected by the disease, including working memory, attention, and language processing [92]. Structural studies such as diffusion tensor imaging (DTI) studies are also common in literature and have revealed alterations in structural connectivity in AD-afflicted subjects [67]. These subjects have been shown to have decreased fractional anisotropy and disrupted the integrity of white matter tracts - such as the fornix and corpus callosum - which indicates reduced structural connectivity and has been associated with cognitive impairment and memory deficits in Alzheimer's disease. These disruptions are collectively linked to cognitive impairment and the progression of AD.

In recent years, there has been a focus on developing better non-invasive methods for early identification of AD by studying changes in brain structure, function and connectivity that often occur in the preclinical stages of Alzheimer's. Some promising approaches are identifying disruptions in connectivity through the use of fMRI data and the use of machine learning algorithms on various modalities [94]. Analyses through statistical methods such as the use of energy landscape analysis for characterising Alzheimer's and entropy-based analysis methods are also encouraging approaches to the problem of early identification and intervention [2, 25]. These techniques leverage complex patterns of connectivity alterations and biomarkers associated with the disease to aid in detection.

In AD, multiple studies have found a disruption in criticality, which stems from the abnormal connectivity [44, 85]. AD brains, hence, show signs of behaviour being farther from criticality than cognitively normal brains. This fact can thus be leveraged in order to study what a disruption in criticality would look like through the lens of statistical mechanics models. The deviation from the optimum critical functioning can enable the Alzheimer's-afflicted brain to serve as a useful benchmark of abnormal critical behaviour.

2.7 Relevant Literature

Numerous studies leverage models inspired or directly derived from statistical mechanics to study criticality in the brain. There are resting-state studies that are often used to study the nature of the brain itself or determine the difference caused by neurodegeneration or altered states of mind [78, 25]. Task-based studies implement the perturbations as an external field effect and attempt to study the response of the brain analogous to the model [47, 99, 30]. Many techniques have been developed in this area that have inspired this thesis, and statistical mechanics proves to be a good tool to model the brain and advance our understanding of neural function and dysfunction.

A study by I. Fortel et al. investigates critical-state dynamics using the pairwise maximum-entropy model in an interesting way [28]. In this work, they use resting-state fMRI data from carriers of the apolipoprotein E (APOE)- $\epsilon 4$ - which has widely been linked with a genetic predisposition of susceptibility to Alzheimer’s Disease - and noncarrier control subjects to explore the complex interactions underlying neural activity. Using rs-fMRI data along with structural data, they employ a pairwise maximum-entropy model to simulate the connectivity dynamics of each subject and infer the connectome to generate a Functional-Structural Embedding (FSE) using a likelihood maximisation approach and Monte Carlo simulations over a range of temperatures. Their analysis was able to distinguish between female APOE carriers and noncarriers using the Excitation-Inhibition ratio, but not between male carriers and noncarriers, with the distribution of the female carriers vs noncarriers displaying a statistically significant difference ($p = 0.008$). Their findings displayed a shift towards hyperexcitation for female carriers of APOE, revealing a shift in criticality for female carriers compared with noncarriers of APOE, suggesting an increased vulnerability to AD neuropathology in female carriers.

This study is of significance to us as it demonstrates the potential of the pairwise maximum-entropy model in understanding macroscale dynamics from microscale interactions in fMRI and MRI in general. The excitation-inhibition balance simulated at different temperatures can further shed light on the critical-state dynamics within subjects with possibly abnormal dynamics. This sets a precedent for using the pairwise maximum-entropy model to study dynamics in complex systems such as the brain and investigate the nature of or closeness to criticality in various neurological conditions, states, or disorders.

An interesting investigation by Ezaki et al. employs a similar pairwise maximum-entropy model to infer the functional connectome (J) from resting-state fMRI data [24]. They parametrize the J values using a Sherrington-Kirkpatrick model distribution in the form of $J_{ij} = (\hat{J}_{ij} - \hat{\mu})\frac{\sigma}{\sigma} + \mu$, motivated by the extensive literature surrounding spin-glass physics. A pseudo-maximum likelihood method was used to perform gradient descent in order to estimate the \hat{J} and \hat{h} values for the Ising model using empirical data from the concatenation of all time-series. The J_{ij} values are then swept through to

generate a phase diagram through susceptibility and magnetisation characterised by the μ and σ of J , resulting in a heatmap in each of these order parameters and allowing the separation of phases based on these parameters. The observable magnetisation and susceptibility are then calculated for each subject independently and then placed on the phase diagram according to their susceptibility values. This generates a phase diagram in 2D with subjects lying somewhere in the diagram.

They found that the subjects lay close to the paramagnetic-spin-glass transition approaching from the paramagnetic side and established a mild positive correlation between performance IQ and the spin-glass susceptibility of the subjects, suggesting that those with higher IQ were closer to criticality. They also suggest that the paramagnetic-ferromagnetic transition may be irrelevant in this case. In their case, all subjects seem to approach criticality (of the spin-glass-paramagnetic transition) from the paramagnetic side, and they seem to lie in the paramagnetic phase. This is an artefact of the binarisation procedure followed, as the data was binarised by z-scoring (mean set to 0) and converting to +1 or -1 values based on being greater/lesser than the mean. This leads to the coercion of the data to be in the paramagnetic phase as the mean has all but explicitly been set to 0. The validity of this kind of binarisation is germane to this study as the focus is not, particularly on establishing which phase the brain operates in at default, but it is an important point to note since this could influence the results obtained.

This study is noteworthy as it employs a pairwise-maximum entropy model to study criticality and the relevant phase transition. A correlation is established between the optimum functioning of the brain and criticality. The spin-glass state and the corresponding transition are also acknowledged, although the limitations of the study do not allow further exploration of the importance of the phase itself. The qualitative nature of the fMRI time-series themselves can be further studied in detail in order to shed light on the nature of the relevant phase transition and the existing default phase.

There is a wide range of literature applying concepts from statistical mechanics to study the brain. Criticality, in particular, has been widely studied in statistical physics but is only recently seeing application in the field of neuroscience. In this thesis, we employ similar concepts and methods to investigate the nature of criticality in the human brain through the use of resting-state fMRI data from Alzheimer's and cognitively normal subjects.

2.8 Overview

There is extensive literature on statistical physics and their applications in neuroscience. In this chapter, we explored numerous concepts from neuroscience and statistical mechanics. We started with a review of the predominant modalities in neuroscience and their applications in recent years. Next, we explore popular statistical models that are often used to model complex systems, followed by an examination of the concept of criticality in the context of these systems. We then investigate the emergence of the

concept of brain criticality and the application of this concept to better understand neural function. We further analyse certain signatures of criticality in detail and the characterisation of critical state dynamics using these signatures. We then take a look at neural dysfunction in the form of Alzheimer's Disease and examine how its study can be used to deepen our comprehension of the human brain. Finally, we review some relevant literature that has applied similar methodologies to study the brain. In this thesis, we use many of the concepts discussed here in order to further our understanding of neural function and dysfunction. We attempt to leverage existing literature and build on top of it to study the nature of criticality in the brain through fMRI data by using statistical mechanics models.

Chapter 3

Investigating Disrupted Criticality in Alzheimer's through the Pairwise Maximum-Entropy Model

3.1 Introduction

Criticality of the brain has often been said to be crucial to living organisms and has been suggested to be a valuable paradigm for understanding the sophisticated functioning of the brain. Behaviour at the critical state is well-studied in the realm of statistical physics, and statistical modelling serves as an excellent analogue to further explore the unique features exhibited at this state. Alzheimer's Disease (AD) is a neurodegenerative disorder characterised by progressive cognitive decline and memory impairment that afflicts millions around the world. The underlying pathophysiology of AD involves the disruption of neural connectivity and dynamics, which play a crucial role in cognitive functions and disrupt the functioning of the brain, pushing it away from the ideal critical state. In this work, we employ the Pairwise Maximum-Entropy Model (pMEM) as a statistical modelling approach to study this disruption. We infer neural connectivity from resting-state functional magnetic resonance imaging (rs-fMRI) data in AD and Cognitively Normal (CN) subjects and derive the critical temperature of the two classes of subjects by studying the susceptibility linked to this characteristic connectivity in order to understand the deviation from criticality caused by the progressive neurodegeneration of Alzheimer's.

Functional MRI (fMRI) has emerged as the primary imaging modality over the past decades used to provide information about both spatial and temporal dynamics. The popularity of fMRI is partly due to its non-invasive nature, allowing recording of the human brain while it is in working. This is particularly helpful when working with people with neurological diseases. Functional connectivity, as measured from the fMRI signal, has been shown to be predictive of the diagnosis and characterisation of multiple neurological diseases [11, 57].

Alzheimer's accounts for a substantial percentage of dementia cases worldwide and is the most common form of it. A significant marker of Alzheimer's Disease is disrupted neural connectivity and

dynamics. This is frequently observed particularly in areas crucial for memory and cognition, such as the hippocampus and neocortex [3]. This neuronal loss disrupts the connections between brain regions and alters the transmission of signals within the network. AD hence exerts profound effects on the criticality of brain networks, perturbing the delicate balance necessary for optimal function in neural activity. Studies have demonstrated that as the disease advances, the neurodegenerative processes, characterised by neuronal loss and synaptic dysfunction, significantly reduce the complexity and flexibility of brain networks. This hampers the brain's ability to achieve an optimal state for information processing and adaptability, consequently contributing to the symptoms observed in individuals with AD. The study contributes to our understanding of the disruption of criticality within the brain due to Alzheimer's and the greater connection between the deterioration of neuronal circuitry and its effect on criticality.

Modelling the brain using concepts from statistical mechanics has emerged as a potent tool for researching various phenomena. There is extensive literature investigating the capability of statistical models in capturing the nuances of the reaction between neurons at multiple levels [66, 46, 58, 25]. Statistical physics-based methods have the necessary formalism to analyse complex spatio-temporal dynamics at the micro-scale and capture them into a few macroscopic variables. By treating the brain as a system of interacting microscopic parts, namely neurons, we can study the dynamics at scale and better understand their collective behaviour. Models such as the Ising model have long been employed to understand critical behaviour within the brain. Statistical mechanics has extensive literature on the connectivity and dynamics of spin systems and on the phases observed in these systems. This allows the study of phase transitions by constructing systems analogous to the brain. Models such as this are adept at capturing the intricate dynamics between brain regions, which more superficial metrics such as functional connectivity are unable to capture. Considerable simulations can also be performed using such techniques, and well-established signatures can be studied to infer the states of the system. These models help bridge the microscopic and macroscopic scales.

The pairwise maximum-entropy model, or pMEM for short, is a variant of the Ising model that accommodates long-range interactions - a spin-lattice system with possible connectivity between every pair of spins. The connectivity is not explicitly modelled but is inferred from empirical data through optimisation techniques such as maximum-likelihood estimation. Recent investigations have shown that the unconstrained pMEM is proficient in generating functional connectivity representations. The pMEM is an ideal model to link excitation-inhibition interactions at the neuronal level to the larger functional connectome.

Using the pMEM, we can generate a connectivity model between pairs of the spins of the lattice. These connectivity models then allow us to perform Monte-Carlo simulations for this spin-lattice model at various temperatures, enabling us to compute a myriad of metrics at these temperatures, such as the average magnetisation and susceptibility of the system. In typical statistical mechanics models, the

susceptibility is often used to understand the phase transition boundary through critical temperature. At this temperature, the model is said to be at a critical point or a critical state. We perform a similar analysis here to infer the critical temperature of our modelled spin-lattice system derived from empirical data.

In this work, we explore the extent to which Alzheimer’s Disease affects critical state functioning by computing the critical temperature of the two classes - AD and CN - through the pseudo-likelihood maximisation of a pairwise maximum-entropy model. We study the fMRI data of 34 AD and 55 CN subjects from the Alzheimer’s Disease Neuroimaging Initiative (ADNI) dataset, which are parcellated into various regions of interest (ROIs), with each ROI representing a spin. The signals are binarised (to +1 or -1 values) and act as spins in a lattice that evolves over time. The connectivity of the model for each class is inferred through the time series of this lattice using a pseudo-likelihood maximisation. This connectivity is then used to study their magnetisation and susceptibility curves. The functional connectivity of each class is also explored to serve as a baseline. The critical temperature of each class can then be inferred from their susceptibility, enabling us to understand the extent of the disruption in critical state functioning due to the neurodegeneration resulting from Alzheimer’s. This helps us deepen our understanding of the dynamics of the brain itself, as we can then study the exact physical and functional changes caused by AD and correlate these to the changes observed in proximity to criticality. This could also lead to the potential identification of biomarkers for AD, which would add to the literature on early detection, intervention, and treatment of the disease that afflicts millions of people around the world. Through this investigation, we aim to quantify the disruption of critical dynamics due to Alzheimer’s and link this disruption to brain function.

3.2 Methods

3.2.1 Dataset

The study utilised resting-state fMRI data from the Alzheimer’s Disease Neuroimaging Initiative (ADNI) database [71] from the ADNI-2 phase. The ADNI dataset is a collaborative effort among multiple institutions. It is a widely used collection of neural data, including MRI, PET scans, biomarkers, and genetic data, focused on accelerating the diagnosis, treatment, and understanding of Alzheimer’s Disease.

Data collection was performed through the portal available at adni.loni.usc.edu. The samples consisted of both Cognitively Normal (CN) individuals and patients with Alzheimer’s Disease (AD). A total of 89 subjects were selected, comprising 34 AD patients and 55 CN individuals. The details for the dataset are documented in Table 3.1. Each time-series was 140 time points long with a repetition rate (TR) of 3s. Some subjects contained extended resting-state fMRI studies consisting of 200 time points, which were truncated to 140 time points for uniformity. Anatomical MRI scans corresponding to each resting-state fMRI scan were used for preprocessing.

Detail	AD	CN	Total
Number of Subjects	34	55	89
Number of Male Subjects	16	25	41
Number of Female Subjects	18	30	48
Age Mean (years)	73.09	78.85	76.65
Age STD (years)	± 7.38	± 6.51	± 7.41
Age Range (years)	56 – 89	66 – 91	56 – 91
Repetition Rate (s)	3		
Scan Duration (s)	420		
Parcellation Atlas	Automated Anatomical Labelling		
Number of RoIs	116		

Table 3.1: Dataset Information

3.2.2 Preprocessing and Parcellation

The fMRI data underwent preprocessing primarily using tools from the FMRIB Software Library (FSL) [43, 83]. The preprocessing steps involved motion correction, coregistration, and parcellation. The entire process was done programmatically using the Nipype package for orchestration of various plugins and command-line tools using Python 3.9.

For motion correction, FSL’s MCFLIRT [42] was employed to align all volumes to the mean volume, resulting in motion parameters and mean images. Slice-timing correction was performed using FSL’s SliceTimer. The coregistration process involved several procedures. First, the anatomical image was skull-stripped using FSL’s BET. Then, it was segmented with FSL’s FAST, and the resulting white matter probability image was thresholded. The fMRI data was pre-aligned and coregistered to the anatomical images using FSL’s FLIRT. The computed coregistration transformation was applied to both the functional and mean images. Spatial smoothing using SPM was done with a full-width at half-maximum (FWHM) of 5mm. The ArtifactDetect algorithm from NITRC’s RapidArt artefact detection module [32] was used to identify and separate artefacts from the functional images, utilising a norm threshold of 2 and a z-intensity threshold of 3. The images were then spatially normalised to the Montreal Neurological Institute’s (MNI) ICBM-152 template with a resolution of 2mm through the anatomical transformation computed using Advanced Normalisation Tools (ANTs). Finally, Nilearn [1] was utilised to compute and implement a brain mask, which employed the histogram of the mean fMRI image intensity, discarding the bottom 20% and top 15% of the histogram values.

After preprocessing, the data was parcellated to enable a more comprehensible and computationally feasible analysis. The `nilearn` package in Python was used to perform the parcellation. The Automated Anatomical Labelling (AAL) Atlas [64] was used, which divides the entire brain into 116 Regions of Interest (ROIs) based on brain anatomy, and the mean signal from each of these areas is computed.

3.2.3 Functional Connectivity

Functional connectivity, also known as static functional connectivity (sFC), quantifies the strength of connection by measuring the correlation between the activity patterns of a pair of regions of interest (ROIs). In mathematical terms, it represents the correlation between the time series data of two ROIs.

The sFC is generally represented as a square matrix of size $N \times N$, denoted as F , where N corresponds to the total number of ROIs. The entry F_{ij} in the matrix represents the correlation between the ROIs labelled as i and j .

The calculation of F_{ij} involves computing the correlation using the following formula:

$$F_{ij} = \frac{\sum_{t=1}^{t_{max}} (\sigma_i(t) - \bar{\sigma}_i)(\sigma_j(t) - \bar{\sigma}_j)}{\sqrt{\sum_{t=1}^{t_{max}} (\sigma_i(t) - \bar{\sigma}_i)^2 (\sigma_j(t) - \bar{\sigma}_j)^2}} \quad (3.1)$$

Here, $\sigma_i(t)$ represents the signal value of the i^{th} ROI at time t in the fMRI scan. \bar{x} denotes the mean of $x(t)$ over all time points. The numerator captures the covariance between the signals of the two ROIs, while the denominator normalises the correlation by the standard deviations.

Functional connectivity has demonstrated considerable promise in differentiating between Alzheimer's Disease (AD) and Cognitively Normal (CN) subjects. It is a metric that is frequently used in neuroscience to quantify the relationships between different regions of the brain. FC can hence be used to characterise subjects or entire classes and is employed as a baseline measure for neuronal dynamics in this study.

3.2.4 Pairwise Maximum-Entropy Model

The Pairwise Maximum Entropy Model (pMEM) is a version of the Sherrington-Kirkpatrick Model (a variant of the Ising model that allows for long-range interactions), which is used to infer connectivity from empirical data. This model is based on the principle of maximising the overall system entropy while preserving discrete pairwise connections between nodes, specifically the regions of interest (ROIs) in this context. This approach allows for capturing complex patterns and relationships within the brain network. It considers the interplay between different brain regions, taking into account their functional associations, which can provide valuable insights into the underlying neural processes and communication dynamics in the brain.

The connectome can be represented as a graph consisting of nodes (ROIs) and the connections (edges) between them. The strength of the connection between two ROIs, such as nodes i and j , can be quantified using the static functional connectivity (sFC) matrix denoted by F , where F_{ij} represents the correlation value.

The activity pattern of the ROIs is represented by $\sigma = (\sigma_1, \sigma_2, \dots, \sigma_N)$. Each $\sigma_i \forall i \in \{1, \dots, N\}$ is a timeseries of the BOLD signal from the i^{th} ROI. Thus, it can be represented as $\sigma(t) = (\sigma_1(t), \dots, \sigma_N(t)) \forall t \in \{1, \dots, t_{\text{max}}\}$ where t_{max} is the total number of time points in the series. $\sigma_i(t)$ hence represents the signal value of the i^{th} ROI at time point t from the parcellated fMRI scan of a selected subject. These raw activity patterns are then binarised, and all the signal values are updated to spins, taking the values +1 or -1 according to a set binarisation strategy (discussed in the next section).

The empirical probability distribution $P_e(\sigma)$ of the activity pattern over its time series σ is computed. This probability distribution is fitted onto the probability distribution of the model using a likelihood-maximisation method.

The pMEM can be characterised by two fundamental equations. The probability of a state σ is given by the Boltzmann distribution:

$$P(\sigma|h, J, \beta) = \frac{e^{-\beta E(\sigma|h, J, \beta)}}{\sum_{\sigma} e^{-\beta E(\sigma|h, J)}} = \frac{e^{-E(\sigma|h, J, \beta)}}{Z} \quad (3.2)$$

where $Z = \sum_{\sigma'} e^{-\beta E(\sigma'|h, J)}$ is the partition function, and σ' is an activity pattern with the summation over it representing all possible activity patterns. h is the field strength, which usually represents external factors, and $J = \{J_{ij}\}$ represents the connection strength between the sites i and j . $\beta = \frac{1}{T}$ is a parameter known as the inverse temperature and T is the temperature.

The energy of a state σ is given by:

$$E(\sigma|h, J) = - \sum_{i=1}^N h_i \sigma_i - \sum_{i=1}^N \sum_{j>i}^N J_{ij} \sigma_i \sigma_j$$

h and J are parameters to the model that can be learned to fit the pMEM probability distribution P onto the given empirical probability distribution P_e , for a given value of β which represents a certain temperature value. Since we consider resting-state fMRI data in our study, there is assumed to be no external stimulus. This can be taken as no external force acting on the model itself, thus not requiring the use of the field term. Hence, we set the field parameter h to null, and we only estimate the parameter J . The model can simplified and be represented as:

$$P(\sigma|J, \beta) = P(\sigma|0, J, \beta)$$

$$E(\sigma|J) = E(\sigma|0, J)$$

3.2.5 Binarisation

Since the pMEM works on the principle of spins, which can take values of $+1$ or -1 , the complete activity pattern is then binarised. Binarised signals can be represented as spins in the pMEM. This enables the model to emulate its states as an activity pattern. Common binarisation strategies include z-scoring the signals first and then setting the values above the mean to be $+1$ and below it to -1 . However, the inherent problem with this is that it effectively coerces the empirical systems into the paramagnetic phase since the average magnetisation values per site are now equal to 0, i.e., $m_i = 0 \forall i$, which is a characteristic feature of the paramagnetic phase. To avoid this issue, we compute the threshold value ($\bar{\sigma}_i$) differently. We take this value to be the average of the most significant 10 values (Z_{max}) and the smallest 10 values (Z_{min}) in the time series of the signal.

We employ the following strategy: Let z be an array of values of some time-series σ_i sorted in descending order. Then, we have $z_1 \geq z_2 \geq \dots \geq z_K$ where $K = t_{max}$ is the length of the time-series. We can then compute the average maximum (Z_{max}) and average minimum (Z_{min}) as such:

$$Z_{max} = \frac{1}{10} \sum_{i=1}^{10} z_i \quad (3.3)$$

$$Z_{min} = \frac{1}{10} \sum_{i=1}^{10} z_{K-i+1} \quad (3.4)$$

Then, we can compute the threshold as:

$$\bar{\sigma}_i = \frac{Z_{max} + Z_{min}}{2} \quad (3.5)$$

Finally, the binarised activity pattern time series for each subject is thus updated as follows:

$$\sigma_i(t) = \begin{cases} 1, & \text{if } \sigma_i(t) \geq \bar{\sigma}_i \\ -1, & \text{if } \sigma_i(t) < \bar{\sigma}_i \end{cases} \quad \forall i \in \{1, \dots, N\} \quad (3.6)$$

3.2.6 Pseudo-likelihood Maximisation

There exist various methods for estimating parameters in a probability distribution, one of which is Maximum-likelihood Estimation (MLE). This widely-used approach involves utilising a gradient ascent scheme to maximise a likelihood function. The likelihood function is defined as the product of conditional probabilities given by:

$$\mathcal{L}(J, \beta) = \prod_{t=1}^{t_{max}} P(\sigma(t)|J, \beta) \quad (3.7)$$

The calculation of this likelihood, however, becomes exceptionally computationally expensive as the number of spins in the system increases. Hence, we use a form of MLE known as pseudo-likelihood

maximisation here, which simplifies the calculation of the likelihood through a mean-field approximation, which is defined by the likelihood:

$$\mathcal{L}(J, \beta) = \prod_{t=1}^{t_{max}} \prod_{i=1}^N P(\sigma_i(t) | J, \beta, \sigma_{-i}(t)) \quad (3.8)$$

In contrast to likelihood maximisation, where the likelihood function is computed for the entire system $\sigma(t)$ with parameters J and β , pseudo-likelihood maximisation calculates the conditional probability of an individual spin $\sigma_i(t)$. It incorporates the same parameters J, β , along with the additional term $\sigma_{-i} = \sigma \setminus \sigma_i$, representing the remaining elements of σ excluding σ_i . Pseudo-likelihood maximisation is much more computationally efficient as it estimates the conditional probabilities of individual spins instead of computing the joint likelihood for the entire system, thereby simplifying the problem with a minute degree of loss in accuracy. This makes it advantageous for analysing large datasets with high-dimensional variables. Additionally, pseudo-likelihood maximisation is robust to complex or unknown dependencies between variables, allowing for flexible modelling approaches that capture localised dependencies in intricate network structures such as the pMEM.

The log pseudo-likelihood is hence maximised for the estimation of the parameters:

$$\begin{aligned} \ell(J, \beta) &= \frac{1}{t_{max}} \ln(\mathcal{L}(J, \beta)) \\ &= \frac{1}{t_{max}} \sum_{t=1}^{t_{max}} \sum_{i=1}^N \ln \left(\frac{\exp \left[\beta \sum_{k=1}^N J_{ij} \sigma_i(t) \sigma_k(t) \right]}{Z_i} \right) \end{aligned} \quad (3.9)$$

where the partition function is represented as

$$Z_i = \exp \left[\beta \sum_{k=1}^N J_{ij} \sigma_i(t) \sigma_k(t) \right] + \exp \left[-\beta \sum_{k=1}^N J_{ij} \sigma_i(t) \sigma_k(t) \right] \quad (3.10)$$

with $\exp[x] = e^x$ simply being the exponential function.

This equation can be further simplified by setting

$$C_i(t) = \beta \sum_{k=1}^N J_{ik} \sigma_k(t) \quad (3.11)$$

giving:

$$\ell(J, \beta) = \frac{1}{t_{max}} \sum_{t=1}^{t_{max}} \sum_{i=1}^N C_i(t) \sigma_i(t) - \ln(e^{C_i(t)} + e^{-C_i(t)}) \quad (3.12)$$

The gradient ascent scheme on J can be computed by taking the partial derivative of ℓ with respect to J_{ij} :

$$\frac{\delta \ell}{\delta J_{ij}} = \frac{\beta}{t_{max}} \sum_{t=1}^{t_{max}} (\sigma_i(t) \sigma_j(t) - \sigma_j(t) \tanh(C_i(t))) \quad (3.13)$$

Then the connectivity matrix J is updated as:

$$J_{ij}^{n+1} = J_{ij}^n + \alpha \frac{\delta \ell}{\delta J_{ij}} \Big|_n \quad (3.14)$$

where n is the iteration of the gradient ascent and α is the learning rate.

This procedure allows the fitting of a probability distribution onto the pMEM to calculate the matrix J , thus inferring connectivity using a complex model. Pseudo likelihood-maximisation is a method that is commonly used in neuroscience to infer connectivity from neural recordings due to its computational efficiency [78, 24, 28], and we employ this method in our investigation of disrupted criticality in the AD brain.

3.2.7 Hyperparameter Optimisation

The optimisation process involves gradient ascent to optimise the connectivity matrix J over a range of values of the inverse temperature β . The pMEM is then simulated using the Metropolis-Hastings Monte-Carlo algorithm at each β where the simulation paradigm can be split into two phases: the phase equilibration for a number of n_{seq} timesteps which allow the system to stabilise; and then followed by the simulation phase for a number of n_{sim} timesteps. The Metropolis-Hastings Monte-Carlo algorithm is widely used to simulate probabilistic systems [36, 50]. In this algorithm, we iterate through spins on a random basis and allow them to flip upon meeting these conditions: (i) if it is energetically favourable or (ii) based on a random probability that increases with temperature. During the equilibration phase, the spins are allowed to flip, but no metrics are recorded, and metrics such as functional connectivity are only calculated over the simulation time series. Each timestep comprises 116 Monte-Carlo flips, ensuring that each region of interest (ROI) has an opportunity to flip once on average per timestep. After each simulation is completed, i.e., the equilibration followed by simulation steps are done, the loss and gradient are calculated as mentioned above (in Section 3.2.6) and applied to optimise J . This is a single iteration of gradient ascent, and n_{iter} such iterations are performed. The pseudocode for the Monte-Carlo simulation is given in Algorithm 1.

Additionally, an early-stopping criterion is implemented for the gradient ascent, where the normalised Frobenius norm of the gradient is calculated. If this value drops below a certain threshold ϵ_{GA} at any step, the gradient ascent is stopped as the gradient has now converged. The convergence criteria can be written as:

$$\frac{\|\Delta\|_F}{N \cdot (N + 1)} < \epsilon_{GA} \quad (3.15)$$

where $\Delta = \frac{\delta \ell}{\delta J_{ij}}$ is the computed gradient, $\|\cdot\|_F$ represents the Frobenius norm, N is the number of RoIs, and ϵ_{GA} is the threshold value. The Frobenius norm for a matrix $A_{M \times N} = \{a_{ij}\}$ can be calculated as

$$\|A\|_F = \sqrt{\sum_i^M \sum_j^N |a_{ij}^2|}.$$

The details of the parameters used for optimisation are given in Table 3.2.

Algorithm 1 Monte Carlo Simulation using the Pairwise Maximum-Entropy Model

```

0 procedure INITIALIZE(spins, J)
0   Initialize spins randomly or with a specified configuration
0 end procedure
0 procedure CALCULATEENERGY(spins, J)
0   energy  $\leftarrow$  0
0   N  $\leftarrow$  length of spins
0   for i  $\leftarrow$  1 to N do
0     for j  $\leftarrow$  i + 1 to N do
0       energy  $\leftarrow$  energy + J[i][j] · spins[i] · spins[j]
0     end for
0   end for
0   return energy
0 end procedure
0 procedure MONTECARLOSTEP(spins, J, T)
0   Randomly select a spin
0   current_energy  $\leftarrow$  CALCULATEENERGY(spins, J)
0   Flip the selected spin
0   new_energy  $\leftarrow$  CALCULATEENERGY(spins, J)
0   delta_energy  $\leftarrow$  new_energy – current_energy
0   if delta_energy < 0 or RANDOM(( )) < exp(–delta_energy/T) then
0     Accept the flip
0   else
0     Reject the flip
0   end if
0 end procedure
0
0 for step  $\leftarrow$  1 to n do // Main Monte Carlo simulation loop
0   // Perform N Monte Carlo steps on average (determined by temperature T)
0   for i  $\leftarrow$  1 to N do
0     MONTECARLOSTEP(spins, J, T)
0   end for
0   M  $\leftarrow$  CALCULATEMAGNETISATION(spins)

```

```

0  $\chi \leftarrow \text{CALCULATE\_SUSCEPTIBILITY}(spins)$ 
0 end for
0
=0

```

Parameter	Value
Equilibration Iterations (n_{seq})	500
Simulation Iterations (n_{sim})	1000
Gradient Ascent Iterations (n_{iter})	1000
Convergence Threshold (ϵ_{GA})	0.0001
Learning Rate (α)	0.05
Inverse Temperature Range (β)	(0.10, 0.30, ..., 1.10, 1.20, 1.22, ..., 1.70, 1.80, 2.00, ..., 4.00)
No. of Flips per Timestep	116

Table 3.2: Parameters for Gradient Ascent on J

From the simulated time series at each iteration of gradient ascent, the simulated functional connectivity, denoted as $FC_{sim}(\beta)$, is computed as defined previously. The value of β that maximizes the Pearson correlation (denoted by r) between the simulated functional connectivity $FC_{sim}(\beta)$ and the observed functional connectivity FC_{obs} obtained from fMRI data is determined as follows:

$$\beta_{best} = \underset{\beta}{\operatorname{argmax}} [r(FC_{sim}(\beta), FC_{obs})] \quad (3.16)$$

Thus, the parameter β is swept to generate a landscape of reconstruction accuracy r , which will allow us to study the ability of the model to capture dynamics accurately across a range of temperatures and select the J matrix for the best-performing β_{best} .

3.2.8 Archetype Construction

In order to study the proximity to criticality, archetypes of each of the two classes are constructed. The archetype is defined by the connectivity matrix J obtained from the process of pseudo-likelihood maximisation. The activity pattern of each subject $\sigma^a(t) = (\sigma_1^a(t), \dots, \sigma_N^a(t))$ (where a is the index of

the subject) is concatenated to form a single activity pattern corresponding to the class - AD or CN.

$$\sigma^c(t) = \begin{cases} \sigma^1(t) & \text{if } 1 \leq t \leq t_{max} \\ \sigma^2(t - t_{max}) & \text{if } t_{max} + 1 \leq t \leq (2t_{max}) \\ \dots & \\ \sigma^{K_c}(t - (K_c - 1)t_{max}) & \text{if } ((K_c - 1)t_{max}) + 1 \leq t \leq (K_c t_{max}) \end{cases} \quad (3.17)$$

where c is either AD or CN and K_c is the total number of subjects belonging to the respective class. The functional connectivity FC_{obs} is calculated separately for each class over this combined activity pattern and is used in the optimisation process. In addition to that, a global archetype (*Global*) utilising data from all the subjects (both AD and CN) is also computed to serve as an overall benchmark. This activity pattern is then fit to the pMEM in order to calculate J , which represents the entire class.

3.2.9 Magnetisation and Susceptibility

The key observable in the simulation is the magnetisation of the lattice, which is defined as the average spin. The magnetisation per site can be calculated as:

$$M = \sum_{i=0}^N \langle \sigma_i \rangle \quad (3.18)$$

where $\langle \sigma_i \rangle$ is the time average of the time-series $\sigma_i(t)$. Average magnetisation of the lattice is the most straightforward order parameter of the system, and it can represent the order of the system in the ferromagnetic-paramagnetic transition.

The other important variable computed is the magnetic susceptibility of the lattice. The susceptibility is the variance of the magnetisation and can be defined as:

$$\chi = \frac{1}{\beta} (\langle M^2 \rangle - \langle M \rangle^2) \quad (3.19)$$

Susceptibility describes the sensitivity of the magnetisation of the system and is a measure of how easily the system can be magnetised on the application of an external field. This quantity is of particular interest to us as it exhibits interesting behaviour near criticality. In the Ising model, as we approach the critical temperature, i.e., as $T \rightarrow T_c$, there is a sharp increase in the number of fluctuations of the magnetisation. During this stage, the system is very sensitive to changes as the second-order phase transition approaches at $T = T_c$. In the immediate vicinity of T_c , the susceptibility of the system is expected to diverge and follow a power-law distribution, which can be expressed as:

$$\chi \propto |T - T_c|^{-\gamma} \quad (3.20)$$

where γ is the critical exponent. Hence, the susceptibility of the system peaks at T_c . The peak of the susceptibility-temperature curve allows us to estimate the T_c of a system.

Parameter	Value
Equilibration Iterations (n_{seq})	10000
Simulation Iterations (n_{sim})	10000
Convergence Threshold (ϵ_χ)	0.005
Inverse Temperature Range (β)	(0.10, 0.11, ..., 1.10, 1.20, 1.30, ..., 1.60, 1.80, 2.00, ..., 4.00)
No. of Flips per Timestep	116

Table 3.3: Simulation Parameters for M and χ Calculation

In order to study the susceptibility and magnetisation of the system, we first estimate the connectivity strengths J for a given archetype. We can then simulate a Sherrington-Kirkpatrick model in a Metropolis-Hastings Monte-Carlo simulation across various inverse temperature values (β) using the characteristic J calculated at β_{best} from the hyperparameter optimisation step. The simulation (for a given β) is first run for a set number of equilibration iterations (n_{seq}) where no calculations are recorded, and the spins are allowed to flip to come to a stable state, and then simulated for a set number of simulation iterations (n_{sim}) where the metrics are recorded. An early-stopping convergence criterion is implemented on susceptibility for the simulation wherein once the susceptibility value stabilises, the simulation is allowed to stop before the maximum number of simulation iterations are reached. The simulation stops when the criteria $\frac{STD(\chi)}{Mean(\chi)} < \epsilon_\chi$ is met where ϵ_χ is a set threshold. The parameters for this simulation are listed in Table 3.3. For each temperature, we calculate the average magnetisation and susceptibility, resulting in an M vs T and a χ vs T curve, which will allow us to analyse these systems.

3.3 Results

3.3.1 Reconstruction

The first step involves sweeping over a range of β values and optimising J for each value. From these values, we then select the β and J pair such that the functional connectivity FC_{obs} is best recreated. To quantify the quality of emulation of the empirical data, the reconstruction accuracy metric is used. The

reconstruction accuracy $r(FC_{obs}, FC_{sim}(\beta))$ is a simple Pearson correlation was calculated between the empirical functional connectivity of the archetype (FC_{obs}) and the functional connectivity derived from the simulation using the characteristic J obtained from the gradient ascent at the β value (FC_{sim}). We observe a noticeable peak in the reconstruction accuracy values of both the AD and the CN classes. The peaks occur $\beta_{r,AD} = 1.56$ with $r(FC_{obs}, FC_{sim})_{AD} = 0.957$ for the AD archetype and $\beta_{r,CN} = 1.60$ and $r(FC_{obs}, FC_{sim})_{CN} = 0.966$ for the CN class (represented in Fig. 3.1). Additionally, a global archetype is also computed, which contains all the subjects. This archetype acts as a general benchmark for the entire dataset. The peak for the global archetype was found to be at $\beta_{r,Global} = 1.4$ with $r(FC_{obs}, FC_{sim})_{Global} = 0.945$. The functional connectivity is hence reconstructed to a very high degree of accuracy.

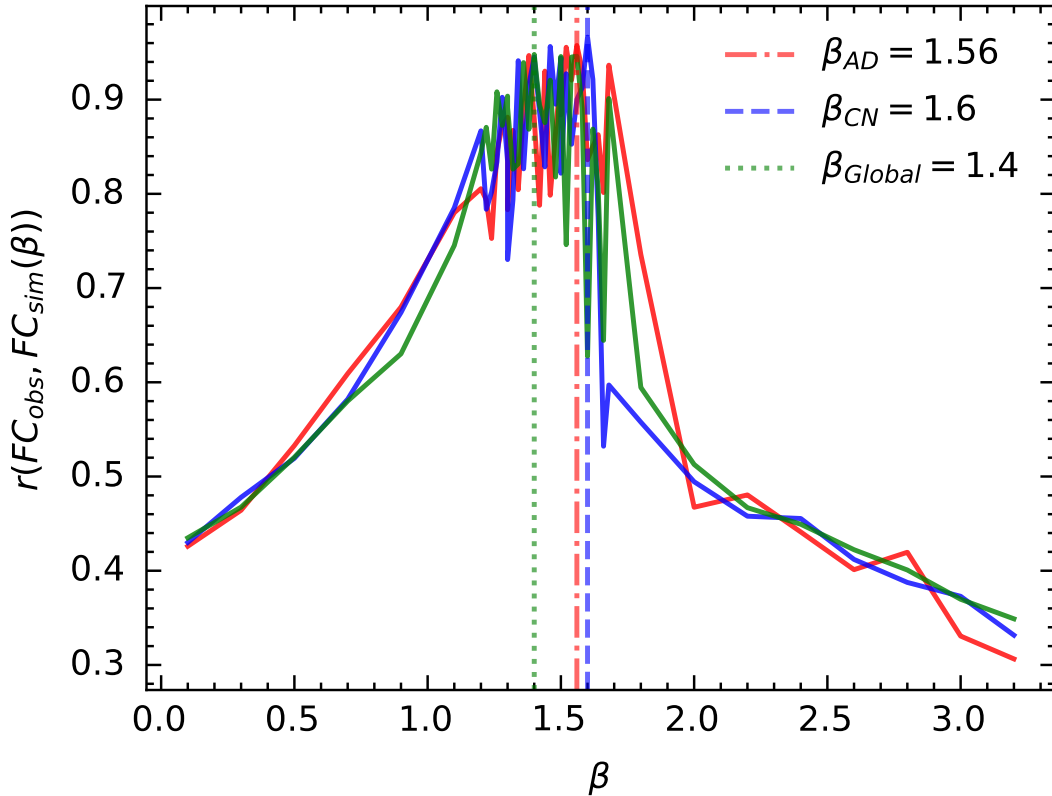


Figure 3.1: Reconstruction Accuracy

Pearson correlation between FC_{obs} and the derived connectivity matrix J at the inverse temperature of maximum reconstruction accuracy (β_r) was also calculated for both classes. The correlation obtained for AD was $r(FC_{obs,AD}, J_{AD}) = 0.393$ and for CN was $r(FC_{obs,CN}, J_{CN}) = 0.346$, and $r(FC_{obs,Global}, J_{Global}) = 0.362$. The correlation of J with the actual functional connectivity is quite weak, suggesting that the pMEM is able to capture the underlying factors required to recreate the dy-

namics to an exceptional extent as evidenced by the high $r(FC_{obs}, FC_{sim})$ values for all classes. This is consistent with other works which have found similar results using the maximum-entropy principle [24]. This matrix has often been found to be correlated with structural connectivity, but this calculation is outside the scope of this work as there was no structural (DTI) data available for the selected subjects. These correlations represent that the connectivity matrix is not simply a proxy for functional connectivity but is able to capture signatures of dynamics between the RoIs, reinforcing our rationale for using the pairwise maximum-entropy model.

3.3.2 Magnetization and Susceptibility

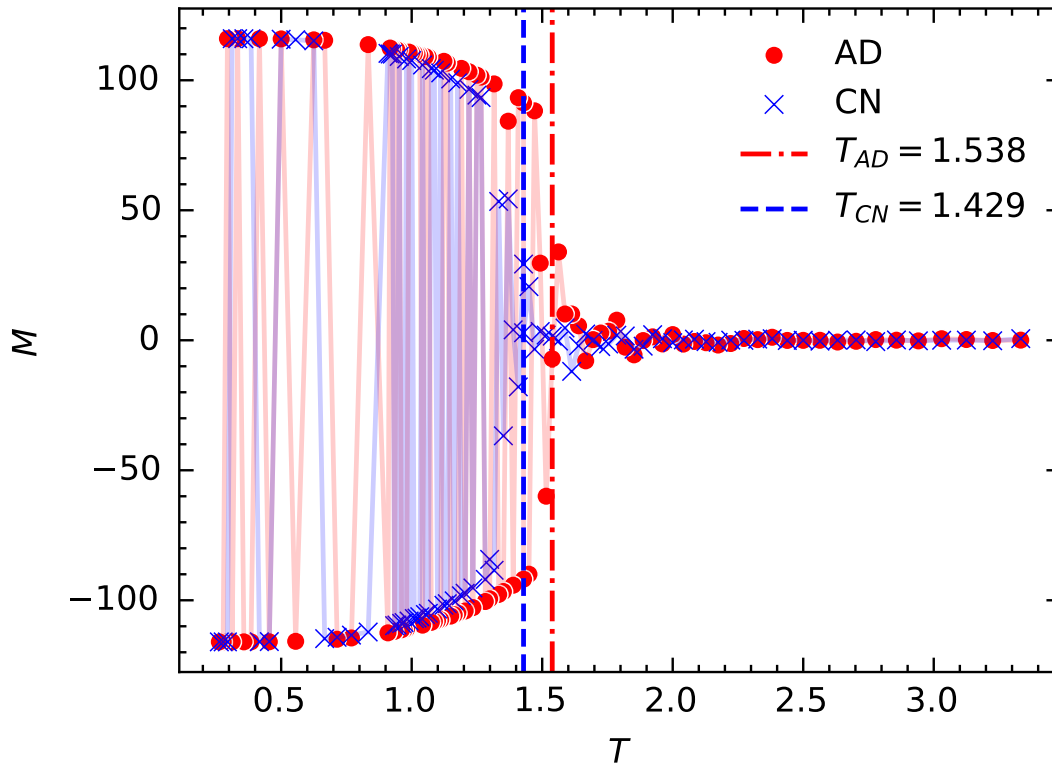


Figure 3.2: Variation in Average Magnetization with Temperature

The average magnetisation of the archetypes was calculated by simulating the pMEM at different temperatures with the J derived from the earlier hyperparameter optimisation. Fig. 3.2 visualises the average magnetisation of the two classes against the temperature $T = \frac{1}{\beta}$. It is apparent that in the low-temperature regime, there is a large amount of fluctuation between positive and negative magnetisation values, i.e., between average spins of +1 and -1. This non-zero average magnetisation occurs due to the spins having a strong tendency to align with each other. Most of the spins either become +1 or -1

throughout the simulation, leading to a highly polarised system. At the lowest temperatures ($T < 0.5$), the spins almost instantly align with each other, leading to an M value almost equal to ± 1 .

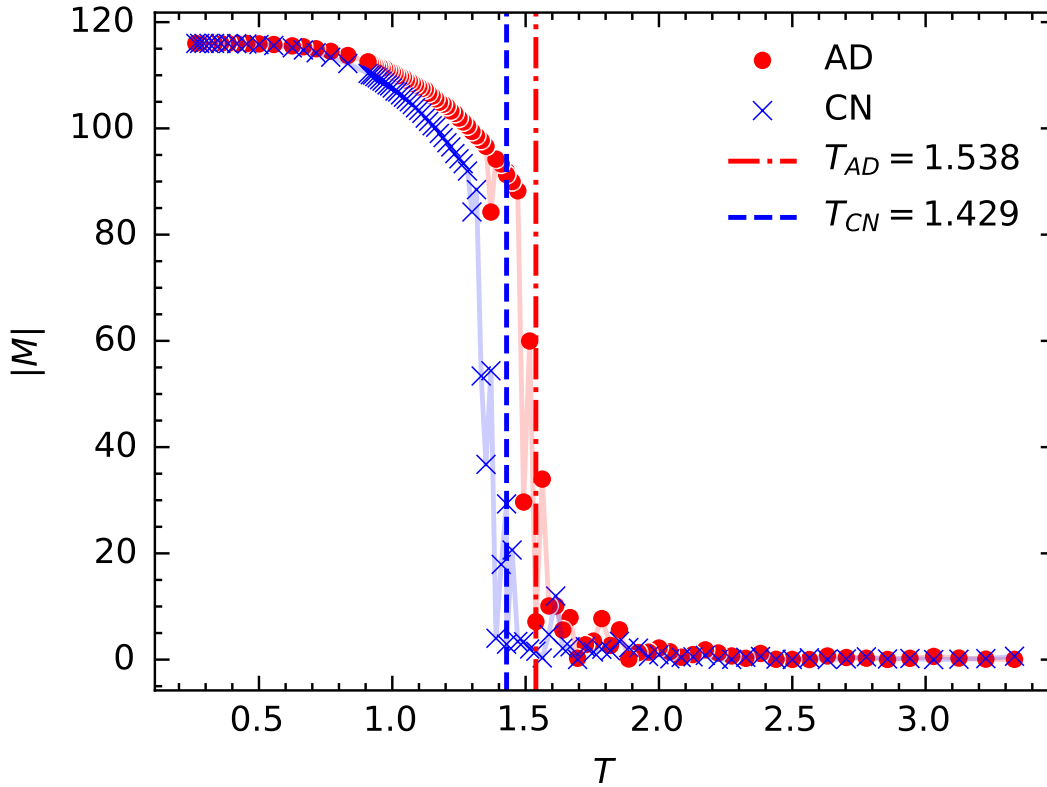


Figure 3.3: Absolute Average Magnetization vs Temperature along with critical Temperature marked using the dotted-dashed lines

To more clearly visualise the overall magnitude of polarisation, the absolute value of the magnetisation, $|M|$, is plotted in Fig. 3.3. As the temperature increases, the randomness introduced to the system increases, resulting in a lesser degree of polarisation. After a certain point, the randomness is so high that the spins do not tend to align with each other at all. This leads to an average magnetisation nearly equal to 0, i.e., $|M| \approx 0$. The temperature is high enough for there to be random flips at nearly every step of the simulation.

We observe two distinct regions in these plots. The left half of the plot corresponding to low temperatures has fluctuations, whereas the right half of the curve is almost static. There is a rough separation along the temperature axis into two distinct regimes. These regimes are the ferromagnetic and the paramagnetic phases, and the boundary at which it transitions from one to the other can be roughly demarcated. This boundary is known as the phase transition and is marked by the critical temperature T_c .

This temperature is chosen such that:

$$T_c = \operatorname{argmax}_T [\chi(T)] \quad (3.21)$$

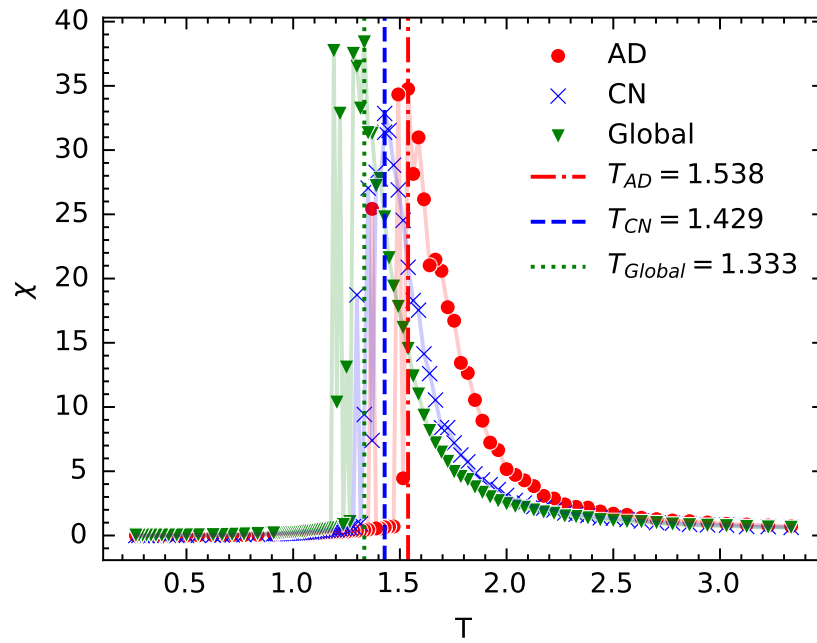
The temperature range can now be split into two clearly separated domains for a more detailed study according to the critical temperature T_c .

Fig. 3.4 shows the susceptibility of the system as the temperature varies. The corresponding results are tabulated in Table 3.4. There is negligible susceptibility in the low-temperature regime, corresponding to strong polarisation in one direction. In this phase of ferromagnetism, the system is resistant to change as all the spins align with each other, and an external field cannot influence it easily. As the temperature is increased, there is a sharp rise in susceptibility.

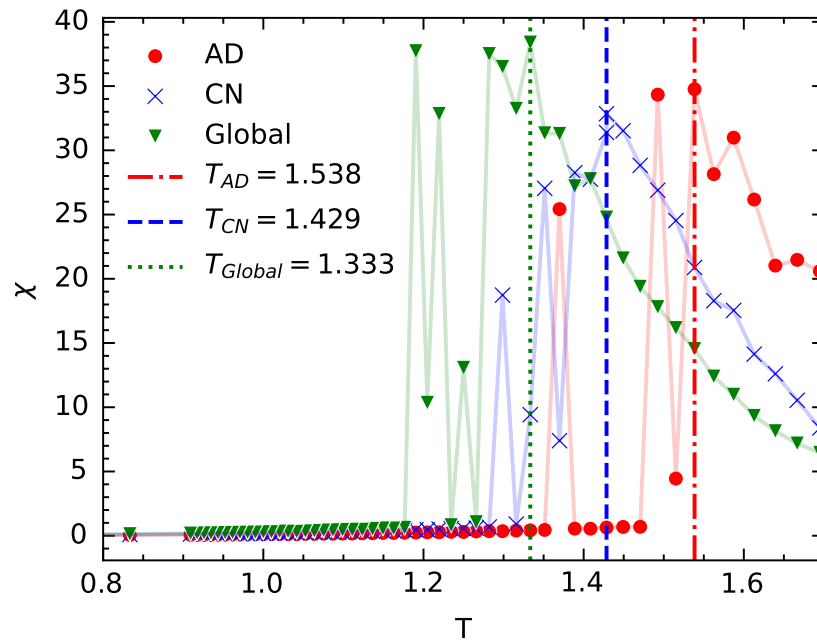
Past the T_c , we note a gradual decrease in the susceptibility, eventually plateauing at $\chi = 0$. As the system enters the paramagnetic phase, it is more vulnerable to external stimuli since the spins do not strongly align with each other, and strong randomness leads to lesser polarisation. A few random flips might allow the system to influence connected spins and align with the external field.

At the critical temperature (or the critical state), however, the Ising model undergoes a second-order phase transition - a transition where order parameters such as magnetisation smoothly transition from one value to the other. Here, there exists a delicate balance between the ordered (ferromagnetic) and disordered (phases). The system is not too resistant to changes as in the ferromagnetic phase since the magnetisation is not strongly polarised. It is also not too disordered to the point where randomness dominates. Therefore, in the critical state, the system is the most vulnerable to change and is able to respond quickly to external stimuli. Hence, this is the state that the resting-state brain is hypothesised to operate at - an intricate balance between order and chaos where its capacity to respond to stimulus is maximised.

At higher temperatures, the system has a larger amount of randomness and hence cannot be polarised as easily. This means that a system at higher temperatures is less malleable and requires stronger stimuli to cause a change in state.



(a) χ vs T plot: The peaks of susceptibility are $\chi_{AD} = 34.756$, $\chi_{CN} = 32.849$, and $\chi_{Global} = 38.390$



(b) A closer look at the near T_c regime of χ vs T : A distinctive discontinuity is observed at T_c for all three classes

Figure 3.4: Susceptibility vs T along with critical Temperature (marked using the dotted-dashed lines)

Detail	Range	AD	CN	Global
Critical Temperature	T_c	1.538	1.429	1.333
Magnetisation ($ M $)	$[T = T_c]$	7.129	2.906	6.383
$Mean(M) \pm STD(M)$	$[T < T_c]$	105.336 ± 13.887	98.854 ± 24.662	96.354 ± 27.943
$Mean(M) \pm STD(M)$	$[T > T_c]$	2.871 ± 5.893	1.785 ± 3.576	1.562 ± 3.190
$Median(M)$	$[T < T_c]$	109.331	106.859	105.527
$Median(M)$	$[T > T_c]$	0.684	0.555	0.541
Susceptibility (χ)	$[T = T_c]$	34.756	32.849	38.390
$Mean(\chi) \pm STD(\chi)$	$[T < T_c]$	1.214 ± 5.325	2.83 ± 7.641	4.165 ± 10.610
$Mean(\chi) \pm STD(\chi)$	$[T > T_c]$	7.783 ± 8.825	6.908 ± 8.572	7.723 ± 9.306
$Median(\chi)$	$[T < T_c]$	0.139	0.213	0.255
$Median(\chi)$	$[T > T_c]$	3.084	2.624	2.829

Table 3.4: Magnetisation and Susceptibility Results

We observe that the susceptibility of the system shows a sharp peak at the critical temperature for both the AD and CN classes. This T_c also coincides with the point of phase transition in the magnetisation curve. For the AD archetype, $T_c = 1.538$ was obtained, and $T_c = 1.429$ was obtained for CN. The global archetype yielded a critical temperature of $T_c = 1.333$. The difference between the AD and CN temperatures is $\Delta T_{AD,CN} = 0.109$. Upon testing between random splits of two groups to establish the significance of this number, we obtained differences of $\Delta T_{random} = 0.073 \pm 0.046$, thereby telling us that this difference is overall on the higher side of random, its statistical significance is weak at best.

From the T_c obtained, we observe that $T_c^{CN} < T_c^{AD}$, suggesting that the Alzheimer’s archetype requires more potent stimuli than the control group. The AD group is less malleable or “susceptible” to change. The implication, then, is that the control group is in a less disordered state and can respond more effectively to stimuli as compared to the AD group. The T_c of the global archetype is also calculated to be lesser than both the CN and AD subjects, with the difference between CN and the global T_c being lesser than that of AD. These results seem to suggest that the CN class is closer to T_c , and hence closer to criticality, albeit this difference is not significant. This weak distinction warrants further investigation as it does not support existing literature on the disruption in critical dynamics that occurs during the progression of Alzheimer’s Disease.

3.4 Discussion

In this work, we employed a statistical modelling approach using the Pairwise Maximum-Entropy Ising Model to study the disruption in proximity to criticality caused by affliction of Alzheimer’s Disease. Resting-state fMRI data from the ADNI-2 dataset was used, containing 34 AD subjects and 55 CN subjects. The archetype of each of the classes was constructed by utilising all the subjects.

The hyperparameter inverse temperature (β) was first optimised to find the ideal Ising connectivity J for each archetype. A gradient ascent approach using the pseudo-likelihood-maximisation process was applied at each value of the hyperparameter to derive the J for the archetypes, which was then used in a Metropolis-Hastings Monte-Carlo simulation to generate functional connectivity (FC_{sim}). This FC was refined to recreate the empirical functional connectivity of each archetype (FC_{obs}), and the J matrix corresponding to the maximum reconstruction accuracy ($r(FC_{obs}, FC_{sim})$) was selected. We observed that the reconstruction accuracy values were high ($r_{AD} = 0.957$ and $r_{CN} = 0.966$) for both classes, with the empirical functional connectivity being reconstructed almost completely.

Once J is fixed, the system is simulated at various temperatures T , and the magnetisation as well as susceptibility of the system is calculated at each T value. For each of the two archetypes, the magnetisation shows two distinct regimes along the T -axis. The low-temperature regime displays considerable oscillations in the magnetisation value, and the magnitude of these oscillations gradually decreases as the temperature is increased. At high temperatures, we note a sharp decrease in oscillation, which then fluctuates at low magnitudes until the point where no oscillations are displayed past a specific temperature and the overall magnitude of average magnetisation $|M| = 0$.

The susceptibility curves start off with negligible susceptibility at low temperatures (in the ferromagnetic phase) and display a sharp increase up to a specific temperature where it peaks. After the peak, in the high-temperature regime (paramagnetic phase), there is a gradual decline in susceptibility as it returns to 0. The critical temperature T_c is then selected as the peak inflexion point in the susceptibility curve. At this point, the system is noted to be most vulnerable to change and can effectively respond to stimulus. We obtain the critical temperatures $T_c^{AD} = 1.538$ and $T_c^{CN} = 1.429$. The higher T_c of AD suggests that its capacity to respond to stimulus is hindered as compared to the control subjects CN, thereby pushing it away from the ideal critical state. However, this difference does not seem to be as significant as expected. It is possible that the ferromagnetic-paramagnetic phase transition is too simplistic of a paradigm to understand the complex dynamics of the human brain and hence warrants a deeper inquiry into the nature of the phase transition at the critical state.

The susceptibility of a system is essentially the change in average magnetisation of it. This change serves to quantify how sensitive the system is to external changes. In complex systems that involve frustrated and non-uniform interactions, the spins struggle to align together in any meaningful way. Hence, the response of individual regions of spins to an external field can vary significantly throughout

the lattice, thereby making the average change in magnetisation a much more complicated property than it is in simple Ising systems. The complexity makes it so that this property is simply not as sensitive in a spin-glass-like phase transition as it is in a simple Ising-like phase transition. Therefore, this necessitates a deeper inquiry into the spatial dynamics within the human brain. Determining the nature of the critical phase transition through the study of spatial growth will allow us to gain great insight into neural function and enable us to study it in a significantly more nuanced fashion.

Chapter 4

Spatial Aspects of Criticality in fMRI

4.1 Introduction

The brain exhibits highly complex dynamics at rest, where the capacity for information processing and response to stimuli are maximised. It exhibits emergent behaviour through intricate interactions between neurons. This complex functioning is often likened to that found in statistical mechanical systems, as these systems comprise a large number of interacting components whose collective behaviour cannot be simplified to the sum of their parts. This sets the stage to study the brain as a system operating at a phase transition - a point where the system has the potential to undergo drastic changes and exhibits highly complex dynamics - and has given rise to the notion of the brain operating at a critical state.

The simplest model often used to study criticality is the Ising model. The basic Ising model is composed of a lattice of spins. These spins can take values of either up (+1) or down (-1). In the simple version, these spins typically only interact with their nearest neighbours in the lattice. This model can be extended further to interact with spins farther away. These connections generally tend to be defined uniformly and cause the other interacting spins to align towards the same state as the system evolves to minimise its energy. However, the evolution of the system is hindered by randomness in the form of temperature. The temperature causes spins to flip randomly - the higher the temperature, the more likely this random flip occurs. At low temperatures, all the spins align with each other due to the connections causing their neighbouring spins to align to their state. This results in most spins having the same state and is known as the “ferromagnetic” phase, where there is a net magnetisation of the system in one direction. At high temperatures, the randomness dominates, and most of the spins do not align. This results in a “paramagnetic” phase with the net magnetisation typically being zero.

The transition between these two phases occurs at a certain temperature and is defined as the phase transition boundary. At this tiny range of temperature(s), the system could either tend to align or misalign, and it is extremely sensitive to perturbations. A flip in just one of the spins could cause changes at a much larger scale throughout the system. This state of the system is known as the “critical state”. In the

Ising model, the critical state is at the phase boundary between the ferromagnetic and the paramagnetic phases. It exhibits some interesting phenomena, such as scale-free behaviour in various metrics. The existence of this kind of criticality between the two states is referred to as “Ising criticality”.

A more complex variant of the Ising model is the Sherrington-Kirkpatrick model or the SK model for short. In this model, the interactions between the spins are not limited to the nearest neighbours. There can be interactions between any two spins in the system with varying degrees of strength. Given the right set of conditions where there is disorder in the interactions, i.e., the interactions between spins are random and even negative, there can be many competing interactions within the system. Compared to the case in the Ising model at low temperatures, where most of the spins would align to the dominant state, there could be numerous spins out-of-phase with the dominant state in the SK model. Flipping these spins to conform with the other spins could, in fact, lead to an increase in energy due to competing interactions, and the system finds itself in a state of local minima within the energy landscape. An immense amount of random spin flips might be required to get the system out of this minima. This phase is then known as the “spin-glass” phase. The existence of this phase complicates the phase diagram as there are now three phases instead of the two in the Ising model. This would lead to a complex phase boundary at the interface of the three, which could be approached from numerous directions. A phase transition of this kind could lead to further convoluted behaviour and cannot simply be studied like the Ising model. The existence of the spin-glass phase leads to a new transition boundary, and criticality in this type of system is referred to as “spin-glass criticality”.

The Ising model undergoes a second-order phase transition at T_c and displays collective behaviour. As the temperature is brought closer to T_c , localised regions of the same spin known as ‘domains’ emerge. Domains form due to the elaborate interaction dynamics between the spins and the random behaviour of the temperature parameter. The magnetisation is uniform within a domain, and that of its neighbouring domains is opposite in direction. In a spin-lattice system, we can analyse the formation of these domains and characterise them using their spatial correlations. Quantifying the spatial correlation will allow us to study the behaviour near criticality in greater detail. Numerous metrics, such as the susceptibility, correlation lengths, and specific heat are typically expected to follow a power-law distribution as we approach criticality [15]. Mathematically, the power-law can be expressed as $\xi \propto |T - T_c|^{-\nu}$ where ξ is the property in question and ν is the criticality exponent associated with it. In particular, we study here two properties of the system at criticality: domain formation and self-averaging.

Domains are regions of uniform and distinct magnetisation that emerge due to complex interactions between the spins. All the spins are oriented in the same direction throughout a single domain. The neighbouring domains will have spins in the opposite direction. Networks of correlated and anti-correlated regions have been shown to exist in the brain, which can be likened to the domains found in spin-lattice systems. The dynamics of these domains typically depend on the proximity to criticality and spatial

propagation of signals through the brain. The formation of domains in spin systems can be investigated to characterise criticality through their spatial and temporal behaviours [15].

Self-averaging is a fundamental concept in thermodynamics when studying systems at scale, and it can be observed in disordered systems. It is the phenomenon where the averaging of measurements leads to more reliable and stable estimates of underlying signals or phenomena. The statistics of the system tend to improve when averaged over a larger system size [4]. Self-averaging (or the lack thereof) can be considered a proxy for closeness to criticality. Given the same realisation size, the closer the system is to the critical state, the worse the self-averaging would be in the system due to increasing long-range correlations. Self-averaging can be studied even in systems with quenched disorder - such as the SK model here in question. Even with the inherent disorder, these systems exhibit self-averaging to a reasonable extent at criticality, and the examination of this self-averaging can give us useful insights into the nature of the system [77]. Hence, the extent of self-averaging within the brain is an important indicator of its criticality [104, 4]. The relative variance metric is used to quantify this extent.

Alzheimer's Disease is a neurodegenerative disorder characterised by cognitive decline and memory impairment. The disruption of neuronal connectivity - both functional and structural - plays a key role in the progression of this disease. Numerous studies have investigated connectivity alterations using various modalities. Resting-state connectivity studies using fMRI investigate the functional connectivity of the subject in a state where there is no stimulus, and the subject is typically in a resting position [3]. Disrupted connectivity within the default mode network (DMN), which is a set of brain regions associated with memory and introspection, has often been observed in these studies [60, 35]. Abnormal connectivity within other networks, such as the salience network and executive control network, have also been identified. Additionally, task-based studies have shown disrupted connectivity patterns in various cognitive domains affected by the disease, including working memory, attention, and language processing [92]. Structural studies such as diffusion tensor imaging (DTI) studies are also common in literature and have revealed alterations in structural connectivity in AD-afflicted subjects [67]. These disruptions are collectively linked to cognitive impairment and the progression of AD. Numerous studies have found links between changes in neural connectivity and disruption in critical-state functioning [44, 100, 85]. Hence, brains afflicted with Alzheimer's Disease have disrupted the functioning of the critical state, leading to a deviation from their proximity to the standard critical state.

Standard parameters such as susceptibility are often investigated in order to quantify the criticality in the human brain, which is posited to be similar to the one found in the Ising model. The critical-state phase transition that is typically investigated is the ferromagnetic-paramagnetic transition found in the Ising model. Motivated by deficient differences found in the susceptibility parameter between criticality-disrupted and cognitively normal subjects, we set out to investigate the nature of the phase transition (and, in turn, the nature of criticality) that the brain exhibits. We study the spatial aspects of criticality between

Alzheimer's-afflicted and normal subjects and quantify the distinction found. A similar approach is also used to quantify the temporal distinction. The distinction found in these two metrics would vary depending on the type of phase transition that the brain exhibits between the three phases typically found in Ising models - paramagnetic, ferromagnetic, and spin-glass. We focus on discerning the variations within these metrics between AD and CN subjects in order to classify the underlying criticality [69].

4.2 Methods

4.2.1 Datasets

The data used in this study is resting-state fMRI data from the Alzheimer's Disease Neuroimaging Initiative (ADNI) database [71]. Specifically, data from the ADNI-2 phase was used. The ADNI dataset is a widely used collection of neural data, including MRI, PET scans, biomarkers and genetic data. It is the collaborative effort of multiple institutions aimed at accelerating the diagnosis, treatment and understanding of Alzheimer's Disease. The portal at adni.loni.usc.edu was used for the collection of the data. The subjects selected were a mix of Cognitively Normal (CN) and patients with Alzheimer's Disease (AD). 34 AD and 55 CN subjects were selected, totalling 89 subjects. There were 121 AD and 243 CN scans in total, but only one scan was selected for each subject for generalisability. Each rs-fMRI scan has a corresponding structural MRI scan as well, which was used in the preprocessing. Resting-state data was selected as it is the most representative of the critical state of the brain. Without any stimulus, rs-fMRI captures spontaneous activity within the brain, which is a key phenomenon in criticality. It allows for exploration of the brain without any predefined hypotheses or stimulus design and is also easily extensible as it can be repeated without any significant prerequisites [51].

4.2.2 Preprocessing

The fMRI data underwent preprocessing primarily utilising tools from the FMRIB Software Library (FSL) [43, 83]. Initially, motion correction was performed employing FSL's MCFLIRT [42], aligning all volumes to the mean volume. This process yielded motion parameters and mean images as output. Subsequently, FSL's SliceTimer was utilised for slice-timing correction. The coregistration step encompassed several procedures:

1. Skull-stripping the anatomical image using FSL's BET
2. Segmenting it with FSL's FAST and thresholding the resulting white matter probability image
3. Pre-alignment and coregistration of the fMRI to the anatomical images using FSL's FLIRT
4. Applying the computed coregistration transformation to the functional and mean images.

The images were spatially smoothed using SPM with a full width at half-maximum (FWHM) of 5mm. Nipype’s ArtifactDetect algorithm [32] was employed to identify and separate artefacts from the functional images, utilising a norm threshold of 2 and a z-intensity threshold of 3. Finally, Nilearn [1] was utilised to compute and implement a brain mask, which employed the histogram of the mean fMRI image intensity, discarding the bottom 20% and top 15% of the histogram values.

4.2.3 Self-Averaging

The first of the spatial measures we shall study is self-averaging. Self-averaging is numerically well-researched in the realm of statistical physics. We can quantify the extent of self-averaging through the use of a metric known as “relative variance”. We transform the data into a suitable form to calculate relative variance and compare the evolution of the metric between the AD and CN classes.

4.2.3.1 Relative Variance (R_X)

Consider a system in the form of a flat array with S total points. Let the array be X . Then, each point in this array can be denoted by X_i where $i \in 1, \dots, S$. The metric Relative Variance (R_X) can be defined as such:

$$R_X = \frac{\Delta V}{[X]^2} = \frac{[X^2] - [X]^2}{[X]^2} \quad (4.1)$$

where [...] denotes the average over the points. The relative variance of a set of data is a measure of error which quantifies the amount of “noise” in the system. It is often used to quantify self-averaging in physical systems [4].

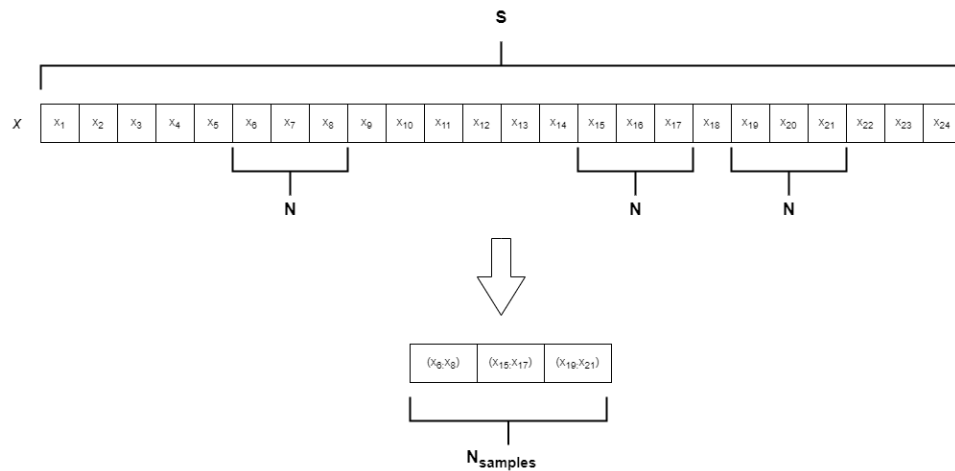


Figure 4.1: Visualisation of Subsystems Generated from the Primary System for R_X calculation.

In the system X , each observation X_i is derived by averaging over a set of realisations. Let each realisation be of size N , and let the primary system from which X is derived be labelled A . Then, each point in X can be defined as:

$$X_i = \frac{\sum_j^N = 1 A_{r+j}}{N} \quad (4.2)$$

where r is some offset representative of the realisation set in indices $\{r + 1, \dots, r + N\}$ and $0 \leq r \leq |A| - N$. Let this set be represented by $\{A\}_r = \{A_{r+1}, \dots, A_{r+N}\}$.

According to the Central Limit Theorem (CLT), the relative variance $R_X \rightarrow 0$ as the realisation size $N \rightarrow \infty$ in a self-averaging system. In such a case, the entire system can be completely described by the average $[X]$ as this average will be unchanging regardless of realisation size. Hence, self-averaging within a system can be investigated by generating derivative systems of varying realisation sizes from a single “primary system”. The process of splitting the system into subsystems is visualised in Fig. 4.1.

As the CLT stipulates, the relationship between R_X and N is in the form of a power-law where the exponent can determine the extent of self-averaging in the system:

$$R_X \sim N^{-\alpha} \quad (4.3)$$

For a system of independent and identically distributed (i.i.d.) spins, the relationship will always be an exact linear power-law, i.e., the exponent α will be exactly equal to 1. This is a system with perfect self-averaging. If $0 < \alpha < 1$, then the system is said to be experiencing weak self-averaging. The extent of self-averaging can be quantified by the difference between 1 and α . The closer α is to 1, the better the self-averaging in the system [62].

4.2.3.2 Generating Systems to Study Self-Averaging

In order to investigate self-averaging, we study the fMRI scan of each subject separately. All the scans are studied at the same time point $t = T$, which is varied. We can consider each scan at some point $t = T$ to be a system where each voxel is treated as a random variable. To simplify the problem, we can convert the 3-D volume of length L , width W and height H into a flat 1-D array of size $L \times W \times H$. There is a slight loss of spatial information here since the neighbours are not maintained in all dimensions, but it is an adequate approximation as the neighbours in a single dimension are still retained. Each point in this array now represents the voxel strength at that location. This flattening can be represented by the equation:

$$\text{index}(x, y, z) = i = x + y \cdot W + z \cdot W \cdot H \quad (4.4)$$

where x , y , and z are the coordinates of the voxel in the initial volume, and i is its position in the flattened array. From now on, we shall use the label “primary system” or the symbol A to refer to the flattened array in the context of a single scan taken at time $t = T$.

To investigate the effect of the realisation size of the system, we need to generate a series of derivative systems, each varying in their realisation size. Let this realisation size be N . To quantify self-averaging, we need to calculate a metric R_X for each of these systems.

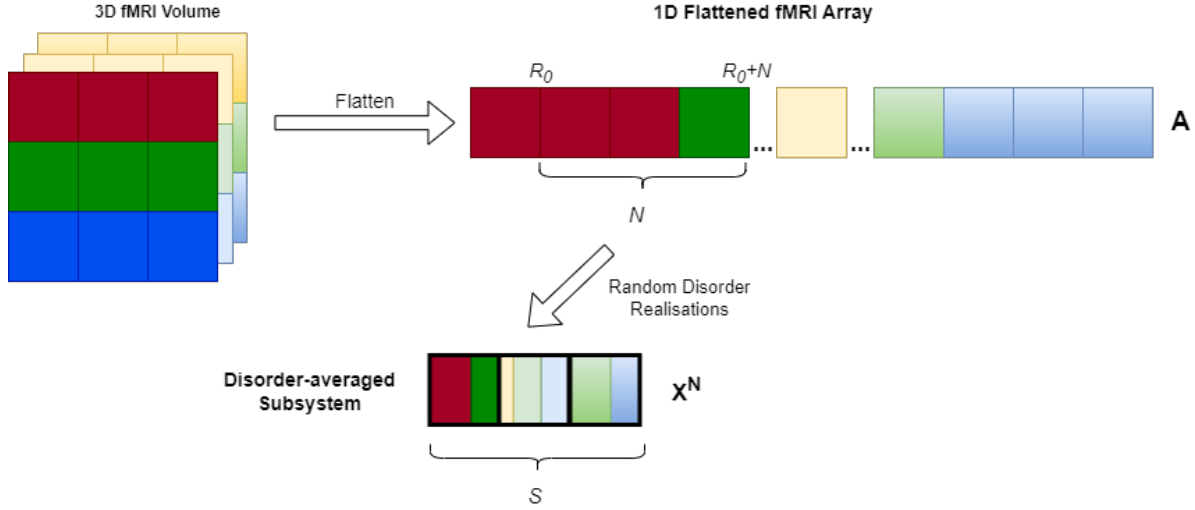


Figure 4.2: Generating subsystems from fMRI

First, we explain how these systems are generated. N represents the number of lattice points (A_i) that are averaged over to get one lattice point in the derivative system. That is, N points in the primary system correspond to a single point in a derivative system. Derivative systems can be generated from A by setting the parameter N . Although a theoretical maximum of $|A|/N$ points can be generated in the derivative system, we set the size of the derivative systems to a constant S as N will be varied.

Let us call a derivative system with realisation size as X^N . Then, each point in X_i^N where $i \in 1 \dots S$ corresponds to a realisation set A_r (according to the notation defined in the previous section). Thus, S such sets have to be generated, implying that S unique r values have to be generated. To generate a derivative system X^N , we generate a set of random integers $R \in \{0, \dots, |A| - N\}$ of size S . We also ensure that the realisation sets are non-overlapping, i.e., $|R_a - R_b| \geq N$ for $a, b \in \{1 \dots S\}$ and $a \neq b$. Thus, we now have S realisation sets of size N each, represented by $(A_r | r \in R)$. Then, the derivative system of size N can be defined as:

$$X_i^N = [A_{R_i}] = \frac{\sum_{j=R_i+1}^{R_i+N} A_j}{N} \quad (4.5)$$

N is varied at regular intervals (of V) to generate N/V such derivative systems. The relative variance R_X for each of these is then calculated. Additionally, a system of independently and identically-distributed (i.i.d.) random Gaussian spins - with mean $\mu = 1$ and standard deviation $\sigma = 1$ and the same size as the

flattened fMRI data - is generated to serve as a baseline for a system that exhibits perfect self-averaging behaviour.

Parameter	Value
Realisation Sizes Range (N)	1-1000
Interval Size (V)	2
Number of Realisations (S)	30
Number of Generated Subsystems (N/V)	500

Table 4.1: Parameters to Generate Systems for R_X Analysis

The parameters used for the generation of systems are listed in Table 4.1 A visualisation of this entire process is shown in Fig. 4.2. The evolution of this R_X with realisation size N is then studied to understand the nature of self-averaging within the primary system A .

4.2.4 Domain Formation

The next spatial measure we study is domain formation, which is the emergence and evolution of domains through the time series. We study both the quantity and the size of the domains. We use the following methods to compute these values. First, the spins for each time series were first binarised according to the method mentioned above. A domain is defined as a contiguous region of neighbouring sites containing the same spin value at a given time. Each site can then be mapped to a domain depending on its spin value at that time point.

To identify the domains, the Hoshen-Kopelman algorithm [41] was used. The Hoshen-Kopelman algorithm is a commonly-used algorithm for identifying clusters within a lattice. It is often used in materials sciences to study the microstructure of materials, in network analysis to find connected components, in transportation to identify traffic patterns, in social sciences to analyse social networks, and in many more fields as it is a fast and simple clustering algorithm which is extendable to higher dimensions. The pseudocode for this algorithm is given in Algorithm 2. A raster scan is performed throughout the lattice, and each spin site is assigned a cluster label based on its neighbours. The Union-Find data structure is used to store cluster labels, allowing the algorithm to function faster than $O(N \log N)$ (where N is the number of lattice sites). Each site is iterated through starting from one end of the lattice and going through to the other end in all dimensions. The algorithm conditionally assigns cluster labels to a site based on these rules:

- If it has a neighbour that shares the same spin:
 - If it is the only (or first-scanned) neighbour with the same spin, the label from that neighbour ($\text{Find}(a)$) is assigned to the current site.
 - If there exists another previously scanned neighbour with the same spin, the label from the previously scanned ($\text{Find}(a)$) is assigned to the current site. Then, this label is combined with the label of the currently-scanned neighbour ($\text{Find}(b)$), and are considered equivalent henceforth ($\text{Union}(a, b)$).
- If there are no neighbours sharing the same spin, the site is assigned a new, unique cluster label.

By the end of this scan, at every time point, we have a cluster label assigned to each spin of the lattice. We can now obtain cluster sizes (S_{dom}) and number of clusters (n_{dom}) for the lattice at that particular time-point.

Algorithm 2 Hoshen-Kopelman Algorithm for a 3-D Grid

```

0 procedure HOSHENKOPELMAN(grid)
0   current_label  $\leftarrow$  0
0   for each cell  $(i, j, k)$  in the grid do
0     if grid( $i, j, k$ ) is occupied then
0       left_label  $\leftarrow$  label of the left neighbor of  $(i, j, k)$ 
0       above_label  $\leftarrow$  label of the above neighbor of  $(i, j, k)$ 
0       front_label  $\leftarrow$  label of the front neighbor of  $(i, j, k)$ 
0       if left_label and above_label and front_label are all 0 then
0         current_label  $\leftarrow$  current_label + 1
0         label grid( $i, j, k$ ) with current_label
0       else if left_label is not 0 then
0         label grid( $i, j, k$ ) with left_label
0       else if above_label is not 0 then
0         label grid( $i, j, k$ ) with above_label
0       else if front_label is not 0 then
0         label grid( $i, j, k$ ) with front_label
0       end if
0     end if
0   end for
0   for each cell  $(i, j, k)$  in the grid do
0     if grid( $i, j, k$ ) is occupied then
0       label  $\leftarrow$  label of grid( $i, j, k$ )

```

```

0     root_label ← find the root label of label
0     label grid(i, j, k) with root_label
0     end if
0     end for
0 end procedure
0 procedure FIND_ROOT_LABEL(label)
0     while label is not the root label do
0         label ← label of the parent of label
0     end while
0     return label
0 end procedure
=0

```

Additionally, we also track the development of each cluster through time to characterise its size throughout its lifetime. Since the cluster labels vary at each time point, this problem is non-trivial. We iterate through each time-point in order to find the overlap of spin sites corresponding to each cluster g at time-point $t = k$ with every other cluster at $t = k + 1$ and calculate the number of overlap spin sites. A cluster with the label g at time-point $t = k$ is considered to be equivalent to a cluster h at time-point $t = k + 1$ if they have the maximal overlap. If there is a conflict, i.e., if there are two clusters at $t = k$ with maximal overlap at $t = k + 1$, the larger one is selected. The cluster labelling at the next time-point is done in descending order of maximal overlap. This allows small clusters to disappear and spontaneously appear as well. We now have a size evolution of each domain with time. Using this method, we determine the mean lifetimes of the largest domain for each subject. The largest domain ld is selected at time-point $t = 0$ as the one containing the largest number of spins. Then, the size-evolution of this domain S_{ld} is used to calculate the autocorrelation function $\langle S_{ld}(0)S_{ld}(t) \rangle$. This is fit to an exponential decay function, and the calculated decay constant τ_{ld} is taken as the mean lifetime of the largest domain for each subject.

4.2.5 Relaxation Times: τ Calculation

To characterise the temporal dynamics in the brain, the time correlation function of the signals was also studied as the relaxation behaviour of an fMRI signal has been shown to be a good indicator of its underlying dynamics. Studying its form can give us a good idea about the nature of relaxation occurring in the system. An exponential decay is typically observed in the case of fMRI signals. To quantify this exponential decay, the autocorrelation function of the signal from each voxel for every subject throughout

the scan is fitted to an exponential curve of the following form:

$$\rho(t) = A * \exp \left[-\frac{t}{\tau} \right] + B \quad (4.6)$$

The characteristic decay time τ is estimated using a least-squares fit method. A and B are additional constants to account for the scaling and offset and are therefore ignored. A smaller τ value would indicate faster decay, whereas a longer τ value would indicate slower decay. This can also show further insights into the nature of criticality of the system [103].

We also fit another curve known as a “stretched exponential”, also known as the Kohlrausch-Williams-Watts stretched exponential form, to the autocorrelation functions. This involves a two-step relaxation pattern. This is also fit as a comparison of the nature of relaxation with the standard simple exponential fit [103]. The stretched exponential is of the form:

$$\rho(t) = A * \exp \left[-\left(\frac{t}{\tau} \right)^\beta \right] + B \quad (4.7)$$

The characteristic relaxation time τ is estimated in a similar manner to the above, and the stretching exponential β is also calculated additionally, which quantifies the deviation from simple exponential behaviour. The stretched exponential represents a broader range of relaxation behaviours and is often employed to describe relaxation or decay in systems displaying complex dynamics, such as systems approaching criticality [9].

4.3 Results

4.3.1 Self-Averaging

The self-averaging behaviour of the system is an important marker of criticality since non-self-averageness is a characteristic marker of systems operating near the critical state. We study self-averaging within the system to verify that it is indeed functioning near the critical state and to look for distinctions between the self-averageness of AD and CN data. The relative variance of a system is a good measure of the stability of the signal and the amount of disorder or long-range correlations in it as mentioned above. We follow the procedure as described in Section 4.2.3. Derivative systems are generated for each subject from the primary system (which is the fMRI scan) of varying realisation sizes (N) with a set number of realisations (S) randomly selected per realisation size. N is swept over a range of values at regular intervals. The R_X value for the derivative system is then calculated according to Eq. 4.1.

We first compare the relative variance of each system (R_X) with N . Plotted in Fig. 4.3 is a plot of R_X vs $\log(N)$ averaged over Cognitively Normal (CN) and Alzheimer’s (AD) subjects for the time point

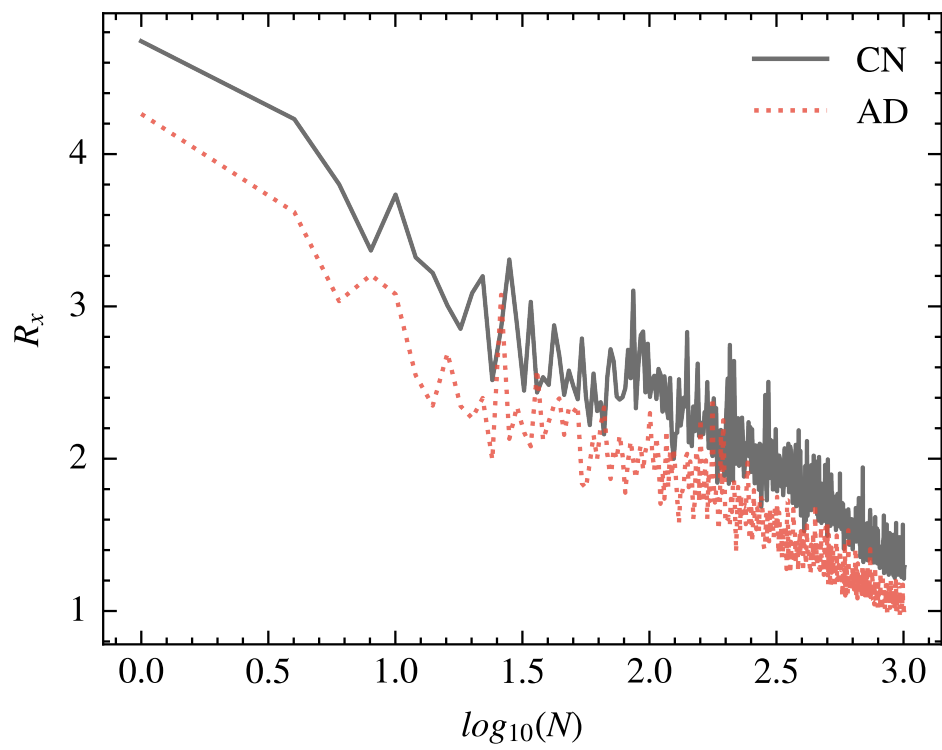


Figure 4.3: R_X vs N after averaging in log-space for $t = 80$

$t = 80$. The R_X values were first converted to the logarithmic space and then averaged over. These were then converted back into the normal space by taking their exponential. Hence, the R_X values plotted here are:

$$R_X(N) = \exp \left[\sum_i \log (R_X^i(N)) \right] \quad (4.8)$$

where $R_X^i(N)$ is the relative variance at realisation size N corresponding to the scan of subject i . This was done since the sensitivity of the R_X values is very high due to the scale, and the mean would diverge significantly due to the influence of outliers.

The power-law is characterised by the equation:

$$y = k \cdot x^a \quad (4.9)$$

A power-law-like relationship is expected between the relative variance and the realisation size at criticality [4], but it is not clearly identifiable here. It is unclear whether there actually is a power-law here as there is considerable variation throughout the range of values. We need to take a more detailed approach to investigate the existence of such a relationship.

A more in-depth analysis can be done by studying the log-log plot of the same. The power-law relationship spans a wide range of values, with varying densities across the y-axis. The variation in the trend is not easily visible to the human eye. Analysing the variables in a log-log plot, i.e., $\log(R_X)$ vs $\log(N)$, would allow us to observe the trends more clearly.

Any power-law relationship is transformed into a linear relationship in a log-log plot. The differences between CN and AD subjects can be quantified more clearly in a linear system, and it would also allow us to confirm if it is indeed a power-law. As mentioned earlier, we want to calculate the exponent α in the relationship $R_X \sim N^{-\alpha}$. To accomplish this, we can take advantage of the linear form of the log-log plot. The relationship is now:

$$\log(R_X) = \alpha \cdot \log(N) + \text{intercept} \quad (4.10)$$

Here, the relationship is in the form of a straight line as long as the power-law relationship is maintained. The intercept can be ignored since we are only concerned with the power-law exponent. Deviation from a straight line would indicate deviations from power-law behaviour, while the slope of the line would indicate the exponent in the power-law relationship. To compute this, we perform a linear fit on portions of the data to confirm that the slope remains the same. If there is a change in the slope, that would indicate a change in the nature of self-averaging within the system.

Plotted in Fig. 4.4 is the mean R_X of the subjects against the system size N in the log-log form. The scatter points indicate the mean values and the less opaque fill colours indicate the standard deviation of each point. All the R_X values were calculated for each subject by generating derivative systems (as

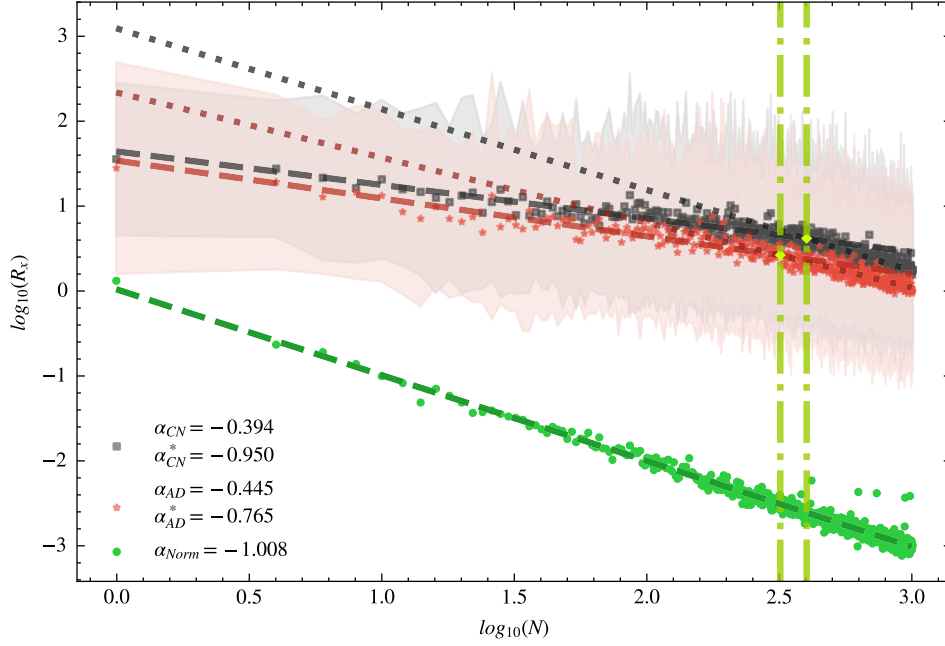


Figure 4.4: $\log(R_X)$ vs $\log(N)$ averaged over subjects for $t = 80$

described in 4.2.3.2) at a representative time point $t = 80$, and this behaviour is generalisable since similar trends were observed at all time-points.

We observe that R_X exhibits two distinct slopes for both the AD and CN cases: the first line (α) is fit on the first 50% of data, and the second line (α^*) is fit on the remaining 50% of the data. There is also another set of data: a primary system of spins generated from a random Gaussian distribution with $\mu = 1$ and $\sigma = 1$, which is displayed in dark green in Fig. 4.4. The line fit on this data seems to show no change and is a straight line with a slope of -1 , as expected from the power-law relationship of a self-averaging system. This means that the randomly generated system of independent spins experiences perfect self-averaging. In the case of our systems generated from fMRI data, however, we notice that the slope seems to undergo a significant transition. This shows a clear deviation from straight-line behaviour, which confirms that the nature of self-averaging within the system indeed changes as the realisation size changes.

For the CN case, we see the exponent $\alpha = -0.394$ and $\alpha^* = -0.950$. These two lines intersect at $N^* \approx 398$. For the AD case, $\alpha = -0.445$ and $\alpha^* = -0.765$ with the intersection point being $N^* \approx 315$. We notice that in both cases, the exponent approaches 1 as the realisation size increases. This demonstrates better self-averaging as the realisation size is increased. Although the size N^* is different for the CN and AD cases, it is around the same scale. These observations prompt us to conclude that an appropriately large system size needs to be chosen for fMRI studies in order to ensure stable, reliable

estimates of self-averaging.

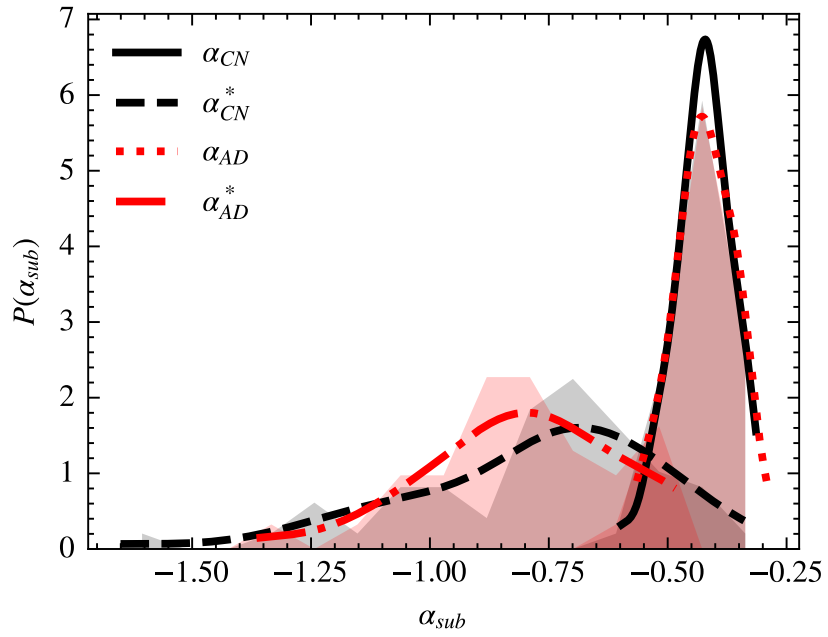
In order to visualise the results for each subject individually, we compute the slopes for the $\log(R_X)$ vs $\log(N)$ plots of each subject individually at every time-point instead of the group mean as plotted above. This results in a α and α^* exponent values for each time-point for every subject. We then take the average α values over the time points, thereby resulting in an α and α^* value for each subject. α_{sub} represents the mean value over all the time points in the time series corresponding to a particular subject. This can give us a quantitative understanding of the average change in self-averageness with an increase in domain size.

Parameter	AD	CN
$Mean(\alpha) \pm STD(\alpha)$	-0.423 ± 0.062	-0.426 ± 0.058
$Mean(\alpha^*) \pm STD(\alpha^*)$	-0.802 ± 0.206	-0.785 ± 0.261
$Median(\alpha)$	-0.422	-0.422
$Median(\alpha^*)$	-0.784	-0.720
$Mean(\alpha - \alpha^*) \pm STD(\alpha - \alpha^*)$	0.380 ± 0.212	0.359 ± 0.244

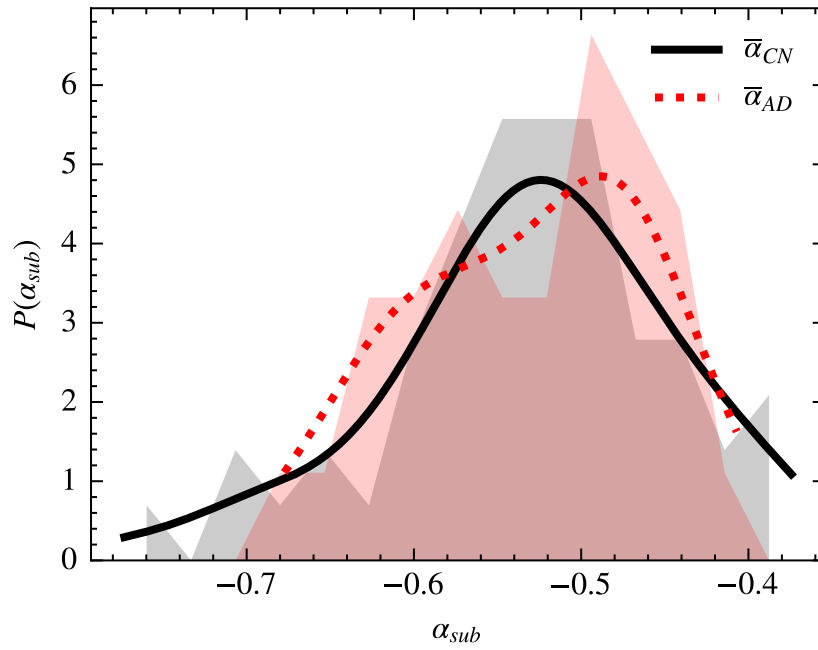
Table 4.2: Results of R_X Fits

The results of the fits are tabuled in Table 4.2. The α and α^* values are plotted in Fig. 4.5a. We observe a clear shift in the distribution of α^* compared to the α values. The α^* for both AD and CN subjects move towards values of -1 , thereby indicating a shift towards better self-averaging in larger system sizes. The behaviour observed for AD and CN is similar, and no statistically significant difference is found in the self-averaging critical exponents. The change from the α fit corresponding to the small realisation-size and α^* corresponding to the large realisation-size regime is distinctive, and this change in the self-averaging behaviour implies that the brain does indeed function at a critical state as the system is non-self-averaging in the small value region near criticality. As we increase the realisation size N , we average over a larger range of spatially distributed spins and account for more randomness, thereby compensating for long-range correlations and leading to an increase in the stability of the observables [104]. The poor self-averaging observed in the initial case of smaller realisation sizes displays the presence of disorder, again indicating criticality in the brain.

The overall fits are displayed in the Fig. 4.5b. $\bar{\alpha}$ is the slope for the fit on the entirety of data without splitting into the first and second halves, as done before. We can look at this metric to understand the



(a) α_{sub} Distribution with Separate Fits for Small and Large Realisation Size



(b) α_{sub} Distribution with Overall Fits

Figure 4.5: Distributions of α_{sub}

overall trend towards power-law behaviour. The mean of $\bar{\alpha}$ for the AD case is ≈ -0.520 and ≈ -0.531 for the CN case. The difference between the two classes appears to be notably less distinct than expected and is statistically insignificant. Although the exponents α for the AD and CN cases are observed to take different values, there does not appear to be a lot of variation between them, thereby not allowing us to definitively determine which is closer to criticality. The weak self-averaging in the small-to-medium realisation sizes confirms the existence of long-range correlations, which require large realisation sizes to compensate for, which is a characteristic marker of frustration and criticality as found in spin-glass states. The results observed indicate that both the AD and CN cases exhibit characteristics of being close to criticality and that the nature of criticality observed is quite complex, more akin to a spin-glass system due to the presence of disorder rather than simple Ising criticality as initially expected.

4.3.2 Domain Formation

The domains formed throughout the time series of each subject are studied. Their sizes (S_{dom}) and number of domains formed (n_{dom}) are calculated for every time point. Our results show the existence of large, percolating domains throughout the scan. These domains are distinctively large in size ($S_{large} \approx 15000$) and typically only a few in number ($n_{large} \approx 2$). A key feature of the critical state is the presence of long-range correlations in the form of domains spanning large portions of the system. The existence of these massive domains suggests that the system is close to the critical temperature T_c [15].

To quantify these domains further, the probability distributions of their sizes and numbers throughout the time series of length T_{max} were calculated:

$$P(S_{dom}) = \frac{1}{N_{sub}T_{max}} \sum_j^{N_{sub}} \sum_k^{T_{max}} \delta(S_{dom} - S^j(k)) \quad (4.11)$$

$$P(n_{dom}) = \frac{1}{T_{max}} \sum_k^{T_{max}} \delta \left(n_{dom} - \frac{1}{N_{sub}} \sum_j^{N_{sub}} n^j(k) \right) \quad (4.12)$$

The variables $n^j(k)$ and $S^j(k)$ represent the number of domains and size at time k for subject j .

For clear visualisation, the distribution for the large domains is isolated for domain sizes $S_{dom} > 500, 2000$ shown in Fig. 4.6 (A) and Fig. 4.7 (A). There also appear to be a large number of smaller domains ($S_{dom} < 50$) that are dominated by sizes $S_{dom} \lesssim 10$, which are visualised in Fig. 4.6 (B) and Fig. 4.7 (B). Studying the domain distributions filtered by their sizes allows us to get a better sense due

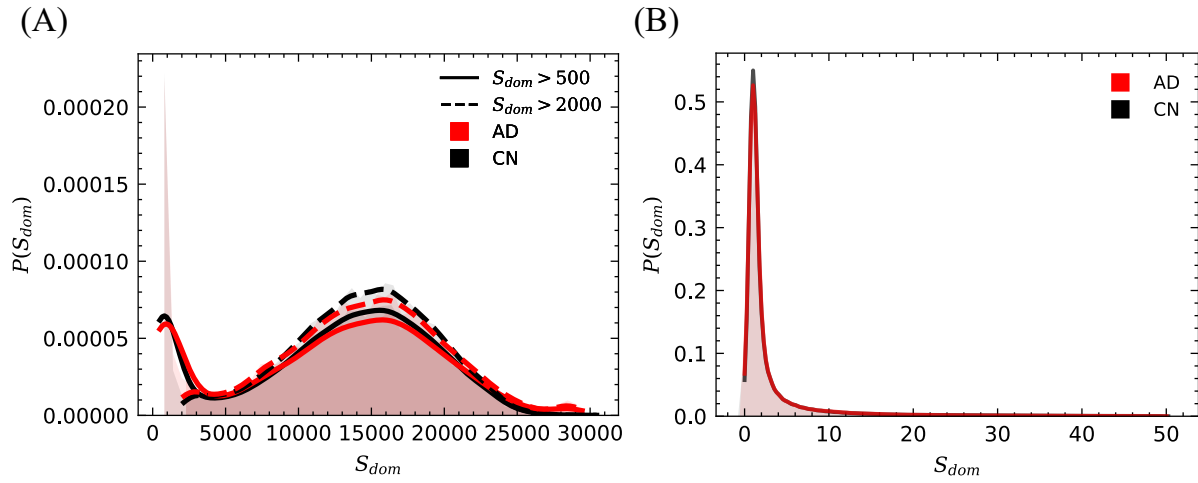


Figure 4.6: Domain Size Distributions

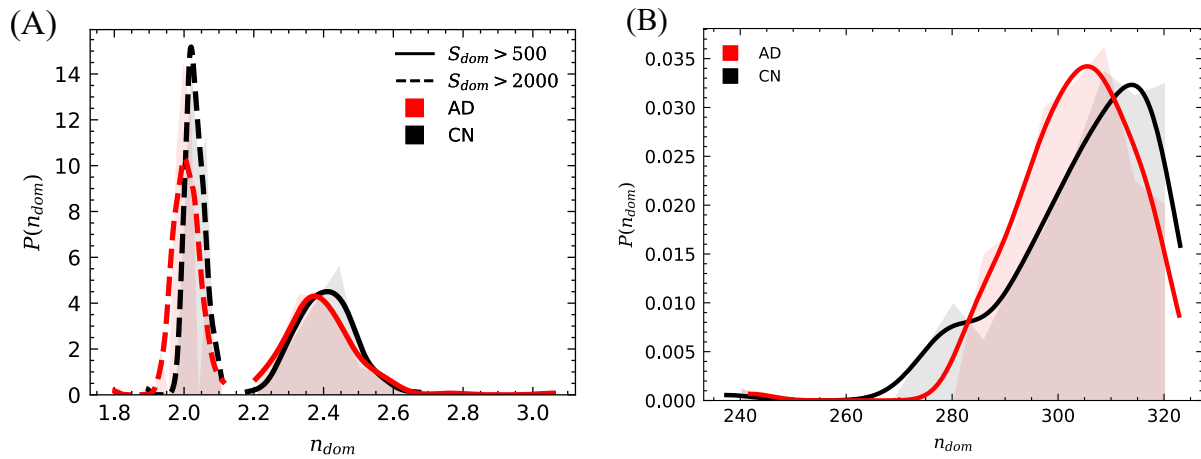


Figure 4.7: Number of Domains Distributions

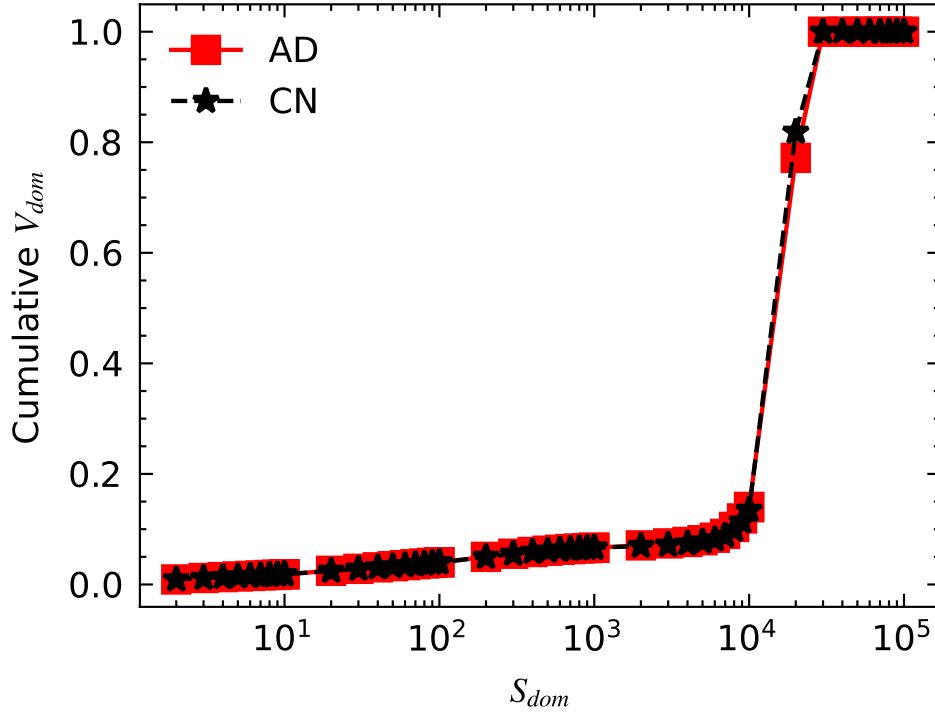


Figure 4.8: Volume of Spins within Domains of Varying Sizes

to the sparse nature of the distributions. We observe no significant differences between the AD and CN in both small and large domain regimes ($p > 0.05$).

In order to understand the size of clusters where the majority of the spins lie, we calculate the volume V_{dom}^i contained within clusters of sizes S_{dom}^i as:

$$V_{dom}^i = (S_{dom}^i * n_{dom}^i) \quad (4.13)$$

This is calculated throughout the time series for all subjects. The cumulative volume is displayed in Fig. 4.8, which represents the total fraction of the volume covered by clusters of sizes up to S_{dom} . We observe that the Cumulative V_{dom} exhibits a rapid increase (from ≈ 0.1 to ≈ 1.0) upon arriving at sizes of $S_{dom} \approx 10^4$, implying that nearly all of the volume ($\approx 90\%$) is contained within domains of sizes 10^4 . This suggests the existence of large, percolating clusters that run throughout the system for both AD and CN classes as Fig. 4.7 shows that there are only ≈ 2 domains of size > 2000 . The two large domains, along with an immense number of smaller domains, seem to imply the existence of percolating stable clusters, while the dynamics through the time series revolve mostly around the small domains. In the case of the Ising type of criticality (ferromagnetic-paramagnetic transition), we would expect a sizable distinction between the two classes as these domain sizes are expected to diverge significantly as we get closer to criticality. As we get closer to the phase transition, the sizes of the percolating clusters are

expected to diverge rapidly, thereby resulting in a significant difference between AD and CN, but this does not seem to be reflected in the results observed above.

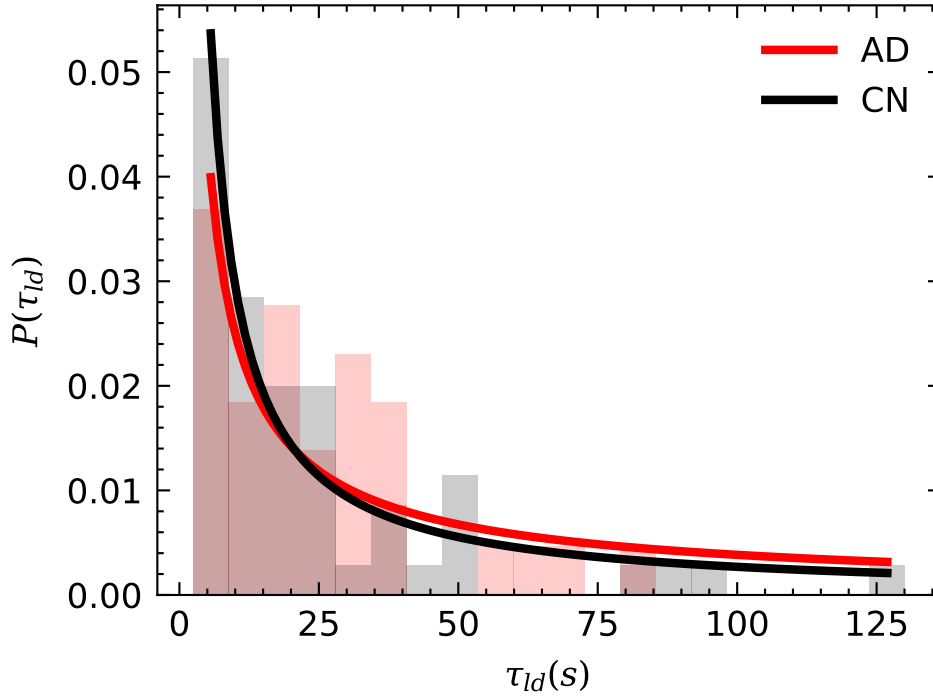


Figure 4.9: Mean Lifetime of Largest Domain

Additionally, we also calculate the mean lifetime τ_{ld} of the largest domain, which is the relaxation time of the autocorrelation of the domain lifetime. Fig. 4.9 displays these results. The distribution of τ_{ld} seems to be similar for both the AD and the CN cases, and no substantial distinction was found between the two ($p > 0.05$). The lifetime relaxation times of the largest domains for both cases seem to follow an exponential-decay pattern, which is to be expected at criticality and points to a state that is near the phase transition. From the lifetimes of the largest domain, we can conclude the existence of large, long-lasting, stable percolating clusters in both the AD and CN cases with no significant distinction, which is a hallmark of criticality.

In summary, the spatial aspects of criticality that we have investigated - self-averaging and domain formation - establish that we are close to criticality due to the nature of the domains formed and the lack of self-averaging at smaller system sizes. However, they do not seem to show an adequate distinction between the AD and CN classes. If the phase transition here is bordering the spin-glass phase, the lack of distinction in spatial correlations might be expected, as it can be attributed to the local frustrations found in this phase. This might prevent the system from reaching equilibrium domain distributions. The

presence of non-self-averageness due to long-range correlations and the existence of percolating clusters both seem to imply a spin-glass type of criticality [22]. In that case, we should be able to see a significant distinction in the temporal correlation lengths as long as there is a sufficient distinction in proximity to criticality. We shall study the temporal aspect to confirm our hypothesis in the next section.

4.3.3 Relaxation Times

The autocorrelation functions (ACF) of each voxel for all the subjects are calculated using an inverse Fourier transform of the power spectral density (PSD) as defined by the Wiener-Khinchin theorem. The ACF $\rho(t)$ is normalised to the value at $t = 0$ [16]. An exponential curve and a stretched exponential curve are both fit to the ACF using the least-squares method. The resulting plots can visually show us the difference between the two fits as well as the nature of the ACF itself, which appears to be roughly an exponential decay. A few representative plots are shown in Fig. 4.10. From the representative plots, it is visually apparent that the simple exponential fit is unable to reconcile the initial drop-off with the leading tail - the drop-off seems to be steeper than the standard exponential fit that is required to match both the initial drop and the tail. However, the stretched exponential appears to capture the drop-off much better while being able to approximate the tail to moderate accuracy.

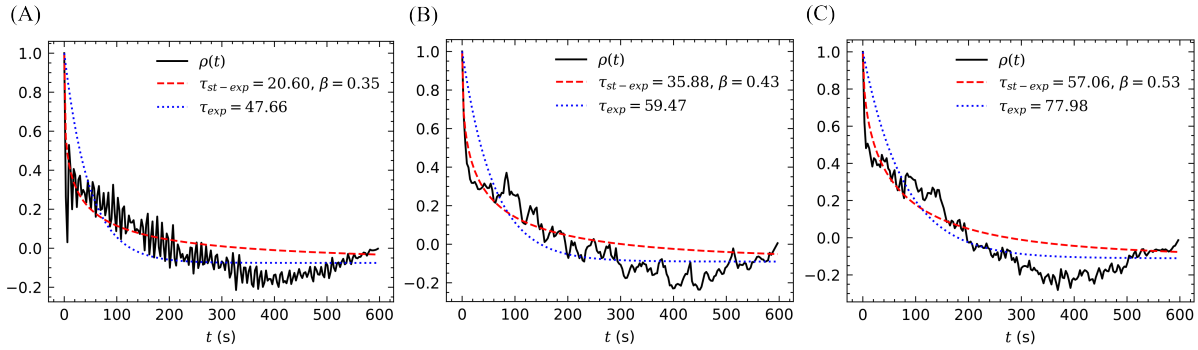


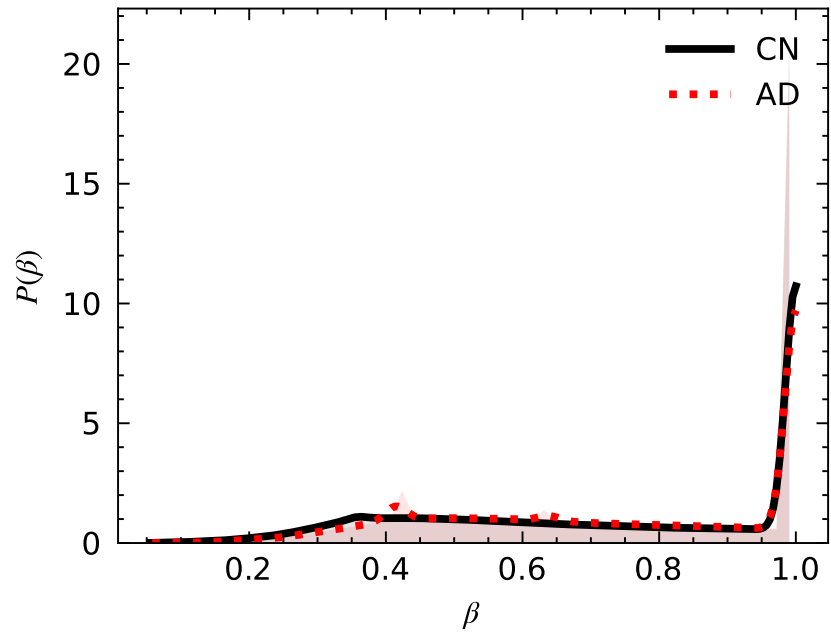
Figure 4.10: Representative exponential and stretched exponential fits on ACF $\rho(t)$

To quantify the extent of deviation from simple exponential behaviour, we can study the *beta* values from stretched exponential fit.

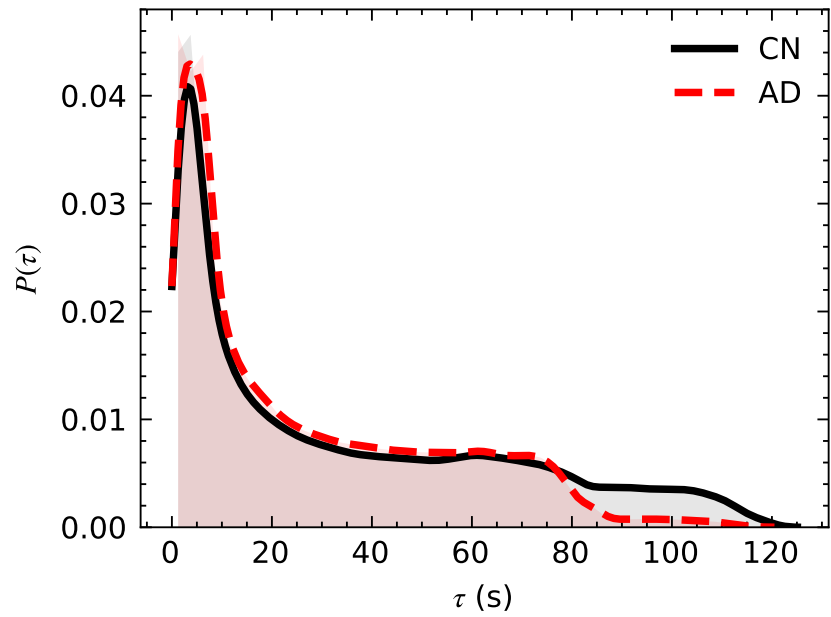
Fig. 4.11 displays the overall distributions of β and τ values for the entire space of voxels across all subjects. The histogram displayed can be quantified by the equation:

$$P(\beta) = \frac{1}{N_{sub}N_{vox}} \sum_i^{N_{sub}} \sum_j^{N_{vox}} \delta(\beta - \beta_j^i) \quad (4.14)$$

$$P(\tau) = \frac{1}{N_{sub}N_{vox}} \sum_i^{N_{sub}} \sum_j^{N_{vox}} \delta(\tau - \tau_j^i) \quad (4.15)$$



(a) β distribution: β quantifies the deviation from standard exponential behaviour



(b) τ distribution: τ is the characteristic time constant of the exponential decay

Figure 4.11: Distributions of the stretched exponential parameters over all voxels for all subjects

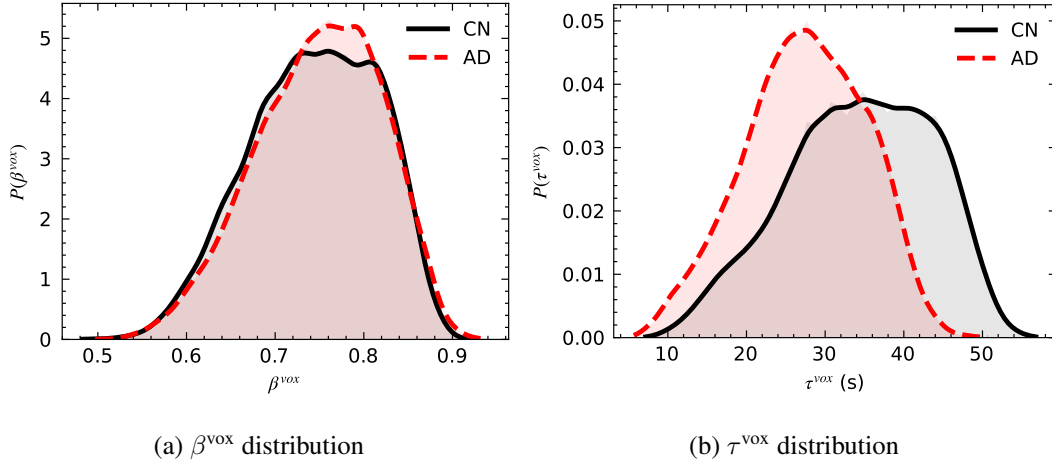


Figure 4.12: Distributions of the stretched exponential parameters across voxels averaged over subjects

We observe that $\approx 59\%$ of the voxels across all subjects have $\beta < 0.95$, indicating that there is ample deviation from simple exponential behaviour. No significant differences are seen between the AD and CN distributions for β . There does, however, appear to be a notable distinction between AD and CN in the τ distributions. The tail end of the τ distribution seems to vary significantly between the classes, with a good amount of the CN values being notably in the higher range of relaxation times. This indicates that a larger percentage of them have slow relaxation times.

These distributions can also be visualised as displayed in Fig. 4.12 by averaging over each voxel:

$$P(\beta^{vox}) = \frac{1}{N_{sub}} \sum_i^{N_{sub}} \delta \left(\beta - \frac{1}{N_{vox}} \sum_j^{N_{vox}} \beta_j^i \right) \quad (4.16)$$

$$P(\tau^{vox}) = \frac{1}{N_{sub}} \sum_i^{N_{sub}} \delta \left(\tau - \frac{1}{N_{vox}} \sum_j^{N_{vox}} \tau_j^i \right) \quad (4.17)$$

In the $P(\tau^{vox})$ distribution, a distinction can be observed between the AD and CN fits, with CN tending towards larger relaxation times on average. These larger relaxation times are suggestive of being closer to criticality. At the critical state, relaxation times diverge to become longer due to increased frustration (or “critical slowing down”) and indicates the presence of long-range correlations in the system [5, 17, 96]. This indicates a slower recovery from external perturbations and is a good marker of closeness to criticality.

$P(\beta^{vox})$ demonstrates clearly that most of the fits for each voxel (on average) are of the stretched exponential nature for both the AD and CN cases. The stretched exponential form of decay is characteristic of metastable states approaching the glass transition in spin-glass systems. As the system approaches criticality, heterogeneous dynamics emerge, leading to a wider range of relaxation times. Critical systems

are characterised by fluctuations and disorder, and the stretched exponential form can account for these by allowing for non-exponential relaxations. These frustrations enable features not found in the paramagnetic phase - such as long-term memory - as evidenced in the deviation from simple exponential behaviour. Therefore, it appears that criticality in the brain is more akin to that found in spin-glass systems and not as simple as the Ising model criticality that is traditionally posited [17].

4.4 Discussion

In our study of the spatial aspects of criticality in the human brain, we have used fMRI data from Cognitively Normal and Alzheimer’s Disease-afflicted subjects from the ADNI dataset.

We first studied two key spatial aspects of criticality in Ising systems - self-averaging and domain formation. The extent of self-averaging was quantified using the metric relative variance (R_X). Derivative systems of different realisation sizes (N) were generated by taking the fMRI scan of the subject at individual time points for each subject. R_X was evaluated for varying realisation sizes, and the relationship between them was studied to determine a minimum size for adequate self-averaging. We determined that the nature of self-averaging is not constant as in the case of a random system, but it changes as the system size increases. There is a breakdown of self-averaging at lower realisation sizes, and the property seems to stabilise as we increase the realisation size. The change appears to be more pronounced in the case of CN subjects as compared to AD, indicating that Alzheimer’s Disease might disrupt critical-state dynamics and be further away from the critical point, although the difference found was not major and less than expected.

The domain formation in the brain was studied by first labelling the domains throughout the time series of all subjects. These domains were then quantified by calculating their sizes and the number of domains at each time point. The size evolution of the largest domains was also tracked. This investigation reveals the existence of large, percolating clusters in both AD and CN cases, which are a hallmark of criticality. The mean lifetimes of the largest domains for both AD and CN classes seemed to follow an exponential decay pattern with an insignificant difference between them. These percolating clusters observed appear to be stable, whereas the dynamics mostly revolve around an enormous number of smaller domains. There was no significant difference found between the AD and CN classes, and both seemed to show similar behaviour in this aspect. This suggests that there might exist a more complex phase transition here - one that involves the spin-glass phase. In this phase, there exist local frustrations that might now allow the system to reach equilibrium domain distributions. This might lead to the proximity to the critical state not adequately affecting the spatial correlation lengths as we would expect in a simple Ising-like phase transition, accounting for the inadequate distinction.

In order to confirm this hypothesis, we then studied the nature of relaxation in resting-state fMRI brains, as the temporal aspect should sufficiently vary between AD and CN subjects regardless of the type of transition as long as there is a tangible difference in the closeness to criticality of the two classes. We find that a stretched exponential curve can be a better fit for the autocorrelation of the BOLD signals derived from the scans. Our examination of relaxation times suggests that CN may be closer to criticality, as indicated by a shift in the tail towards larger values in the distribution of mean relaxation times - which tend to diverge at critical temperature. A significant difference was found in the temporal correlation lengths between the two classes, which suggests that they differ considerably in their proximity to criticality. The stretched exponential behaviour suggest that the brain operates in a spin-glass phase which could enable numerous other properties - such as long-term memory - which are not explainable by simple Ising-like dynamics. This confirms our hypothesis that the nature of criticality is more akin to a spin-glass system rather than simple Ising and also validates our method of treating the brain as a system with quenched disorder.

In summary, our findings indicate that the spatial critical phenomena - such as self-averaging and domain formation - do not differ adequately, whereas the temporal critical phenomena - namely relaxation dynamics - show a significant distinction between the AD and CN classes. We confirm that there is indeed a disruption of criticality through the progression of Alzheimer's Disease. The temporal measures are found to be considerably more sensitive than the spatial measures, which is a characteristic signature of the spin-glass phase. This lack of distinction in the spatial aspect but its presence in the temporal aspect suggests that the phase transition in the brain appears to not be of the Ising type (i.e., ferromagnetic-paramagnetic) but is more akin to a complex spin-glass phase transition (spin-glass-ferromagnetic or spin-glass-paramagnetic). Our investigation prompts further research into the nature of criticality in the brain.

Chapter 5

Conclusion and Future Work

We study the brain through the perspective of statistical mechanics in order to develop a better understanding of the physical systems that can be applied in neuroscience investigations. The objectives of the thesis were to study the disruption in criticality caused by the neurodegeneration of Alzheimer's Disease and then to determine the nature of criticality within the human brain. In particular, we try to determine the type of phase transition and the phase in which the brain functions - paramagnetic, ferromagnetic, or spin-glass.

We start by employing a statistical mechanics model - the Pairwise Maximum-Entropy Ising model - to study the closeness to criticality for Alzheimer's by studying fMRI data. We infer the connectivity of the model through a pseudo-likelihood maximisation procedure and then simulate these systems to compute key properties of the model - namely magnetisation and susceptibility. These properties then allow us to deduce the critical temperature of each of the two classes, thereby allowing us to see the deviation from the critical state in the case of AD.

We found that the magnetisation of both classes starts off with considerable deviations in positive and negative values, with the absolute magnitude being large. The variation stays nearly constant for the low-temperature regime, and it displays a quick drop-off as we approach the vicinity of a specific temperature, presumably the critical temperature T_c , and stays constantly at $m = 0$ after it. Correspondingly, there is a sharp peak in susceptibility at T_c . The trends observed in susceptibility and magnetisation for both classes of data displayed similar behaviour, and they indicate that the brain is indeed near a critical state.

The critical temperature for AD was slightly higher than CN, indicating that it is further away from the regular critical state, although this difference was minor. Motivated by the insignificant differences between the two classes, we hypothesise that susceptibility might be too simple of a parameter to determine the proximity to criticality due to its inherent spatial nature. The spatial sensitivity of such a parameter might be inadequate to accurately characterise systems that exhibit a relatively more complex phase transition compared to simple Ising systems, such as spin-glasses. We set out to investigate the possibility

of the transition involving the spin-glass phase in further detail by studying critical-state properties in order to identify the nature of the phase transition since that would lend justification to the inadequacy of this parameter and give us a clearer picture of the parameters that are applicable for such a study.

We study the nature of criticality in the human brain through resting-state fMRI by likening it to a spin-lattice system. We first study two spatial aspects of criticality - self-averaging and domain formation - which are well-researched concepts in statistical physics.

To study self-averaging, numerous derivative systems averaged over different realisation sizes are generated, and their relative variance is calculated. This metric can be used to quantify the extent of self-averaging in a system. The relative variance in an ideal self-averaging system displays a power-law behaviour with the realisation size for realisations of all sizes, and the exact exponent α can be calculated. We observe that the exponent for larger realisation sizes differs significantly from the smaller realisation sizes, thereby confirming the non-self-averageness of the system, which is a hallmark of criticality. The curves for both AD and CN display similar behaviour.

Then, we analyse the domain formation behaviour within the brain. Domain formation is a crucial aspect of criticality, as domain sizes tend to enlarge at criticality due to long-range correlations. In order to quantify the domain formation behaviour, we compute the domain size (number of spin-sites contained within the domain) and the number of unique domains formed at each time-point. We observe large, percolating domains throughout the time series, which is indicative of the critical state. At criticality, the correlation length increases, and these large domains, which span very large lengths, form. We also observe a good number of small domains - although minuscule by total volume - which are responsible for the majority of dynamic behaviour in the system. The distribution of domain sizes and number of domains were found to be similar for both AD and CN classes. Additionally, we also study the mean lifetimes of the largest domains for each subject, which is the relaxation time of the autocorrelation function of the largest domain's size evolution for each subject - the class-wise distributions for these seem to show no statistically significant difference between both classes.

At this point, there are two possibilities. Either the brain works at a critical state approaching the phase transition from the paramagnetic phase, and there is actually no difference between AD and CN, or it is approaching the transition from a completely different type of phase - the spin-glass phase - and there actually is a difference between the two classes, but it is not reflected in the spatial metrics. Either case can be confirmed by further studying the temporal aspects of criticality. If a significant difference is observed in the temporal metrics, then we can confirm that it is indeed in the spin-glass phase. If there is no difference found, we can confirm that there is no difference in the critical behaviour of the Alzheimer's brain.

Finally, we study the temporal relaxation of the signals from the fMRI data. The autocorrelation function is first calculated. Then, an exponential curve and an alternative form of the exponential decay curve, known as a 'stretched exponential', are fit to this ACF. The stretched exponential involves a two-step relaxation pattern, and the deviation from the simple exponential decay is quantifiable in this form. Two parameters are obtained here for the stretched exponential - the relaxation time τ and the parameter quantifying deviation from criticality β - whereas only the relaxation time τ is obtained for the regular exponential. We observe that a majority of the voxels ($\approx 59\%$) seem to show ample deviation from the regular exponential behaviour through low values of β and are better characterised by the stretched exponential. Significant differences are observed in the tail end of the τ distribution, with a large number of CN values tending towards higher relaxation times, indicating that it is closer to the phase transition as compared to AD. We also calculate the values of each of these parameters - β and τ - averaged over the location of the voxel. The β_{vox} distribution shows a clear deviation from normal exponential behaviour as the majority of values deviate from the values of $\beta_{vox} \approx 1$ (regular exponential). The stretched exponential form of decay is a crucial indicator of criticality in spin-glass systems as it can better characterise for the relaxation observed near the phase-transition by accounting for non-exponential relaxations, which are commonly observed in disordered systems. We also observe key differences in $P(\tau_{vox})$, which augment the differences observed in the $P(\tau)$ distribution, with CN on average tending towards higher relaxation times as compared to AD. With increasing proximity to the critical state, the relaxation times tend to progressively diverge and hence are a good marker of how close a system is to criticality. These results indicate that there is a notable distinction in the temporal dynamics, and the disruption in critical behaviour due to Alzheimer's Disease is tangible.

The study of both spatial and temporal aspects showed signs of being close to the critical state for AD and CN subjects. We observed no differences between the two classes in spatial behaviour but significant differences in temporal behaviour. This indicates that the brain exists in the spin-glass phase and that the phase transition it operates at involves this phase. In this phase, local frustrations might not allow for the system to reach equilibrium domain distributions, causing insignificant differences between the two classes in the spatial behaviour while still allowing for significant differences in the temporal behaviour. This phase allows for the existence of long-term memory, as evident in the stretched exponential behaviour - something that is lacking in the paramagnetic or ferromagnetic phases.

To build upon the work done in this thesis, numerous directions can be pursued. More nuanced order parameters such as four-point correlations can be implemented to further study the phase ordering. Neural recordings from task-based experiments can be studied to understand the effect of activity on brain criticality. Using a similar methodology, other neurodegenerative conditions such as Parkinson's Disease can be investigated to understand their effect on critical-state functioning. Studying the temporal relaxation behaviour of the time-series from Monte Carlo simulations through a pairwise-maximum

entropy model can allow for studying larger time scales beyond the data. Additionally, complex statistical models that incorporate phase transitions can be applied for a perspective that is distinct from spin-models. Finally, other modalities of collecting neural data can also be tested to certify the results.

Our findings hence indicate that the brain operates at a phase transition that involves the spin-glass phase rather than simply involving the two classical Ising phases. These findings allow us to study the brain using statistical mechanics through a more nuanced lens. They pave the way for more intricate models of the brain that integrate long-term memory, a feature that is not found in conventional Ising-like physics. It serves as a bridge between the expansive literature on spin-glass physics and neuroscience, allowing us to apply concepts from statistical mechanics in the context of analysing neural dynamics to understand the mechanisms underlying brain function.

Related Publications

- Anirudh Palutla, Shivansh Seth, S. S. Ashwin, and Marimuthu Krishnan. "**Criticality in Alzheimer's and Healthy Brains: Insights from Phase-Ordering**"; Accepted at **Cognitive Neurodynamics (2023)**; Preprint available at <https://doi.org/10.48550/arXiv.2305.13762>.

Bibliography

- [1] A. Abraham, F. Pedregosa, M. Eickenberg, P. Gervais, A. Mueller, J. Kossaifi, A. Gramfort, B. Thirion, and G. Varoquaux. Machine learning for neuroimaging with scikit-learn. *Frontiers in Neuroinformatics*, 8, 2014.
- [2] D. Abásolo, R. Hornero, P. Espino, D. Álvarez, and J. Poza. Entropy analysis of the EEG background activity in Alzheimer’s disease patients. *Physiological Measurement*, 27(3):241, Jan. 2006.
- [3] F. Agosta, M. Pievani, C. Geroldi, M. Copetti, G. B. Frisoni, and M. Filippi. Resting state fMRI in Alzheimer’s disease: beyond the default mode network. *Neurobiology of Aging*, 33(8):1564–1578, Aug. 2012.
- [4] A. Aharony and A. B. Harris. Absence of self-averaging and universal fluctuations in random systems near critical points. *Physical review letters*, 77(18):3700, 1996.
- [5] P. Bak, C. Tang, and K. Wiesenfeld. Self-organized criticality. *Physical Review A*, 38(1):364–374, July 1988.
- [6] J. R. Banavar, A. Maritan, and I. Volkov. Applications of the principle of maximum entropy: from physics to ecology. *Journal of Physics: Condensed Matter*, 22(6), 2010.
- [7] R. J. Baxter. *Exactly solved models in statistical mechanics*. Elsevier, 2016.
- [8] J. M. Beggs and D. Plenz. Neuronal avalanches in neocortical circuits. *Journal of neuroscience*, 23(35):11167–11177, 2003.
- [9] A. Billoire and I. Campbell. Dynamics in the sherrington-kirkpatrick ising spin glass at and above t_g . *Physical Review B*, 84(5):054442, 2011.
- [10] M. Bleich-Cohen, S. Jamsky, H. Sharon, R. Weizman, N. Intrator, M. Poyurovsky, and T. Hendler. Machine learning fMRI classifier delineates subgroups of schizophrenia patients. *Schizophrenia Research*, 160(1):196–200, Dec. 2014.
- [11] H. Brody. Medical imaging. *Nature*, 502(7473):S81–S81, Oct. 2013. Number: 7473 Publisher: Nature Publishing Group.
- [12] S. G. BRUSH. History of the Lenz-Ising Model. *Reviews of Modern Physics*, 39(4):883–893, Oct. 1967. Publisher: American Physical Society.

- [13] J. M. Campbell, Z. Huang, J. Zhang, X. Wu, P. Qin, G. Northoff, G. A. Mashour, and A. G. Hudetz. Pharmacologically informed machine learning approach for identifying pathological states of unconsciousness via resting-state fMRI. *NeuroImage*, 206:116316, Feb. 2020.
- [14] C. Castellano, S. Fortunato, and V. Loreto. Statistical physics of social dynamics. *Reviews of Modern Physics*, 81(2), 2009.
- [15] P. M. Chaikin and T. C. Lubensky. *Principles of condensed matter physics*. Cambridge University Press, Cambridge, 1995.
- [16] C. Chatfield. *The analysis of time series an introduction*. Chapman and hall, 1989.
- [17] D. R. Chialvo. Emergent complex neural dynamics. *Nature physics*, 6(10):744–750, 2010.
- [18] R. Christopher deCharms. Applications of real-time fMRI. *Nature Reviews Neuroscience*, 9(9):720–729, Sept. 2008. Number: 9 Publisher: Nature Publishing Group.
- [19] B. A. Cipra. An Introduction to the Ising Model. *The American Mathematical Monthly*, 94(10):937–959, Dec. 1987. Publisher: Taylor & Francis eprint: <https://doi.org/10.1080/00029890.1987.12000742>.
- [20] G. Deco and V. K. Jirsa. Ongoing Cortical Activity at Rest: Criticality, Multistability, and Ghost Attractors. *Journal of Neuroscience*, 32(10):3366–3375, Mar. 2012. Publisher: Society for Neuroscience Section: Articles.
- [21] E. L. Dennis and P. M. Thompson. Functional Brain Connectivity Using fMRI in Aging and Alzheimer’s Disease. *Neuropsychology Review*, 24(1):49–62, Mar. 2014.
- [22] V. Dotsenko. *An Introduction to the Theory of Spin Glasses and Neural Networks*. World Scientific, 1994. Google-Books-ID: C8YAcP0kTcIC.
- [23] V. M. Eguiluz, D. R. Chialvo, G. A. Cecchi, M. Baliki, and A. V. Apkarian. Scale-free brain functional networks. *Physical review letters*, 94(1):018102, 2005.
- [24] T. Ezaki, E. Fonseca dos Reis, T. Watanabe, M. Sakaki, and N. Masuda. Closer to critical resting-state neural dynamics in individuals with higher fluid intelligence. *Communications Biology*, 3(1):1–9, Feb. 2020. Number: 1 Publisher: Nature Publishing Group.
- [25] T. Ezaki, T. Watanabe, M. Ohzeki, and N. Masuda. Energy landscape analysis of neuroimaging data. *Philosophical Transactions of the Royal Society A: Mathematical, Physical and Engineering Sciences*, 375(2096):20160287, May 2017. Publisher: Royal Society.
- [26] L. Fadiga, L. Craighero, M. Fabbri-Destro, L. Finos, N. Cotillon-Williams, A. T. Smith, and U. Castiello. Language in shadow. *Social Neuroscience*, 1(2), 2006.
- [27] B. J. Fendler, R. Sknepnek, and T. Vojta. Dynamics at a smeared phase transition. *Journal of Physics A: Mathematical and General*, 38(11), 2005.
- [28] I. Fortel, M. Butler, L. E. Korthauer, L. Zhan, O. Ajilore, I. Driscoll, A. Sidiropoulos, Y. Zhang, L. Guo, H. Huang, D. Schonfeld, and A. Leow. Brain Dynamics Through the Lens of Statistical Mechanics by Unifying Structure and Function. In D. Shen, T. Liu, T. M. Peters, L. H. Staib, C. Essert, S. Zhou, P.-T.

- Yap, and A. Khan, editors, *Medical Image Computing and Computer Assisted Intervention – MICCAI 2019*, Lecture Notes in Computer Science, pages 503–511, Cham, 2019. Springer International Publishing.
- [29] M. D. Fox, A. Z. Snyder, J. L. Vincent, M. Corbetta, D. C. Van Essen, and M. E. Raichle. The human brain is intrinsically organized into dynamic, anticorrelated functional networks. *Proceedings of the National Academy of Sciences*, 102(27):9673–9678, 2005.
- [30] D. Fraiman, P. Balenzuela, J. Foss, and D. R. Chialvo. Ising-like dynamics in large-scale functional brain networks. *Physical Review E*, 79(6):061922, June 2009.
- [31] R. Frigg. Self-organised criticality—what it is and what it isn’t. *Studies in History and Philosophy of Science Part A*, 34(3):613–632, Sept. 2003.
- [32] K. Gorgolewski, C. Burns, C. Madison, D. Clark, Y. Halchenko, M. Waskom, and S. Ghosh. Nipype: a flexible, lightweight and extensible neuroimaging data processing framework in python. *Frontiers in Neuroinformatics*, 5, 2011.
- [33] S. Goswami and A. Chakraborti. Kinetic Exchange Models in Economics and Sociology. *Springer Proceedings in Mathematics & Statistics*, 2015.
- [34] J. Gotman, E. Kobayashi, A. P. Bagshaw, C.-G. Bénar, and F. Dubeau. Combining EEG and fMRI: A multimodal tool for epilepsy research. *Journal of Magnetic Resonance Imaging*, 23(6):906–920, 2006. [eprint: https://onlinelibrary.wiley.com/doi/pdf/10.1002/jmri.20577](https://onlinelibrary.wiley.com/doi/pdf/10.1002/jmri.20577).
- [35] M. D. Greicius, G. Srivastava, A. L. Reiss, and V. Menon. Default-mode network activity distinguishes Alzheimer’s disease from healthy aging: Evidence from functional MRI. *Proceedings of the National Academy of Sciences*, 101(13):4637–4642, Mar. 2004. Publisher: Proceedings of the National Academy of Sciences.
- [36] W. K. Hastings. Monte Carlo sampling methods using Markov chains and their applications. *Biometrika*, 57(1):97–109, Apr. 1970.
- [37] B. He and Z. Liu. Multimodal Functional Neuroimaging: Integrating Functional MRI and EEG/MEG. *IEEE Reviews in Biomedical Engineering*, 1:23–40, 2008. Conference Name: IEEE Reviews in Biomedical Engineering.
- [38] D. J. Heeger and D. Ress. What does fMRI tell us about neuronal activity? *Nature Reviews Neuroscience*, 3(2):142–151, Feb. 2002. Number: 2 Publisher: Nature Publishing Group.
- [39] F. G. Hillary, C. A. Roman, U. Venkatesan, S. M. Rajtmajer, R. Bajo, and N. D. Castellanos. Hyperconnectivity is a fundamental response to neurological disruption. *Neuropsychology*, 29(1):59–75, 2015. Place: US Publisher: American Psychological Association.
- [40] C. Hohenfeld, C. J. Werner, and K. Reetz. Resting-state connectivity in neurodegenerative disorders: Is there potential for an imaging biomarker? *NeuroImage: Clinical*, 18:849–870, Jan. 2018.
- [41] J. Hoshen and R. Kopelman. Percolation and cluster distribution. i. cluster multiple labeling technique and critical concentration algorithm. *Physical Review B*, 14(8):3438, 1976.

- [42] M. Jenkinson, P. Bannister, M. Brady, and S. Smith. Improved optimization for the robust and accurate linear registration and motion correction of brain images. *NeuroImage*, 17(2):825–841, Oct. 2002.
- [43] M. Jenkinson, C. F. Beckmann, T. E. J. Behrens, M. W. Woolrich, and S. M. Smith. Fsl. *NeuroImage*, 62(2):782–790, Aug. 2012.
- [44] L. Jiang, D. Sui, K. Qiao, H.-M. Dong, L. Chen, and Y. Han. Impaired Functional Criticality of Human Brain during Alzheimer’s Disease Progression. *Scientific Reports*, 8(1):1324, Jan. 2018. Number: 1 Publisher: Nature Publishing Group.
- [45] B. D. Johnson, M. Hallett, and S. Slobounov. Follow-up evaluation of oculomotor performance with fMRI in the subacute phase of concussion. *Neurology*, 85(13), 2015.
- [46] B. Kadirvelu, Y. Hayashi, and S. J. Nasuto. Inferring structural connectivity using Ising couplings in models of neuronal networks. *Scientific Reports*, 7(1):8156, Aug. 2017. Number: 1 Publisher: Nature Publishing Group.
- [47] S. Kandeepan, J. Rudas, F. Gomez, B. Stojanoski, S. Valluri, A. M. Owen, L. Naci, E. S. Nichols, and A. Soddu. Modeling an auditory stimulated brain under altered states of consciousness using the generalized Ising model. *NeuroImage*, 223:117367, Dec. 2020.
- [48] N. Karamzadeh, F. Amyot, K. Kenney, A. Anderson, F. Chowdhry, H. Dashtestani, E. M. Wassermann, V. Chernomordik, C. Boccarda, E. Wegman, R. Diaz-Arrastia, and A. H. Gandjbakhche. A machine learning approach to identify functional biomarkers in human prefrontal cortex for individuals with traumatic brain injury using functional near-infrared spectroscopy. *Brain and Behavior*, 6(11):e00541, 2016. eprint: <https://onlinelibrary.wiley.com/doi/pdf/10.1002/brb3.541>.
- [49] M. Khosla, K. Jamison, G. H. Ngo, A. Kuceyeski, and M. R. Sabuncu. Machine learning in resting-state fMRI analysis. *Magnetic Resonance Imaging*, 64:101–121, Dec. 2019.
- [50] D. P. Landau and K. Binder. *A Guide to Monte Carlo Simulations in Statistical Physics*. Cambridge University Press, Nov. 2014. Google-Books-ID: 56ARBgAAQBAJ.
- [51] M. H. Lee, C. D. Smyser, and J. S. Shimony. Resting-State fMRI: A Review of Methods and Clinical Applications. *American Journal of Neuroradiology*, 34(10):1866–1872, Oct. 2013. Publisher: American Journal of Neuroradiology Section: Review Articles.
- [52] J.-M. Lemée, D. H. Berro, F. Bernard, E. Chinier, L.-M. Leiber, P. Menei, and A. T. Minassian. Resting-state functional magnetic resonance imaging versus task-based activity for language mapping and correlation with perioperative cortical mapping. *Brain and Behavior*, 9(10), 2019.
- [53] A. Lipowski. Ising Model: Recent Developments and Exotic Applications. *Entropy*, 24(12):1834, Dec. 2022. Number: 12 Publisher: Multidisciplinary Digital Publishing Institute.
- [54] M. Liu, B. Li, and D. Hu. Autism Spectrum Disorder Studies Using fMRI Data and Machine Learning: A Review. *Frontiers in Neuroscience*, 15, 2021.
- [55] S. Liu, F. Li, and F. Wan. Distance to criticality undergoes critical transition before epileptic seizure attacks. *Brain Research Bulletin*, 200:110684, Aug. 2023.

- [56] N. K. Logothetis. What we can do and what we cannot do with fMRI. *Nature*, 453(7197), 2008.
- [57] A. S. Lundervold and A. Lundervold. An overview of deep learning in medical imaging focusing on MRI. *Zeitschrift für Medizinische Physik*, 29(2):102–127, May 2019.
- [58] D. Marinazzo, M. Pellicoro, G. Wu, L. Angelini, J. M. Cortés, and S. Stramaglia. Information transfer and criticality in the ising model on the human connectome. *PLoS ONE*, 9(4):e93616, Apr. 2014.
- [59] C. Meisel, A. Storch, S. Hallmeyer-Elgner, E. Bullmore, and T. Gross. Failure of Adaptive Self-Organized Criticality during Epileptic Seizure Attacks. *PLOS Computational Biology*, 8(1):e1002312, Jan. 2012. Publisher: Public Library of Science.
- [60] K. Mevel, G. Chételat, F. Eustache, and B. Desgranges. The Default Mode Network in Healthy Aging and Alzheimer’s Disease. *International Journal of Alzheimer’s Disease*, 2011:e535816, June 2011. Publisher: Hindawi.
- [61] M. Mézard, G. Parisi, and M. A. Virasoro. *Spin glass theory and beyond: An Introduction to the Replica Method and Its Applications*, volume 9. World Scientific Publishing Company, 1987.
- [62] A. Milchev, K. Binder, and D. W. Heermann. Fluctuations and lack of self-averaging in the kinetics of domain growth. *Zeitschrift für Physik B Condensed Matter*, 63(4):521–535, Dec. 1986.
- [63] T. Montez, S.-S. Poil, B. F. Jones, I. Manshanden, J. P. Verbunt, B. W. van Dijk, A. B. Brussaard, A. van Ooyen, C. J. Stam, P. Scheltens, et al. Altered temporal correlations in parietal alpha and prefrontal theta oscillations in early-stage alzheimer disease. *Proceedings of the National Academy of Sciences*, 106(5):1614–1619, 2009.
- [64] T.-M. N, L. B, P. D, C. F, E. O, D. N, M. B, and J. M. Automated anatomical labeling of activations in SPM using a macroscopic anatomical parcellation of the MNI MRI single-subject brain. *NeuroImage*, 15(1), Jan. 2002. Publisher: Neuroimage.
- [65] G. F. Newell and E. W. Montroll. On the Theory of the Ising Model of Ferromagnetism. *Reviews of Modern Physics*, 25(2):353–389, Apr. 1953. Publisher: American Physical Society.
- [66] T.-A. Nghiem, B. Telenczuk, O. Marre, A. Destexhe, and U. Ferrari. Maximum-entropy models reveal the excitatory and inhibitory correlation structures in cortical neuronal activity. *Physical Review E*, 98(1):012402, July 2018. Publisher: American Physical Society.
- [67] T. M. Nir, N. Jahanshad, J. E. Villalon-Reina, A. W. Toga, C. R. Jack, M. W. Weiner, and P. M. Thompson. Effectiveness of regional DTI measures in distinguishing Alzheimer’s disease, MCI, and normal aging. *NeuroImage: Clinical*, 3:180–195, Jan. 2013.
- [68] E. Novikov, A. Novikov, D. Shannahoff-Khalsa, B. Schwartz, and J. Wright. Scale-similar activity in the brain. *Physical Review E*, 56(3):R2387, 1997.
- [69] A. Palutla, S. Seth, S. S. Ashwin, and M. Krishnan. Criticality in alzheimer’s and healthy brains: Insights from phase-ordering, 2023.
- [70] F. Pereira, T. Mitchell, and M. Botvinick. Machine learning classifiers and fMRI: A tutorial overview. *NeuroImage*, 45(1, Supplement 1):S199–S209, Mar. 2009.

- [71] R. C. Petersen, P. S. Aisen, L. A. Beckett, M. C. Donohue, A. C. Gamst, D. J. Harvey, C. R. Jack, W. J. Jagust, L. M. Shaw, A. W. Toga, J. Q. Trojanowski, and M. W. Weiner. Alzheimer's Disease Neuroimaging Initiative (Adni): clinical characterization. *Neurology*, 74(3):201–209, Jan. 2010.
- [72] R. C. M. Philip, M. R. Dauvermann, H. C. Whalley, K. Baynham, S. M. Lawrie, and A. C. Stanfield. A systematic review and meta-analysis of the fMRI investigation of autism spectrum disorders. *Neuroscience & Biobehavioral Reviews*, 36(2):901–942, Feb. 2012.
- [73] M. Pievani, W. d. Haan, T. Wu, W. W. Seeley, and G. B. Frisoni. Functional network disruption in the degenerative dementias. *The Lancet Neurology*, 10(9):829–843, Sept. 2011. Publisher: Elsevier.
- [74] G. Pruessner. *Self-Organised Criticality: Theory, Models and Characterisation*. Cambridge University Press, Aug. 2012. Google-Books-ID: TXKcpGqMSDYC.
- [75] A. K. Rehme, L. J. Volz, D.-L. Feis, I. Bomilcar-Focke, T. Liebig, S. B. Eickhoff, G. R. Fink, and C. Grefkes. Identifying Neuroimaging Markers of Motor Disability in Acute Stroke by Machine Learning Techniques. *Cerebral Cortex*, 25(9):3046–3056, Sept. 2015.
- [76] Y. Roudi, S. Nirenberg, and P. E. Latham. Pairwise Maximum Entropy Models for Studying Large Biological Systems: When They Can Work and When They Can't. *PLOS Computational Biology*, 5(5):e1000380, May 2009. Publisher: Public Library of Science.
- [77] S. Roy and S. M. Bhattacharjee. Is small-world network disordered? *Physics Letters A*, 352(1):13–16, Mar. 2006.
- [78] G. Ruffini, G. Damiani, D. Lozano-Soldevilla, N. Deco, F. E. Rosas, N. A. Kiani, A. Ponce-Alvarez, M. L. Kringelbach, R. Carhart-Harris, and G. Deco. LSD-induced increase of Ising temperature and algorithmic complexity of brain dynamics. *PLOS Computational Biology*, 19(2):e1010811, Feb. 2023. Publisher: Public Library of Science.
- [79] P. B. Sederberg, A. Schulze-Bonhage, J. R. Madsen, E. B. Bromfield, D. C. McCarthy, A. Brandt, M. Tully, and M. J. Kahana. Hippocampal and Neocortical Gamma Oscillations Predict Memory Formation in Humans. *Cerebral Cortex*, 17(5), 2006.
- [80] K. Segaert, L. Menenti, K. Weber, K. M. Petersson, and P. Hagoort. Shared Syntax in Language Production and Language Comprehension—An fMRI Study. *Cerebral Cortex*, 22(7), 2011.
- [81] D. Sherrington and S. Kirkpatrick. Solvable model of a spin-glass. *Physical review letters*, 35(26):1792, 1975.
- [82] S. M. Smith. Overview of fMRI analysis. *The British Journal of Radiology*, 77(suppl.2):S167–S175, Dec. 2004. Publisher: The British Institute of Radiology.
- [83] S. M. Smith, M. Jenkinson, M. W. Woolrich, C. F. Beckmann, T. E. J. Behrens, H. Johansen-Berg, P. R. Bannister, M. De Luca, I. Drobnjak, D. E. Flitney, R. K. Niazy, J. Saunders, J. Vickers, Y. Zhang, N. De Stefano, J. M. Brady, and P. M. Matthews. Advances in functional and structural MR image analysis and implementation as FSL. *NeuroImage*, 23 Suppl 1:S208–219, 2004.

- [84] C. J. Stam. Modern network science of neurological disorders. *Nature Reviews Neuroscience*, 15(10):683–695, Oct. 2014. Number: 10 Publisher: Nature Publishing Group.
- [85] C. J. Stam, T. Montez, B. Jones, S. Rombouts, Y. Van Der Made, Y. A. Pijnenburg, and P. Scheltens. Disturbed fluctuations of resting state eeg synchronization in alzheimer’s disease. *Clinical neurophysiology*, 116(3):708–715, 2005.
- [86] D. Stauffer. Social applications of two-dimensional Ising models. *American Journal of Physics*, 76(4):470–473, Apr. 2008.
- [87] D. L. Stein. *Spin Glasses And Biology*. World Scientific, Aug. 1992. Google-Books-ID: SnQGCwAAQBAJ.
- [88] D. L. Stein and C. M. Newman. *Spin Glasses and Complexity*. Princeton University Press, Jan. 2013. Google-Books-ID: pJPaZoK0lq8C.
- [89] R. R. Stein, D. S. Marks, and C. Sander. Inferring Pairwise Interactions from Biological Data Using Maximum-Entropy Probability Models. *PLOS Computational Biology*, 11(7):e1004182, July 2015. Publisher: Public Library of Science.
- [90] E. Tagliazucchi, P. Balenzuela, D. Fraiman, and D. Chialvo. Criticality in Large-Scale Brain fMRI Dynamics Unveiled by a Novel Point Process Analysis. *Frontiers in Physiology*, 3, 2012.
- [91] M. Tahmasian, L. M. Bettray, T. van Eimeren, A. Drzezga, L. Timmermann, C. R. Eickhoff, S. B. Eickhoff, and C. Eggers. A systematic review on the applications of resting-state fMRI in Parkinson’s disease: Does dopamine replacement therapy play a role? *Cortex*, 73:80–105, Dec. 2015.
- [92] V. Taler and N. A. Phillips. Language performance in Alzheimer’s disease and mild cognitive impairment: A comparative review. *Journal of Clinical and Experimental Neuropsychology*, 30(5):501–556, June 2008. Publisher: Routledge .eprint: <https://doi.org/10.1080/13803390701550128>.
- [93] K. Tanahashi, S. Takayanagi, T. Motohashi, and S. Tanaka. Application of Ising Machines and a Software Development for Ising Machines. *Journal of the Physical Society of Japan*, 88(6):061010, June 2019. Publisher: The Physical Society of Japan.
- [94] M. Tanveer, B. Richhariya, R. U. Khan, A. H. Rashid, P. Khanna, M. Prasad, and C. T. Lin. Machine Learning Techniques for the Diagnosis of Alzheimer’s Disease: A Review. *ACM Transactions on Multimedia Computing, Communications, and Applications*, 16(1s):30:1–30:35, Apr. 2020.
- [95] S. L. Thompson-Schill, D. Swick, M. J. Farah, M. D’Esposito, I. P. Kan, and R. T. Knight. Verb generation in patients with focal frontal lesions: A neuropsychological test of neuroimaging findings. *Proceedings of the National Academy of Sciences*, 95(26), 1998.
- [96] E. Tognoli and J. S. Kelso. The metastable brain. *Neuron*, 81(1):35–48, 2014.
- [97] M. E. Tuckerman. *Statistical Mechanics: Theory and Molecular Simulation*. Oxford University Press, Aug. 2023. .eprint: <https://academic.oup.com/book/51892/book-pdf/52062963/oso-9780198825562.pdf>.
- [98] F. Vedaiei, N. Mashhadi, G. Zabrecky, D. Monti, E. Navarreto, C. Hriso, N. Wintering, A. B. Newberg, and F. B. Mohamed. Identification of chronic mild traumatic brain injury using resting state functional MRI and machine learning techniques. *Frontiers in Neuroscience*, 16, 2023.

- [99] T. Vincent, L. Risser, and P. Ciuciu. Spatially Adaptive Mixture Modeling for Analysis of fMRI Time Series. *IEEE Transactions on Medical Imaging*, 29(4):1059–1074, Apr. 2010. Conference Name: IEEE Transactions on Medical Imaging.
- [100] O. Vyšata, A. Procházka, J. Mareš, R. Rusina, L. Pazdera, M. Vališ, and J. Kukul. Change in the characteristics of eeg color noise in alzheimer’s disease. *Clinical EEG and neuroscience*, 45(3):147–151, 2014.
- [101] J.-C. Walter and C. Chatelain. Relaxation at finite temperature in fully frustrated Ising models. *Journal of Statistical Mechanics: Theory and Experiment*, 2012(02), 2012.
- [102] T. Watanabe, S. Hirose, H. Wada, Y. Imai, T. Machida, I. Shirouzu, S. Konishi, Y. Miyashita, and N. Masuda. A pairwise maximum entropy model accurately describes resting-state human brain networks. *Nature Communications*, 4(1):1370, Jan. 2013. Number: 1 Publisher: Nature Publishing Group.
- [103] G. Williams and D. C. Watts. Non-symmetrical dielectric relaxation behaviour arising from a simple empirical decay function. *Trans. Faraday Soc.*, 66:80–85, 1970.
- [104] S. Wiseman and E. Domany. Lack of self-averaging in critical disordered systems. *Physical Review E*, 52(4):3469–3484, Oct. 1995.
- [105] S. Wiseman and E. Domany. Finite-Size Scaling and Lack of Self-Averaging in Critical Disordered Systems. *Physical Review Letters*, 81(1):22–25, July 1998. Publisher: American Physical Society.
- [106] W.-X. Zhou and D. Sornette. Self-organizing Ising model of financial markets. *The European Physical Journal B*, 55(2):175–181, Jan. 2007.
- [107] V. Zimmern. Why brain criticality is clinically relevant: a scoping review. *Frontiers in neural circuits*, 14:54, 2020.